Heating and cooling of accreting white dwarfs

Dissertation
zur Erlangung des Doktorgrades
der Mathematisch–Naturwissenschaftlichen Fakultäten
der Georg–August Universität zu Göttingen

vorgelegt von
Boris T. Gänsicke
aus Berlin

Göttingen 1997

D 7
Referent: Prof. Dr. K. Beuermann
Korreferent: Prof. Dr. W. Kollatschny
Tag der mündlichen Prüfung: 3. November 1997

Die Augen können Dich täuschen, traue ihnen nicht.

Laß Dich von Deinen Gefühlen leiten.

Ben Kenobi

Abstract

Boris T. Gänsicke:
Heating and cooling of accreting white dwarfs

In *cataclysmic variables* (CVs), a white dwarf accretes matter from a main–sequence secondary star which fills its Roche–lobe. The mass accretion affects the temperature of the white dwarfs in these systems by several physical mechanisms, including irradiation and compression. The consequences are an inhomogeneous temperature distribution over the white dwarf surface, short–term heating and cooling of the white dwarf envelope in response to changes in the accretion rate and a retarded core cooling compared to non–accreting white dwarfs. I have analysed these effects in several CVs using ultraviolet spectroscopy obtained with the *International Ultraviolet Explorer* and with the *Hubble Space Telescope*. The systems included in this analysis belong to two different subclasses of CVs, polars and dwarf novae.

I find that a large polar cap which covers 3–10 % of the white dwarf surface and which is heated to $\sim$ 10 000 K above the mean white dwarf temperature is a common feature in the polars V834 Cen, AM Her, DP Leo, QQ Vul and RX J1313–32. In AM Her, the best–studied case, this polar cap is most likely heated by irradiation with cyclotron emission or thermal bremsstrahlung from a rather high standing shock. The luminosity of this heated pole cap proves to be an important, but hitherto neglected ingredient in the energy balance of the accretion process. The white dwarf temperatures derived in this work for seven magnetic cataclysmic variables show a trend to lower temperatures at shorter orbital periods, which can be understood in the general picture of CV evolution where the systems evolve towards shorter periods. Hence, the orbital period can be considered as a clue to the *age* of the system. However, one long–period system, RX J1313–32, is found to have a remarkably low temperature. Viable hypotheses for this low temperature are that RX J1313–32 presently undergoes a prolonged episode of low accretion activity or that the system became a semi–detached binary only "recently", and that the white dwarf had sufficient time to cool during the pre–CV period.

In dwarf novae, the white dwarf envelope is heated on a short timescale during dwarf nova outbursts, e.g. by irradiation from the luminous disc–star interface or by compression by the accreted mass. I could show for the first time that in VW Hyi the decrease of the observed ultraviolet flux following an outburst is due to a decrease of the photospheric temperature of the white dwarf. Furthermore, I could show that the white dwarf responds differently to the two types of outburst that the system undergoes. The declining luminosities and temperatures are in general agreement with models based on radiative or compressional heating of the outer layers of the white dwarf. However, from the present data it is not possible to unequivocally identify the heating mechanism. It is possible that the equatorial region of the white dwarf never reaches an equilibrium state due to the frequent repetitive heating.

A dwarf nova very similar to VW Hyi, but with a much longer outburst cycle is EK TrA. This system, even though fainter than VW Hyi, may be better suited to study the thermal response of the white dwarf to dwarf nova outbursts. I present an analysis based on ultraviolet and optical spectroscopy of EK TrA which yields a temperature estimate for the white dwarf photosphere. In addition, the optical data show emission from a cool accretion disc (or a corona situated on top of a colder disc), possibly extending over much of the Roche radius of the primary.

Contents

Chapter 1

Introduction

Accretion of matter onto a more or less compact object is a very common process in the universe. Examples of objects where mass accretion has impressive observable consequences are e.g. semi–detached binaries harbouring either a neutron star or a stellar black hole, young stellar objects, and active galactic nuclei, where presumably a massive black hole accretes from the inner galactic disc. Even though the phenomenon of accretion is almost banal in itself — the release of potential energy as matter falls into the gravitational well of the accreting object — a large variety of physical processes is usually involved in it. A fine group of stars which is well–suited for a detailed study of accretion physics are the *cataclysmic variables*, semi–detached close binaries consisting of a white dwarf primary star and a late–type main–sequence secondary star. The secondary star fills its *Roche–lobe*, i.e. the largest possible closed equipotential surface encompassing its mass (Fig. 1.1). The gravity of the two stellar components and the centripetal force in the rotating system are cancelled at the inner Lagrangian point L_1 on the line connecting their centres of mass. Through this nozzle, the secondary star loses matter into the gravitational well of the white dwarf. The potential energy released during the accretion of this matter onto the white dwarf is given by

$$L_{\mathrm{acc}} = \frac{GR_{\mathrm{wd}}\dot{M}}{R_{\mathrm{wd}}} \tag{1.1}$$

where G is the gravitational constant, R_{wd} and R_{wd} are the white dwarf mass and radius, respectively, and $\dot{M}$ is the accretion rate. With typical accretion rates of $10^{-11} - 10^{-9} M_{\odot}\,\mathrm{yr}^{-1}$ the resulting accretion luminosities are $10^{31} - 10^{34}$ erg s^{-1}. A large part of this energy is released in relatively small accretion regions near the white dwarf which are, therefore, heated to high temperatures. Consequently, cataclysmic variables are strong sources of X–ray and ultraviolet emission.

One reason for the large fascination that these objects inspired amongst astronomers is probably their liveliness. With a small binary separation (nearby as the distance between the earth and the moon), cataclysmic variables have typical orbital periods of a few hours. It is, therefore,
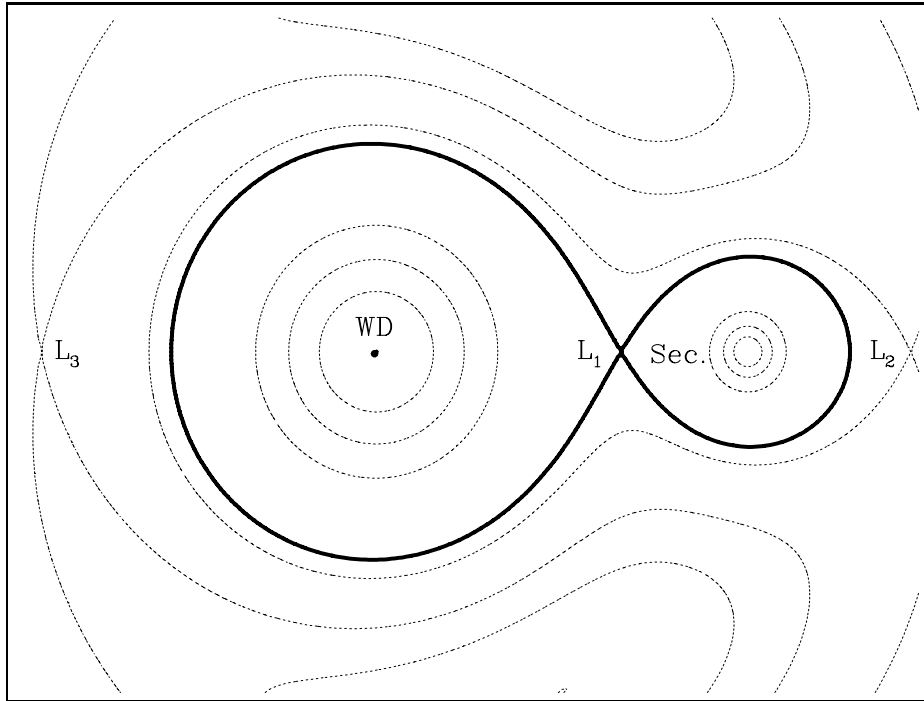
Figure 1.1: Equipotential surfaces in a cataclysmic variable with $R_{wd}/M_{sec} = 5$. The bold line traces the critical Roche–surface, the secondary (Sec.) fills the right *Roche–lobe*. At the inner Lagrangian point L_1, the potential has a saddle point where matter can flow from the secondary into the gravitational well of the white dwarf (WD). The Roche potential has four other saddle points, two of which are, like L_1, located on the line connecting the centres of gravity (L_2 and L_3) while the other two saddle points (L_4 and L_5) are outside the plotted area.

easy to observe the consequences of accretion onto a white dwarf under the gradually changing geometric projection of the system while the two stars rotate around their centre of mass.

Another reason may be the large variety of species within the class of cataclysmic variables. Briefly, cataclysmic variables exist in two flavours (for the most exhaustive review on cataclysmic variables, see Warner 1995):

• If the white dwarf has a strong magnetic field ($B \gtrsim 10 \, MG$), the matter lost from the secondary star is eventually threaded by the field lines and is channelled to rather small regions on the white dwarf near its magnetic poles. Close to the white dwarf surface, the matter falling inwards with supersonic velocities is decelerated in a strong stand–off shock, giving rise to the emission of hard X–rays and cyclotron radiation. Due to the emission of polarized cyclotron radiation these systems were baptised *polars*[1].

---

[1]The classification given here is actually somewhat simplified, because already weaker magnetic fields of $B \gtrsim 1 \, MG$ are sufficient to funnel the accreting matter. In this case, an accretion disc may form in the outer regions of the Roche–lobe of the white dwarf, but is disrupted by the magnetic field near the white dwarf. This type of systems is called *intermediate polars*. The main difference between intermediate polars and polars is that the white

● If the white dwarf has no (or a very weak) magnetic field, the matter lost from the secondary forms an accretion disc around the white dwarf, spiralling slowly inwards while transforming kinetic energy into heat by viscous friction. In this case, the white dwarf will accrete from the inner disc through an equatorial belt.

Both types of systems, however, share a common fate: once a certain amount of hydrogen–rich matter is accumulated on the white dwarf surface, a self–ignited explosive thermonuclear reaction ejects again part of the white dwarf envelope. This *thermonuclear runaway* is the cause of the long–known nova phenomenon.

On one hand, the characteristics of the white dwarf will obviously determine to a large extent the physics involved in the accretion process. The mass of the white dwarf defines the depth of the potential well, and, thereby, both the amount of energy released per gram of accreted matter and the form of the emitted spectrum. The white dwarf mass also strongly affects the mass of the accreted layer of hydrogen which is necessary to ignite a nova explosion. In polars, the accretion geometry sensitively depends on the magnetic field strength of the white dwarf. Also the form of the accretion spectrum is largely determined by the field strength as a substantial part of the released potential energy is emitted in form of cyclotron radiation. In the non–magnetic disc–accreting systems, the white dwarf rotation rate is a crucial parameter which controls the shear mixing of the material from the inner disc (rotating approximatively at Keplerian velocities) into the white dwarf.

On the other hand, the accretion process will modify the white dwarf characteristics. The accreted matter with bona–fide solar abundances will enrich the white dwarf with heavy elements. In disc–accreting systems, the white dwarf, or at least its outer layers, will be spun up by accretion of angular momentum from the disc–material. A larger number of factors will influence the temperature of the white dwarf: X–ray and EUV emission, produced either in the accretion spots of magnetic systems or in the disc–star interface of non–magnetic systems, will heat the white dwarf atmosphere by irradiation. The mass of the accreted matter will compress the envelope of the white dwarf and, thereby, also heat it. In addition, an increase of the white dwarf mass due to accretion will result in an adiabatic contraction of the whole star, resulting in further heating. However, if the mass of the envelope ejected during a nova explosion exceeds the mass of the previously accreted layer, the white dwarf will effectively lose mass and will, consequently, cool by adiabatic expansion. By affecting the white dwarf temperature, accretion perturbs the beat of a usually very reliable stellar clock: The cooling of single (non–accreting) white dwarfs depends only on the thermal energy stored in their degenerate core and can be modelled very well. Hence, for *single* white dwarfs, their observed temperatures can be used as a direct measure of their ages. Also in cataclysmic variables, the white dwarf temperatures may be considered a clue[2] to the age of the systems if the effects of accretion are taken into account. Hitherto, this possibility was only considered by Sion (1991).

---

dwarf spin period is much shorter than the binary orbital period in intermediate polars while the white dwarf rotates synchronously in polars. Throughout this thesis, *magnetic cataclysmic variables* is used equivalent to *polars*

[2]There exists no reliable indicator of the age of cataclysmic variables at present. Apart from the white dwarf temperature discussed here, van Paradijs et al. (1996) and Kolb & Stehle (1996) suggest that the γ velocity of cataclysmic variables could be used as a measure of their age.

The aim of this thesis is to expand our knowledge of the influence that accretion has on the temperature of white dwarfs in cataclysmic variables. I approach this aim by the detailed analysis of ultraviolet observations of a number of magnetic and non–magnetic systems. In order to discuss the observed white dwarf temperatures in the context of the ages of cataclysmic variables, in Chapter 2 I will shortly summarize the evolution of cataclysmic variables as well as the cooling theory for single white dwarfs. Chapter 2 also includes a short discussion of the effect of nova outbursts on the white dwarf temperature. Due to the two–fold nature of cataclysmic variables, the results for the individual stars are presented in two (almost) self–contained sections:

● In polars, the hard X–rays and the cyclotron radiation emitted from the stand–off shock irradiate the polar cap of the white dwarf. Early models (Lamb & Masters 1979) predicted that about half of the post–shock emission is intercepted by the white dwarf and is re–emitted in the soft X–ray regime. However, observations show a large excess of soft X–rays in many systems, a problem known as the *soft X–ray puzzle*. Using orbital phase–resolved ultraviolet spectroscopy of AM Herculis, I show in Chapter 3 that a rather large spot in the polar region of the white dwarf is heated to moderate temperatures. The ultraviolet luminosity of this polar cap matches the sum of the observed luminosities of hard X–rays and of cyclotron radiation, indicating that irradiation from the shock is the most likely heating mechanism. This finding resolves, at least in AM Herculis, the *soft X–ray puzzle* in the sense that the reprocessed post–shock emission emerges in the ultraviolet and not in the soft X–ray regime. A systematic study of the complete archival ultraviolet spectroscopy reveals that a large, moderately heated pole cap is present in many systems. The white dwarf temperatures determined from this study show, in agreement with the work of Sion (1991), a slight trend for lower temperatures at shorter periods, where the systems are likely to be rather old. An exception is, however, the long–period polar RX J1313–32, which contains a much colder white dwarf than all other long–period cataclysmic variables analysed so far. Several possible reasons for this finding are discussed.

● In a subclass of the non–magnetic systems, the *dwarf novae*, the accretion rate through the disc is quasi–periodically enhanced by a large factor. Irradiation, compression and accretion of angular momentum during these *dwarf nova outbursts* cause a short–term heating of the white dwarf envelope. In Chapter 4, I quantitatively show the different thermal responses of the white dwarf in VW Hyi to the two types of outbursts that this system undergoes. The results are discussed in the framework of the various theories suggested for local heating of accreting white dwarfs.

Chapter 2

The age of cataclysmic variables

2.1 The standard scenario of cataclysmic variable evolution

The progenitors of cataclysmic variables are wide binaries with large orbital periods ($P_{\mathrm{orb}} \gtrsim$ 10 d) consisting of a low–mass main sequence star and a more massive primary with $M_{\mathrm{prim}} \simeq$ $1 - 10 M_{\odot}$[1] The massive primary evolves on it's nuclear timescale into a giant and eventually fills its Roche–lobe, starting a dynamically unstable mass transfer which results in a common envelope, engulfing both stars. During that phase, the binary system loses angular momentum due to frictional braking in the common envelope, reducing the distance between the two stars and ejecting the envelope of the giant from the system.

If the core of the giant (the future white dwarf) and the low–mass main–sequence secondary do not merge during this process, a detached close binary (a *pre–cataclysmic variable*) emerges. In order to become a cataclysmic variable, the system has to further shrink its orbit until the secondary fills its Roche–lobe[2], starting the mass transfer onto the white dwarf. Loss of angular momentum may be driven by two mechanisms: (a) by emission of gravitational radiation (e.g. Kraft et al. 1962; Krzeminski & Kraft 1964) or (b) by magnetic stellar wind braking[3] (Verbunt & Zwaan 1981). The timescales for the angular momentum loss are (Kolb & Stehle 1996):

---

[1]More massive primaries will not produce a white dwarf but a neutron star, less massive primaries evolve too slowly.

[2]Nuclear evolution of the secondary will increase its radius and may eventually bring the binary in a semi–detached state. However, the nuclear timescale of the low–mass secondaries in cataclysmic variables are generally too long to be of any importance.

[3]A process known from single stars. The stellar wind consists of ionized matter which corotates on the magnetic field lines out to the Alvén radius before it escapes, carrying off angular momentum. This results in a magnetic braking torque on the star. In cataclysmic variables, magnetic braking of the late–type secondary star withdraws angular momentum from the binary orbit as tidal forces synchronize the spin period of the secondary star with the orbital period.

$$\tau_{\text{GR}} = -\left(\frac{J}{\dot{J}}\right)_{\text{GR}} = 3.8 \times 10^{11} \frac{(R_{\text{wd}} + M_{\text{sec}})^{1/3}}{R_{\text{wd}} M_{\text{sec}}} P_{\text{orb}}^{8/3}(\text{d}) \, \text{yrs} \tag{2.1}$$

and

$$\tau_{\text{MB}} = -\left(\frac{J}{\dot{J}}\right)_{\text{MB}} = 2.2 \times 10^{9} \frac{R_{\text{wd}}}{(R_{\text{wd}} + M_{\text{sec}})^{1/3}} R_{\text{sec}}^{-4} P_{\text{orb}}^{10/3}(\text{d}) \, \text{yrs} \tag{2.2}$$

for gravitational radiation and magnetic braking, respectively. Here R_{wd} and M_{sec} are the masses of the white dwarf and the secondary star in solar masses, respectively, R_{wd} is the radius of the secondary in solar radii, and $P_{\text{orb}}(\text{d})$ is the orbital period in days. For the typical parameters occurring in cataclysmic variables, $\tau_{\text{GR}} \gg \tau_{\text{MB}}$. Typical evolutionary timescales are given in Fig. 2.1. Once the secondary fills its Roche–lobe, the mass transfer rate is determined by the mechanism of angular momentum loss. For periods longer than $\simeq 3\,\text{h}$, magnetic braking is the dominant angular momentum loss mechanism. As the system continues to evolve towards shorter periods, the mass of the secondary decreases. At $P_{\text{orb}} \simeq 3\,\text{h}$ ($M_{\text{sec}} \simeq 0.2\,M_{\odot}$) the secondary becomes fully convective, terminating its magnetic activity. At this point, magnetic breaking ceases and the secondary shrinks somewhat below its Roche–surface, thereby stopping the mass transfer. The binary system now evolves towards shorter periods on the much longer timescale of gravitational radiation. The secondary fills its Roche–lobe again when the systems reaches $\simeq 2\,\text{h}$, restarting the mass transfer. Consequently, the mass transfer rates are higher ($\dot{M} \simeq 10^{-9} \ldots 10^{-8} M_{\odot}\,\text{yr}^{-1}$) above the period gap than below the gap ($\dot{M} \simeq 10^{-11} \ldots 10^{-10} M_{\odot}\,\text{yr}^{-1}$). The binary reaches a minimum period at $P_{\text{orb}} \simeq 80\,\text{min}$ where the secondary becomes a degenerate brown dwarf.

The evolutionary scenario outlined above (for more details see e.g. King 1988; Kolb 1995, 96), known as the *disrupted magnetic braking* model (e.g. Rappaport et al. 1983; Verbunt 1984, McDermott & Taam 1989), satisfactorily describes the observed paucity of cataclysmic variables in the period range 2–3 h. Despite this success, it is difficult to quantify the *age* of a cataclysmic variable at a given orbital period. One reason for this is that the detached binaries emerging from the common envelope phase cover a large range of orbital periods. Hence, the time that the system needs to evolve into a semi–detached configuration may largely differ. Recently, Kolb & Stehle (1996) determined the age distribution in a model population of cataclysmic variables and find that the age[4] of the systems below the period gap peaks at $3 - 5\,\text{Gyr}$ while most systems above the gap are younger than 1.5 Gyr.

---

[4]Their definition of age is the total time elapsed since the formation of the progenitor binary system, including the nuclear evolution of the massive primary, the time spent in the common envelope (usually very short), the time spent in a detached state as a pre–cataclysmic variable and the time in the semi–detached state as a cataclysmic variable.
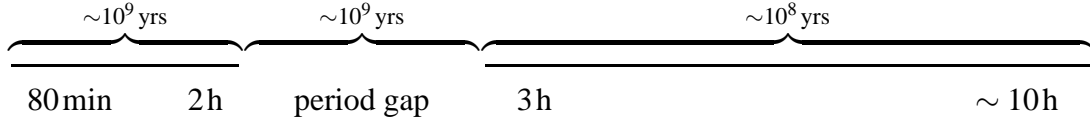
Figure 2.1: Typical evolutionary timescales for cataclysmic variables after McDermott & Taam (1989). Angular momentum loss is driven mainly by magnetic braking for systems above the period gap and by gravitational radiation for systems below the gap.

2.2 The cooling timescale of isolated white dwarfs

The bulk of the white dwarf mass is concentrated in its degenerate core with only a small non–degenerate layer ($\lesssim 10^{-4}\,M_\odot$) floating on top. The core is largely isothermal due to heat conduction by the degenerate electrons. The dominant source of energy[5] powering the luminosity of a white dwarf is the thermal energy of its core, which is if the order of 10^{48} ergs. During the early stages of the white dwarf cooling, when the core is still very hot ($T_{\rm core} \gtrsim 10^7$ K), neutrino emission is a major contribution to the bolometric luminosity. Neglecting the neutrino emission, the cooling timescale of a white dwarf is determined by two factors: the amount of thermal energy stored in its core and the opacity of its non–degenerate envelope, through which the energy is transported by radiation transfer. From the simple envelope solution obtained from the equations of stellar structure and from an appropriately chosen Kramers–opacity, one can estimate the luminosity of the white dwarf $L_{\rm wd}$ as a function of its cooling time (age):

$$t_{\rm cool} = 4.6 \times 10^6 \left(\frac{L_{\rm wd}}{L_\odot} \right)^{-5/7} \text{yrs} \tag{2.3}$$

where $L_\odot$ is the solar luminosity. With $L = 4\pi\sigma R^2 T^4$, where σ is the Stefan–Boltzmann constant and R is the stellar radius, the temperature at a certain age is

$$T_{\rm wd} = T_\odot \left(\frac{t_{\rm cool}}{4.6 \times 10^6\,{\rm yrs}} \right)^{-7/20} \left(\frac{R_\odot}{R_{\rm wd}} \right)^{1/2} \text{K} \tag{2.4}$$

which overestimates the real temperature for $t_{\rm cool} \lesssim 10^7$ yrs because of the neglect of neutrino cooling. Detailed numerical stellar evolution models yield cooling tracks shown in Fig. 2.2. From these calculations and the observed luminosity of white dwarfs their cooling ages can be derived. In fact, the observed cut–off in the luminosity function of white dwarfs in our galaxy at $L \simeq 3 \times 10^{-5} L_\odot$ is used (together with models for the star formation rate) to estimate the age of the galactic disc as $t_{\rm disc} \simeq 10^{10}$ yrs (e.g. Oswalt et al. 1996).

---

[5]In a white dwarf, the central nuclear burning is extinguished. However, the following processes can still produce some energy: (a) release of potential energy due to contraction, (b) *slow* nuclear reactions in the core due to the very high densities (so–called *pyconuclear* reactions, in contrast to the usual thermonuclear reactions in stellar interiors which are driven by the large kinetic velocities of high–temperature ions) (c) release of latent heat due to the cristallization of the core at low temperatures.
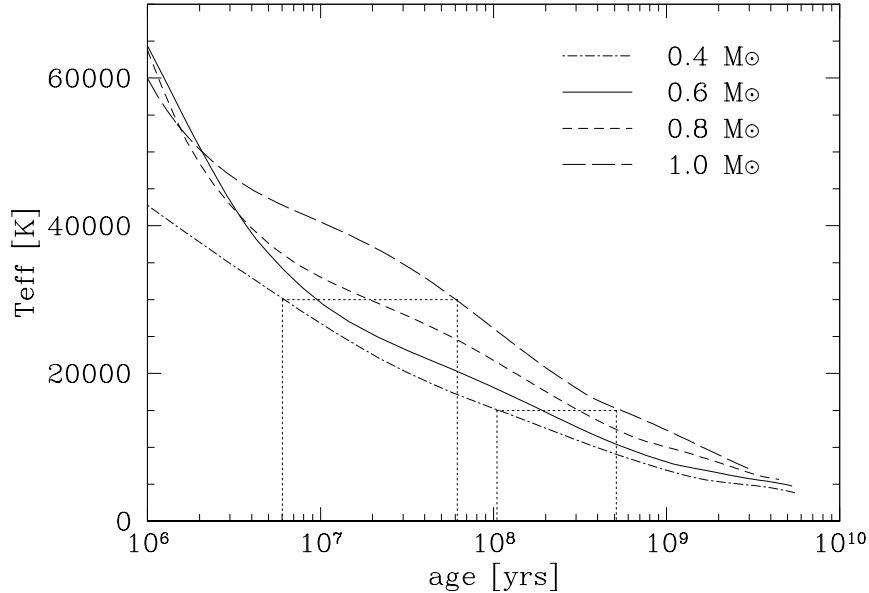
Figure 2.2: Cooling tracks for single (non–accreting) white dwarfs after Wood (1995). The cooling timescale depends on the mass of the white dwarf. Tracks for four different masses are plotted. Two typical temperatures for (accreting) white dwarfs in cataclysmic variables are indicated: 30 000 K as e.g. in the dwarf nova U Gem and 15 000 K as in the polar V834 Cen.

2.3   Photospheric white dwarf temperatures in cataclysmic variables

As outlined above (Sect. 2.1), the orbital period of an individual cataclysmic variable is *no* direct indicator of the age of the system, due to the unknown time spent as a detached pre–cataclysmic variable. Considering that the effective temperatures of single white dwarfs are rather precise "clocks", there is the hope that the white dwarf temperature in cataclysmic variables may be a clue to the age of the systems. I have included in Fig. 2.2 the white dwarf temperatures for two typical cataclysmic variables, the dwarf nova U Gem ($P_{\mathrm{orb}} = 254\,\mathrm{min}$, above the gap) and the polar V834 Cen ($P_{\mathrm{orb}} = 102\,\mathrm{min}$, below the gap). The corresponding ages for *non–accreting* white dwarfs are, depending on the white dwarf mass, a few $10^7\,\mathrm{y}$ for U Gem and a few $10^8\,\mathrm{y}$ for V834 Cen. Comparing these values with the predictions of the standard evolutionary scenario, the estimated age of V834 Cen appears to be rather low or, vice versa, the star is too hot considering its likely evolutionary age.

Apparently, the interpretation of the observed white dwarf temperatures in terms of ages is not straightforward: (a) The photospheric temperatures of white dwarfs in cataclysmic variables depend on the *long–term accretion–induced heating* which counteracts the secular core
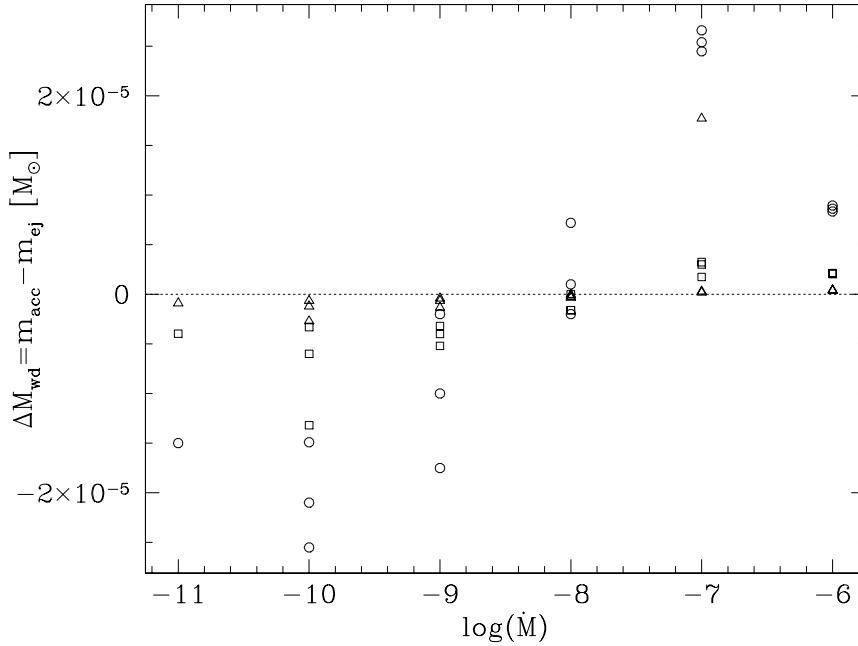
Figure 2.3: Change of the white dwarf mass during one nova outburst (adopted from Table 1 of Prialnik et al. 1995). The initial white dwarf mass is coded as follows: (○) $0.6\,M_\odot$, (□) $1.0\,M_\odot$ and (△) $1.25\,M_\odot$. For each white dwarf mass, three different effective temperatures were considered.

cooling to some extent. Long–term fluctuations of the accretion rate around the secular mean dictated by the angular momentum loss mechanism (gravitational radiation or magnetic braking) will introduce some scatter in the observed temperatures. (b) Short–term variations of the accretion rate (high/low states in polars (Sect. 3.3) or dwarf novae outbursts (Sect. 4.1.2)) will cause an instantaneous thermal response of the white dwarf envelope. The accretion–induced equilibrium temperature has to be measured, therefore, in a phase of low accretion activity (low state/quiescence). (c) Additional heating occurs during nova outbursts when the accreted hydrogen layer ignites a thermonuclear runaway and temperatures of several 10^5 K are reached on the white dwarf surface. (d) The mass of the accreting white dwarf in a cataclysmic variable and, hence, its radius, is not constant. Accretion of matter will result in first place in a contraction of the white dwarf, freeing additional gravitational energy which will cause further heating. However, once enough matter has been accreted[6] a nova explosion occurs which ejects again part of the white dwarf envelope. The long–term mass balance depends, therefore, on the ratio of accreted and ejected mass per nova outburst. Recently, Prialnik et al. (1995) computed evolutionary sequences of nova outbursts through several cycles for a large range of white dwarf masses, white dwarf temperatures and accretion rates. They find that for accretion rates $\dot{M} \lesssim 10^{-9} M_\odot \mathrm{yr}^{-1}$ the white dwarf mass is decreasing gradually and that only for

---

[6]Depending on the white dwarf mass, its temperature and the accretion rate $\sim 10^{-7} - 10^{-4} M_\odot$.
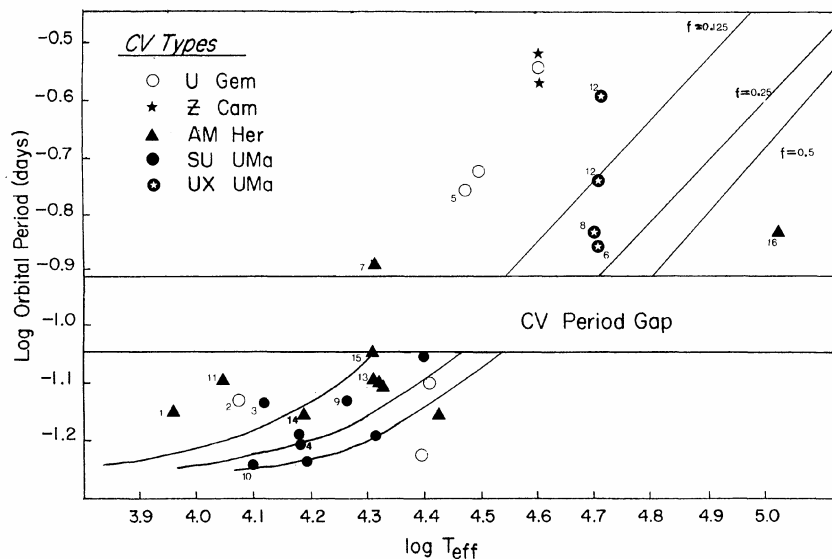
**Figure 2.4:** Orbital period vs. observed photospheric white dwarf temperatures in cataclysmic variables (from Sion 1991). Plotted along with the observed data points is the relation $T_{\text{eff}} = (L_{\text{acc}}/4\pi R_{\text{wd}}^2 \sigma)^{0.25}$ as an approximate description of the accretion–induced heating of the accreting white dwarfs. Here, the accretion luminosity is given by $L_{\text{acc}} = fGR_{\text{wd}}\dot{M}/R_{\text{wd}}$, where f is the fraction of the total accretion energy which heats the white dwarf, and $\dot{M}$ is a function of P_{orb} taken from McDermott & Taam (1989). Three curves are plotted for $f = 0.125, 0.25, 0.5$.

$\dot{M} \geq 10^{-8} M_\odot \text{yr}^{-1}$ an increase of the white dwarf mass is possible (Fig. 2.3). It seems, therefore, that the mass of the white dwarf in typical cataclysmic variables ($\dot{M} = 10^{-11} - 10^{-8} M_\odot \text{yr}^{-1}$) should gradually decrease. Accreting over its lifetime several $0.1 M_\odot$, a cataclysmic variable will undergo a few 10^4 nova eruptions, resulting in a reduction of the white dwarf mass by $\sim 10\%$ or more. The compilation by Ritter & Kolb (1997) indicates indeed a decrease of the white dwarf mass towards lower periods, which will be discussed in more detail in Sect. 5. However, precise mass determinations of most likely old cataclysmic variables (below the period gap) would be desirable to test this hypothesis. *If* the white dwarfs in cataclysmic variables lose mass due to nova eruptions, they will expand accordingly and, thereby, cool adiabatically throughout their interior.

Observationally, Sion (1991) found that the photospheric temperatures of white dwarfs in cataclysmic variables decrease towards shorter periods, with a distinct tendency for rather hot ($T_{\text{wd}} \gtrsim 30000\,\text{K}$) and rather cold ($T_{\text{wd}} \lesssim 20000\,\text{K}$) white dwarfs in systems above and below the period gap, respectively (Fig 2.4). He derived empirically lower limits on the age of the systems which are in general agreement with the evolutionary timescales of McDermott & Taam (1989). Sion (1991) found also a weak evidence for lower temperatures in polars. However, he concluded that the number of polars with reliable temperature determinations in his sample was too small for definite conclusions.

My analysis in Sect. 3.5 and Sect. 3.6 results in the largest sample of reliable white dwarf temperatures for polars obtained so far and I will compare my findings to those of Sion (1991) in Sect. 3.7.

Chapter 3

Polars

3.1 Overview

In 1924, a short notice was published by M. Wolf in *Astronomische Nachrichten* on the discovery of a new variable star in the constellation Hercules, later to be known as AM Her. In the decades to follow, AM Her remained a Sleeping Beauty. Only fifty years later it attracted again attention as possible optical counterpart for the unidentified *Uhuru* X–ray source 3U 1809+50 (Berg & Duthie 1977). Competing identifications were the galaxies OU 1809+516 or NGC 6582 (Bahcall et al. 1976). A refined position of the X–ray source derived from SAS–3 observations (Hearn et al. 1976) ruled out all ambiguities, settling the score for AM Her. Flickering observed at optical and X–ray wavelengths raised the suggestion that AM Her is a cataclysmic variable of the U Geminorum type.

However, the detection of linear and circular polarized radiation (Tapia 1976a,b) revealed the true nature of this so far unique object: a cataclysmic variable containing a strongly magnetized white dwarf. Tapia interpreted the observed polarized optical flux as cyclotron emission from hot electrons gyrating in a strong magnetic field and estimated a field strength of $B \sim 200\,\mathrm{MG}$ (which later turned out to be overestimated by a factor of ~ 10, see Sect. 3.5; 3.6.4). The strong magnetic field of the white dwarf has two important implications. (a) The white dwarf and the mass–losing secondary star rotate synchronously, i.e. the two stars show each other always the same face. (b) The formation of an accretion disc is prevented. The accretion flow is channelled along the magnetic field lines onto one or both poles of the white dwarf where the kinetic energy is released as thermal bremsstrahlung, cyclotron radiation and soft X–ray emission.

The natural observational consequence after such an exciting discovery was the hunt for other cataclysmic variables harbouring a magnetic white dwarf. Searching the emission of known variable binaries for polarized radiation yielded two quick hits: VV Pup (Bond & Wagner 1977; Tapia 1977) and AN UMa (Krzeminski & Serkowski 1977). The latter authors coined the name *polars* for this new class of cataclysmic variables from their most outstanding property, the strong optical polarization. After the first quick discoveries, the search for polars
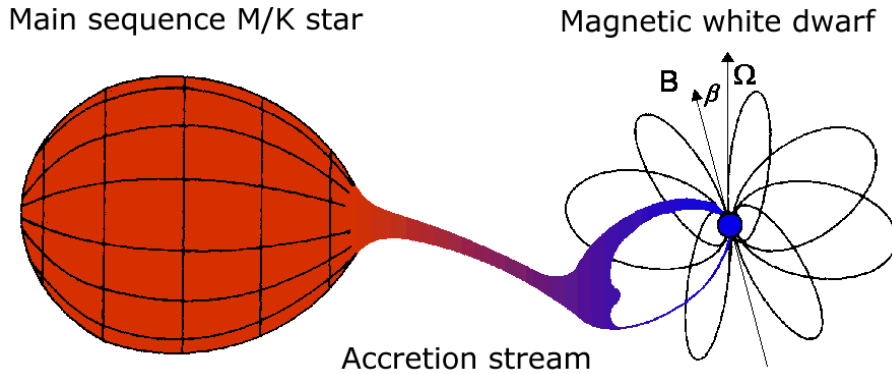
Figure 3.1: Schematic view of a polar, adapted from Cropper (1990). The magnetic dipole axis is inclined against the rotation axis by the angle β.

became a tedious work. Due to their strong X–ray emission, most of the systems were found from the *HEAO–1*, *EINSTEIN* and *EXOSAT* X–ray satellite missions. However, a few objects were also found from optical surveys for blue stars (Palomar Green) or for emission line objects (Case Western). The first all sky survey at X–ray wavelengths performed by *ROSAT* was *the* chance for new offsprings for the polar family. Beuermann & Thomas (1993) started an identification program for all bright soft X–ray sources (count rates $\gtrsim 0.5\,\mathrm{cts\,s^{-1}}$), supplemented by similar efforts of our British colleagues. This efforts quickly lead to the discovery of $\simeq 30$ new polars (e.g. Buckley et al. 1993; Burwitz et al. 1996, 1997a,b; Mittaz et al. 1992; O'Donoghue et al. 1993; Osborne et al. 1994; Reinsch et al. 1994; Singh et al. 1995; Staubert et al. 1994; Schwope et al. 1993a; Sekiguchi et al. 1994; Szkody et al. 1995; Thomas et al. 1996; Tovmassian et al. 1997; Walter et al. 1995).

The fascination for accreting magnetic white dwarfs keeps on spawning continuous observational and theoretical work. In 1995 the first workshop dedicated solely to magnetic cataclysmic variables was hold in Cape Town, South Africa (Buckley & Warner 1995).

3.2   The accretion scenario

The matter lost from the secondary star through the L_1 point follows a free–fall trajectory until the magnetic pressure exceeds the ram pressure in the stream, i.e.

$$\frac{B^2}{8\pi} \gtrsim \rho v^2 = (\dot{M}/\pi\sigma^2 v)v^2 \tag{3.1}$$

where v and σ are the free–fall velocity and the cross–section of the accretion stream, respectively, and $\dot{M}$ is the accretion rate. The matter, ionized to a high degree by the ultraviolet and X–ray emission from the hot accretion region on the white dwarf, then couples to the magnetic field lines and is channelled to one or two accretion spots near the magnetic poles (Fig. 3.1).
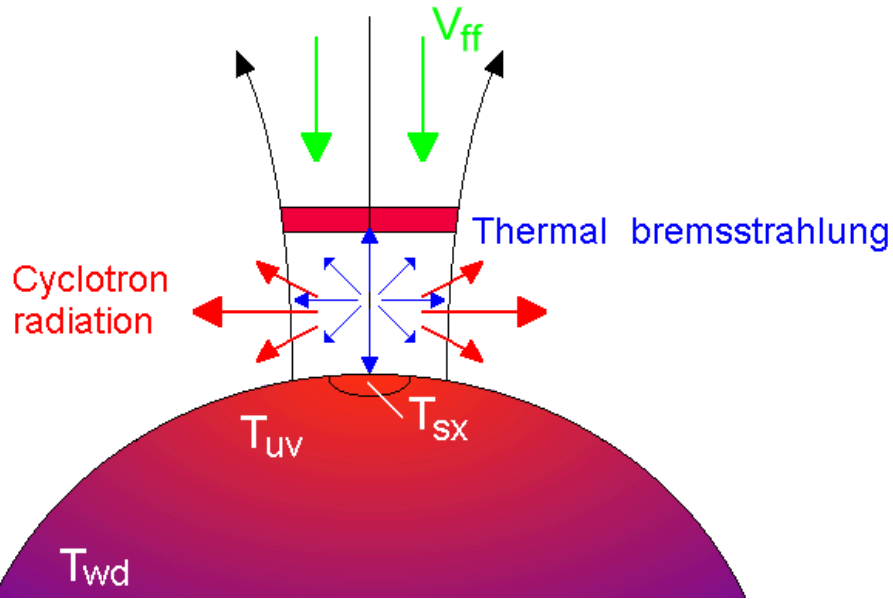
Figure 3.2: Schematic view of the accretion region. The matter falls inwards quasi–radially with supersonic velocities and is decelerated in a stand–off shock. The cyclotron radiation originating in the hot post–shock plasma is beamed perpendicular to the magnetic field lines (gray arrows), the thermal bremsstrahlung is emitted isotropically (black arrows).

Early theories for accretion onto a magnetic white dwarf (e.g. Lamb & Masters 1979; King & Lasota 1979) predict that the matter falling in with supersonic velocities (a few $1000 \, \mathrm{km \, s^{-1}}$) is decelerated by a factor of ~ 4 and heated to $\sim 10^8 \, \mathrm{K}$ in a strong shock standing above the white dwarf surface. The kinetic energy is released from the post–shock flow in the form of thermal bremsstrahlung (hard X–rays) and cyclotron radiation. About half of the bremsstrahlung and cyclotron flux is intercepted by the white dwarf photosphere and re–emitted as soft X–rays (Fig. 3.2). Hence, the following ratio should hold:

$$L_{\mathrm{SX}} \simeq L_{\mathrm{tb}} + L_{\mathrm{cyc}} \tag{3.2}$$

where L_{SX}, L_{tb} and L_{cyc} are the accretion–induced luminosities in form of soft X–rays, thermal bremsstrahlung and cyclotron radiation, respectively. The thermal bremsstrahlung will be reflected to a certain degree from the partially ionized atmosphere of the white dwarf due to Compton scattering, so that equation 3.2 should be corrected for the reflection albedo of the hard X–ray component.

Nevertheless, in many polars the observed soft X–ray flux exceeds the sum of thermal bremsstrahlung and cyclotron radiation by a large factor (recent compilations are given by Beuermann 1997; Ramsay et al. 1994). This deviation from the predictions, known as the *soft X–ray puzzle*, has been discussed in the literature for many years (e.g. Frank et al. 1988). However, considering that the accretion flow is neither homogenous nor constant in time allows to solve this puzzle.
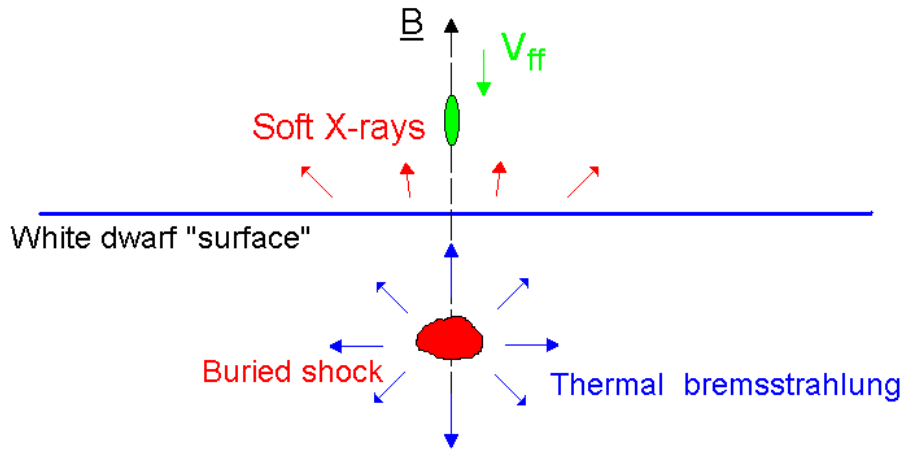
Figure 3.3: Blobby accretion.

(a) At low mass flow rates, $\dot{m} \lesssim 0.1\,\mathrm{g\,cm^{-2}}$, the infalling protons[1] cool within one mean free path due to Coulomb collisions. No shock is formed, the protons rather diffuse into the white dwarf photosphere, a situation known as the *bombardment solution*. In this case, the outer layers of the white dwarf photosphere are heated to a few 10^7 K only, and cyclotron radiation is the dominant cooling mechanism. The radiation transfer for particle heated atmospheres has been numerically solved by Woelk & Beuermann (1992; 1993).

(b) For moderate mass flow rates, $0.1\,\mathrm{g\,cm^{-2}} \lesssim \dot{m} \lesssim 10\,\mathrm{g\,cm^{-2}}$, a hydrodynamic shock forms and the post–shock plasma cools through emission of thermal bremsstrahlung and cyclotron radiation (just as described in the standard model above). The shock height is a function of both, $\dot{m}$ and B. With increasing B, cyclotron cooling becomes more and more efficient, reducing the maximum temperature in the shock and, hence, increasing the ratio $F_{\mathrm{cyc}}/F_{\mathrm{tb}}$. As a consequence, the shock height decreases with increasing B. The shock height is also reduced with increasing $\dot{m}$ due to the higher ram pressure of the accretion stream. However, a higher $\dot{m}$ results in a higher shock temperature, decreasing the ratio $F_{\mathrm{cyc}}/F_{\mathrm{tb}}$. A numerical simulation of the radiation transfer through the hydrodynamic shock was presented by Woelk & Beuermann (1996), for further discussions of the shock height see Beuermann & Woelk (1996) and Beuermann (1997).

(c) For high mass flow rates, $\dot{m} \gtrsim 10\,\mathrm{g\,cm^{-2}}$, the shock is rammed by the accretion column (at this point more an *accretion piston*) deep into the atmosphere of the white dwarf, where *deep* implies several pressure scale heights and large optical depths for hard X–ray photons. The thermal bremsstrahlung produced in this submerged shock is then reprocessed within the atmosphere into soft X–ray and EUV radiation emitted from a small fraction of the white dwarf surface (Fig. 3.3). The regime of very high mass flow rates has been suggested as a solution to the *soft X–ray puzzle* by Kuijpers & Pringle (1982), where the authors envision a time–

---

[1]As the proton mass exceeds the electron mass by a factor of ~ 2000, the kinetic energy of the accreting electrons may be neglected
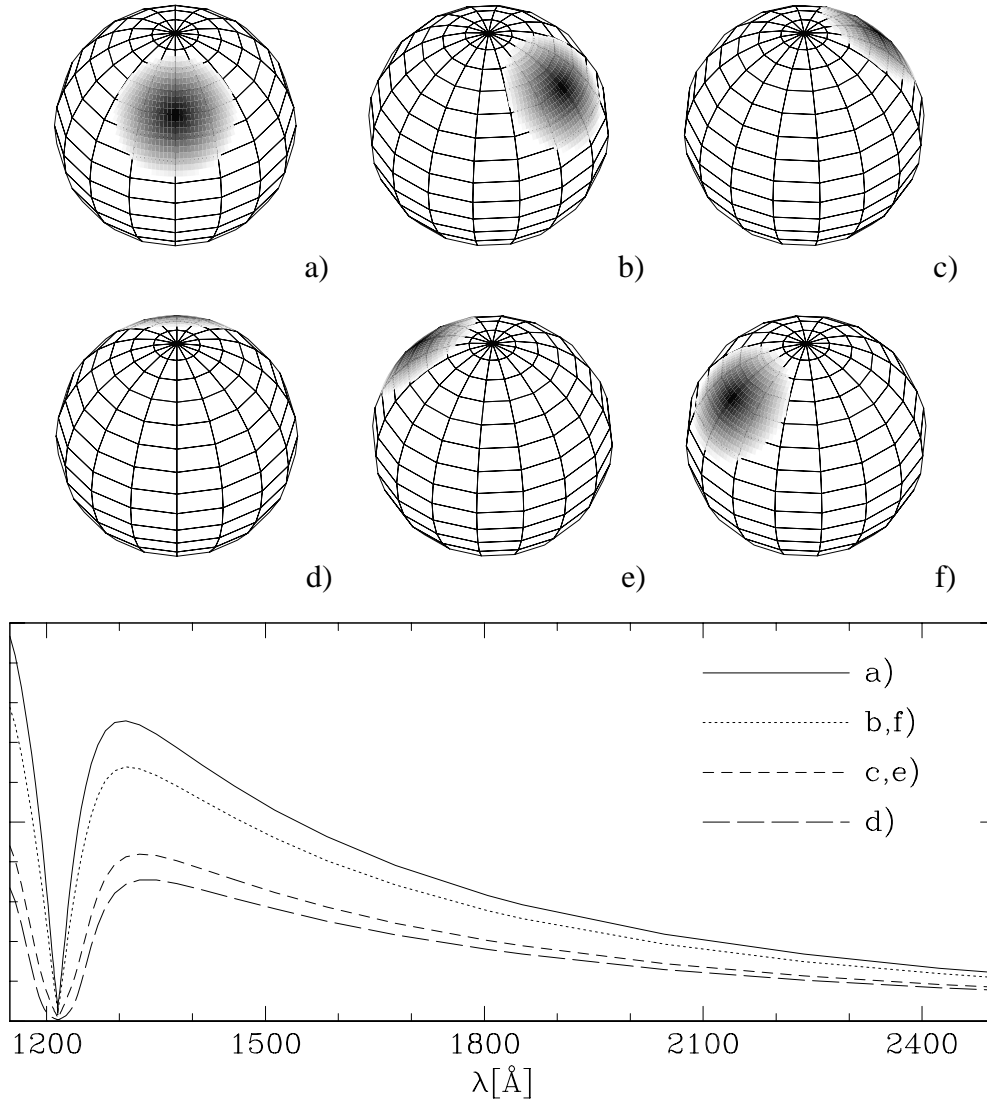
Figure 3.4: Simulated phase–resolved spectra of a white dwarf of $T_{wd} = 17\,000$ K with a hot spot of $T_{cent} = 40\,000$ K; $i = 50°$ and $\beta = 45°$. The integrated spectra are shown for the six phases displayed above.

dependent mass flow rate made out of single dense chunks. A simple simulation of the expected X–ray light curves of this so–called *blobby accretion* was computed by Hameury & King (1988). However, a self–consistent numerical treatment of the time–dependent radiation transfer of these buried shocks has not been carried out so far.

The overall spectrum of a polar will, therefore, depend on the spectrum of mass flow rates hitting the white dwarf. Observational evidence underlines that the accretion stream has in fact a structured density cross–section with the *local* mass flow rates varying over several orders of magnitude (Rousseau et al. 1996). Additionally, at any given point within the accretion spot,

the mean flow rates may be highly time dependant with substantial fluctuation observed down to $100\,\mu$s.

With the standard model outlined above in mind, it is clear that for moderate mass flow rates the hot post–shock plasma will still irradiate the white dwarf surface with thermal bremsstrahlung and cyclotron radiation. The question I will try to answer in this chapter is

from which part of the stellar surface and at
which wavelengths is the reprocessed radiation emitted?

Apparently, the *size* and the *shape* of the irradiated region on the white dwarf strongly depend on the geometry of the accretion column: for low accretion rates and low magnetic fields the shock can stand high ($\sim 0.1 R_{\rm wd}$) above the white dwarf surface (Beuermann & Woelk 1996); thermal bremsstrahlung and cyclotron radiation will cover a substantial fraction of the white dwarf surface. This is the case for the low–density regions in the structured accretion flow as well as for the low state in polars, where accretion is reduced to a trickle. If the magnetic field lines are not perpendicular to the white dwarf surface, the cyclotron radiation beamed $\sim 90°$ to the field line will preferably irradiate a spot offset from the foot point of the accretion column. The exact geometry depends on the inclination of the magnetic field line relative to the radial direction.

Summarized, it seems plausible that, for certain accretion parameters, a large spot can be heated to moderate temperatures by irradiation with thermal bremsstrahlung and cyclotron radiation. Fig. 3.4 exemplifies the expected observational consequence of such a large, heated spot. I represent the white dwarf surface with a fine grid of several 1000 elements; each surface element can be assigned an effective temperature and a corresponding white dwarf model spectrum[2]. The stellar spectrum is then obtained by integrating the flux at each wavelength over the visible hemisphere. For the sake of simplicity, I chose a circular spot with a radius $R_{\rm spot}$ and with the temperature decreasing linearly from the central value $T_{\rm cent}$ until meeting the temperature of the underlying white dwarf $T_{\rm wd}$ at $R_{\rm spot}$. The center of the spot is offset from the rotational axis by an angle β. As the hot spot rotates out of sight, the flux level decreases and the photospheric Lyα absorption profile becomes broader. In a zero–order approximation this fact can be considered as a decrease of the *average* temperature over the visible hemisphere, an approach which will be used in the data anlysis below (Sect. 3.5). At the orbital phase displayed in Fig. 3.4(d), the spot is *self–eclipsed* by the white dwarf, a situation which is found in several AM Her stars, as e.g. in ST LMi, allowing in principle a very reliable measurement of the white dwarf photospheric temperature.

Even though I will concentrate in the present work on the observational and theoretical implications of the locally confined accretion–induced heating, I would like to comment on the

---

[2] Unless noted otherwise, I use throughout this chapter non–magnetic pure–hydrogen line–blanketed model atmospheres computed with a standard fully frequency and angle dependent plane–parallel LTE atmosphere code. Opacities included were bound–free and free–free transitions of hydrogen; Paschen, Balmer and Lyman line blanketing; and Thomson scattering. Stark–broadening was treated according to Vidal et al. (1973). The code is described in full detail in Gänsicke (1993).

following point: the accreted matter will enrich the white dwarf atmosphere at the footpoint of the accretion column with heavy elements. The material is coupled to the magnetic field lines and, therefore, will sink into the white dwarf atmosphere until the gas pressure exceeds the magnetic pressure.

For field strengths of $10 - 100\,\text{MG}$ this occurs at geometrical depths of $\sim 20 - 50\,\text{km}$ which corresponds to very large optical depths. Hence, it seems likely that the white dwarfs in polars show low metal abundances, in contrast to their non–magnetic relatives in dwarf novae (see Chapter 4).

3.3 High states and low states

At irregular intervals, the accretion rate in polars decreases to a trickle. This on/off behaviour is known to occur in many systems (e.g. V834 Cen; MR Ser; BY Cam) but observational details are known only for AM Herculis itself, as it is the only system bright enough to be accessible to regular observations with small telescopes, e.g. by observers of the AAVSO (Fig. 3.5). The system reaches maximally $V \simeq 12.5$ and can fade down to $V \simeq 15$. In the bright state, the *high state*, most optical emission originates in the accretion stream. During the *low state*, the light from the system is dominated in the blue by the white dwarf and in the red by the secondary star (see e.g. Fig 3.10). The absence of an accretion disc is reflected in the small amplitude of the high–to–low state variations of $\simeq 3$ mag. In dwarf novae (see Sect. 4.1.2), the brightening of the large accretion disc during outburst easily raises the luminosity of the system by 5 magnitudes[3].

The light curve of AM Her shows that changes in brightness (=accretion rate) can occur on a wide variety of timescales: the system can drop into the low state in a couple of days (e.g. $\text{HJD} = 2\,447\,650$), but can also gradually fade (e.g. $\text{HJD} = 2\,448\,350$). On some occasions a sudden brightening occurred (e.g. $\text{HJD} = 2\,448\,900$), reminiscent of dwarf nova outbursts, although the mechanism must be of completely different nature. Similarly, short drops in brightness are observed (e.g. $\text{HJD} = 2\,449\,130$). The origin of this long–term variation is still not understood. Even though claimed several times (e.g. Götz 1993), there is no convincing evidence for a periodicity in the long–term light curve of AM Her. Basically, two mechanisms have been proposed so far to explain the changes in brightness. (a) The strong soft X–ray and ultraviolet radiation from the accreting white dwarf may lead through irradiation of the secondary to instabilities in the mass loss rate (King 1989). (b) Star spots may form on the secondary in the L_1 point yielding a locally decreased scale height of the photosphere and, hence, a reduced mass loss rate (Livio & Pringle 1994). However, no detailed modelling of the long–term light curve has been done so far.

As evident from Fig. 3.5, the polar caps of the white dwarfs in AM Her systems are heated

---

[3]It is important to notice that the changes in brightness in polars reflect *directly* a variation of the mass loss rate of the secondary star. In dwarf novae, the matter lost from the secondary is buffered in the accretion disc. During an outburst only a small percentage of the stored matter flows onto the white dwarf. Hence, in dwarf novae every fluctuation in the mass loss rate of the secondary will be largely smoothed out.

by accretion over long periods of time (years). It is, therefore, imaginable that the white dwarf atmosphere is heated to great depth, resulting in an afterglow during the low states. The observational evidences for such a deep heating will be discussed below.

3.4 Observational status

Until recently, temperatures of white dwarfs in polars were published only for a handful of systems; even rarer are reports of an inhomogenous temperature distribution over the white dwarf surface. The main reasons for this scarcity are:

(a) In the easily accessible optical wavelength band, the white dwarf photospheric emission is often diluted by cyclotron radiation and by emission from the secondary star and from the accretion stream. Even when the accretion switches off almost totally and the white dwarf becomes a significant source of the optical flux (e.g. Schmidt et al. 1981; Schwope et al. 1993b), the complex structure of the Zeeman–splitted Balmer lines and remnant cyclotron emission complicate a reliable temperature determination.

(b) The most promising wavelength region to derive the effective temperature of the white dwarf is the far ultraviolet, including the photospheric Lyα absorption profile. During a low state, the white dwarf/its heated pole cap are the only noticeable sources of ultraviolet emission; also during the high state they contribute a significant part to the flux at $\lambda \lesssim 1500$. However, due to the relative faintness of polars, observations with the *International Ultraviolet Explorer (IUE)* resulted in most cases in orbitally averaged spectroscopy of modest signal–to–noise ratio (S/N).

I have summarized in Table 3.1 the white dwarf temperatures published so far. These temperatures have been derived from ultraviolet and optical spectroscopy, from eclipse light curves or simply from observed *V* magnitudes and distance estimates. I include in the table a flag which gives my own judgment of the goodness of the temperature estimate, with A being the best and C being mediocre.

In the sections 3.5 and 3.6 I will present the results of my project to improve the temperature scale of white dwarf temperatures in polars. The analysis is examplified for the case of AM Her, by far the brightest member of its class, with the largest body of data.

System	alternative name	P_{orb}[min]	T_{wd}[K]	T_{spot}[K]	Quality	Ref.
RX J1015+09		80	10 000		C	1
DP Leo[a]	E 1114+182	90	16 000	50 000	A/B	2
VV Pup		100	9000		C	3
V834 Cen[b]	E 1405−451	102	12 000		B	4
			26 500		C	5
			15 000 − 20 000	50 000	B	6
			15 000	30 000	A	7
V2301 Oph	1H 1752+081	113	27 500		C	8
BL Hyi	H 0139−68	114	13 000		C	9
			20 000		C	10
ST LMi	CW 1103+254	114	12 000 − 25 000		C	11
			12 000 − 30 000		C	12
			11 500		C	13
			13 400		C	14
			$\geq 13 000$	$\geq 30 000$	C	15
MR Ser	PG 1550+191	114	9000		C	16
			8500 − 10 000		C	17
			20 000		C	18
AN UMa		115	20 000		C	18
HU Aqr	RX J2107.9−0518	125	$< 13 000$		C	19
UZ For	EXO 033319−2554.2	127	20 000		B	20
			11 000		C	21
			18 000 − 20 000	30 000	B	22
QS Tel	RE J1938−461	140	20 000		B	23
			20 000	45 000	B	24
AM Her[c]	3U 1809+50	186	50 000		C	25
			13 000 − 20 000		B	26
			20 000		A	27
BY Cam[d]	H 0538+608	202	$> 70 000$		C	28
V1432 Aql	RX J1940.2−1025	204	15 000 − 20 000		C	29
V1500 Cyg	Nova Cyg 1975	201	70 000 − 120 000		C	30
V1309 Ori	RX J0515.6+0105	480	20 000		C	8

[a] Sect. 3.6.3; [b] Sect. 3.6.2; [c] Sect. 3.5; [d] Sect. 3.6.1

Table 3.1: Published temperatures of white dwarfs in polars.

Table 3.1 continued

I include a "quality" flag for the temperatures as defined below. For details, see the references given below.

(A) very reliable temperature derived from fits with model spectra to Lyα and/or other absorption lines. E.g. AM Her

(B) good estimate, but may still be wrong by many 1000K. Overall UV & optical continuum as well as distance estimates are consistent with the WD fit. E.g. QS Tel.

(C) Rough estimate only. T_{wd} may not be consistent over large wavelength ranges; T_{wd} may disagree with the distance/no distance known; T_{wd} superseded by better value. E.g. AN UMa

[1]Burwitz et al. 1997b; [2]Stockman et al. 1994; [3]Liebert et al. 1978; [4]Puchnarewicz et al. 1990; [5]Maraschi et al. 1984; [6]Ferrario et al. 1992; [7]Schwope 1990; [8]Szkody & Silber 1996; [9]Schwope et al. 1995; [10]Wickramasinghe et al. 1984; [11]Schmidt et al. 1983; [12]Bailey et al. 1985; [13]Mukai & Charles 1986; [14]Szkody et al. 1985; [15]Stockman & Schmidt 1996; [16]Mukai & Charles 1986; [17]Schwope et al. 1993b; [18]Szkody et al. 1988; [19]Glenn et al. 1994; [20]Beuermann et al. 1988; [21]Bailey & Cropper 1991; [22]Stockman & Schmidt 1996; [23]de Martino et al. 1995; [24]de Martino et al. 1995; [25]Szkody et al. 1982; [26]Schmidt et al. 1981; [27]Heise & Verbunt 1988 [28]Szkody et al. 1990; [29]Friedrich et al. 1996; [30]Schmidt et al. 1995;

3.5   AM Herculis

3.5.1   Introduction

Observationally, AM Her ($P_{\mathrm{orb}} = 107\,\mathrm{min}$) is characterized by a soft X–ray flux much in excess of what is expected from the original reprocessing model (Rothschild et al. 1981; Heise et al. 1985; van Teeseling et al. 1994; Paerels et al. 1994), a classical case of the *soft X–ray puzzle* described in Sect. 3.2. Measurements of the soft X–ray temperature suggested that the ultraviolet flux in AM Her does not represent the Rayleigh–Jeans tail of the blackbody component. Furthermore, the ultraviolet flux always originates from the main hard X–ray emitting pole; the occasional soft X–ray emission from the second pole (reversed mode) is not associated with additional ultraviolet emission (Heise & Verbunt 1988).

An earlier version of this section has been published in Gänsicke et al. (1995).

3.5.2   Observations

3.5.2.1   Low state

Three ultraviolet spectra of AM Her were taken on 21 September 1990 with the Short Wave Prime Camera (SWP) onboard of *IUE*[4] in the framework of the *ROSAT IUE All Sky Survey* (RIASS) program. At this time, AM Her was in a sustained low state for approximately 150 days (Fig. 3.5). The exposure times ranged from 35 to 70 minutes. All spectra were taken in the low–resolution mode of *IUE* and through the large aperture, resulting in a spectral resolution of $\sim 6\,\text{Å}$.

I complemented these data by all available low–state spectra from the *IUE* archive (Table 3.2). Several of these spectra were surprisingly low in the overall flux level. After reprocessing with the most recent *IUESIPS* software and critical inspection of the observation log, some of the spectra were rejected because of non–reconstructable flux losses.

The June 1992 spectra are of very low S/N ratio due to short exposure times; the continuum shows strong wiggles, probably related to a high background signal as *IUE* was located in the radiation belt during the observation. The complete set of analysed data consists of 20 SWP low–state spectra.

The simultaneous *IUE/ROSAT* observations of AM Her in September 1990 show the system without a noticeable soft X–ray component. The mean orbital *ROSAT PSPC*[5] count rate was $0.135 \pm 0.051\,\mathrm{cts\ s^{-1}}$, corresponding to a $0.1 - 2.4\,\mathrm{keV}$ energy flux of $1.3 \times 10^{-12}\,\mathrm{erg\ cm^{-2}s^{-1}}$. For an assumed 20 keV thermal bremsstrahlung spectrum, the total X–ray flux integrated over all energies is $6.1 \times 10^{-12}\,\mathrm{erg\ cm^{-2}s^{-1}}$. At orbital maximum, both values are higher by a factor

---

[4]For a description of the satellite see Boggess et al. (1978)

[5]*Position Sensitive Proportional Counter*

of ~ 1.3. This continued X–ray emission indicates that accretion did not cease completely in this low state. This may be a general feature of AM Her, as suggested by the fact that the system was never observed in a complete off–state, i.e. without X–ray emission. During a pointed *ROSAT* observation in September 1991, it was encountered at a level of $0.6\,\text{cts s}^{-1}(0.1–2.4\,\text{keV})$ and in three *EXOSAT* observations on 3 November 1983, 8 March 1984, and 30 May 1984 at LE count rates of $0.035\,\text{cts s}^{-1}$, $0.012\,\text{cts s}^{-1}$and $0.030\,\text{cts s}^{-1}$, respectively (Heise 1987, private communication). During all these observations, AM Her was in its normal mode accreting at the main pole.

Fig. 3.8, below, shows the *ROSAT PSPC* light curve of the September 1990 low state together with all the *IUE* low–state data from five different epochs.

3.5.2.2   High state

Twelve high–state SWP spectra of AM Her were obtained on 12/13 April 1991 (Table 3.3), all with exposure times of 25 minutes. This is so far the most complete and homogeneous dataset of a single high state. A quasi–simultaneous *ROSAT* pointing showed AM Her in its normal mode with a soft X–ray spectrum and a mean bright–phase count rate of $\sim 130\,\text{cts s}^{-1}(0.1–2.4\,\text{keV})$. The simultaneous *IUE* data and *ROSAT* hard X–ray data $(0.5 - 2.4\,\text{keV})$ are displayed in Fig. 3.9 below.

3.5.3   Analysis

3.5.3.1   Orbital flux variation

I considered all spectra in Tables 1 and 2 which are labeled with the quality signatures '+' or 'o'. Magnetic phase convention and the ephemeris of Heise & Verbunt (1988) were used:

$$\text{HJD}(\phi_{\text{mag}} = 0) = 244\,3014.76614(4) + 0.128927041(5)\text{E} \tag{3.3}$$

where $\phi_{\text{mag}} = 0$ is defined by the middle of the linear polarization pulse, i.e. when the line of sight is closest to perpendicular to the accretion column. The phases quoted in Tables 1 and 2 refer to mid exposure. In both, the high and the low state, the orbital X–ray and ultraviolet light curves (Figs. 3.8 and 3.9) show maxima at $\phi_{\text{mag}} \simeq 0.6$ when the main accreting pole is facing the observer most directly and minima at $\phi_{\text{mag}} \simeq 0.1$ when the line of sight is almost perpendicular to the magnetic field (Cropper 1988). The dashed curves were determined by fitting sinusoidals to the ultraviolet light curves. The error bars of the ultraviolet fluxes in Figs. 3.8(b) and 3.9(b) are of purely systematic nature, representing an adopted 10% uncertainty in the overall flux calibration. The formal statistical error, computed as the ratio of the mean flux deviation in the interval 1420–1500 Å to the square root of the number of bins in that interval, turned out to be negligibly small.

Frame No.	Obs. date	ϕ_{mag}	Δ_ϕ	Quality
SWP 9343L	22 Jun 1980	0.69	0.49	$+^{1)}$
SWP 9403L	30 Jun 1980	0.77	0.32	$-^{2)}$
SWP 9404L	30 Jun 1980	0.39	0.32	$+$
SWP 9405L	30 Jun 1980	0.03	0.32	$-^{2)}$
SWP 9406L	30 Jun 1980	0.69	0.32	$-^{2)}$
SWP10235L	28 Sep 1980	0.68	0.22	$-^{6)}$
SWP10236L	28 Sep 1980	0.45 / 0.23	0.22 / 0.22	$+^{4)}$
SWP21437L	03 Nov 1983	0.34 / 0.12	0.06 / 0.11	$-^{5)}$
SWP21438L	03 Nov 1983	0.42 / 0.52	0.06 / 0.11	$-^{5)}$
SWP21439L	03 Nov 1983	0.94	0.16	$+^{1)}$
SWP21440L	03 Nov 1983	0.46	0.53	$+^{1)}$
SWP21441L	03 Nov 1983	0.08	0.21	$+^{1)}$
SWP39670L	21 Sep 1990	0.61	0.19	$+$
SWP39671L	21 Sep 1990	0.12	0.38	$+$
SWP39672L	21 Sep 1990	0.70	0.32	$+$
SWP44841L	03 Jun 1992	0.97	0.15	$o^{3)}$
SWP44842L	03 Jun 1992	0.31	0.15	$o^{3)}$
SWP44843L	03 Jun 1992	0.60	0.15	$o^{3)}$
SWP44844L	03 Jun 1992	0.87	0.15	$o^{3)}$
SWP44845L	03 Jun 1992	0.15	0.16	$o^{3)}$
SWP44846L	03 Jun 1992	0.43	0.15	$o^{3)}$
SWP44847L	03 Jun 1992	0.71	0.16	$o^{3)}$
SWP44848L	03 Jun 1992	1.00	0.16	$o^{3)}$
SWP44849L	03 Jun 1992	0.27	0.15	$o^{3)}$
SWP44850L	03 Jun 1992	0.54	0.14	$o^{1,3)}$

$+$: data considered reliable

o: data has to be used with care

$-$: data severely harmed, useless

[1] Additional cosmics identified

[2] Bad centering, target partially out of aperture

[3] Low S/N exposures

[4] Double exposure

[5] Uncertain location in aperture, two segments

[6] Flux has been lost

Table 3.2: *IUE* low–state observations of AM Her. Listed are the *IUE* frame number, the observation date, the orbital phase at the middle of the observation, the phase interval of the exposure and the quality of the data determined from the raw two–dimensional data.
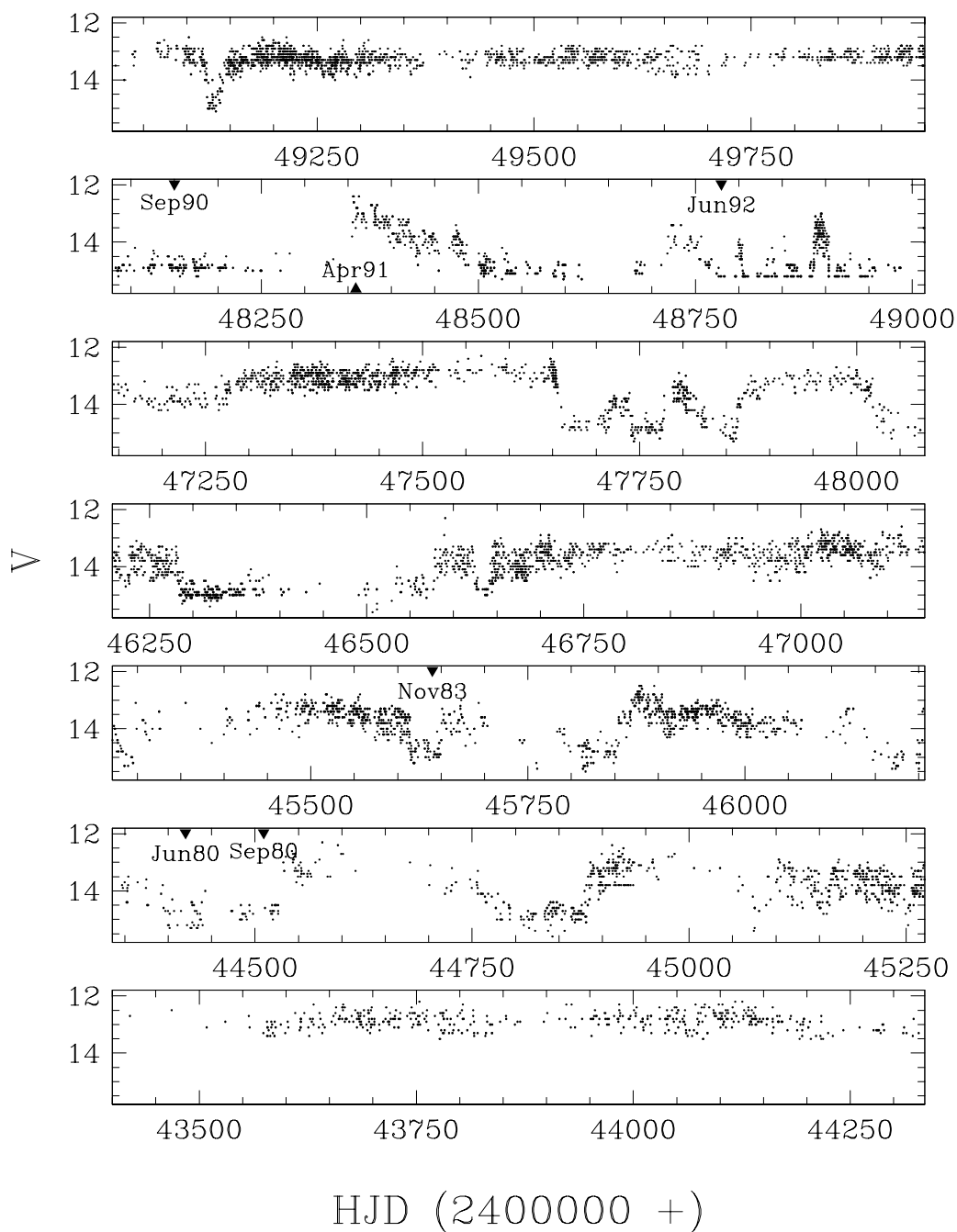
Figure 3.5: Long–term optical light curve of AM Her. The times of the *IUE* observations used in this work are indicated by triangles. The optical data shown here have been kindly provided by J. Mattei

Frame No.	Obs. date	ϕ_{mag}	Δ_ϕ	Quality
SWP41358L	12 Apr 1991	0.79	0.135	+
SWP41359L	12 Apr 1991	0.12	0.135	+
SWP41360L	12 Apr 1991	0.59	0.135	+
SWP41361L	12 Apr 1991	0.96	0.135	+
SWP41362L	12 Apr 1991	0.26	0.135	+
SWP41363L	12 Apr 1991	0.55	0.135	+
SWP41367L	13 Apr 1991	0.38	0.135	+
SWP41368L	13 Apr 1991	0.74	0.135	+
SWP41369L	13 Apr 1991	0.04	0.135	+
SWP41370L	13 Apr 1991	0.43	0.135	+
SWP41371L	13 Apr 1991	0.73	0.135	+
SWP41372L	13 Apr 1991	0.12	0.135	+

Table 3.3: *IUE* high–state observations of AM Her. Listed are the *IUE* frame number, the observation date, the orbital phase at the middle of the observation, the phase interval of the exposure and a quality flag as defined in Table 3.2.

3.5.3.2 Orbital temperature variation

Along with the flux variation, a phase–dependent change of the spectral shape can be found in the *IUE* data, indicating a non–uniform temperature distribution over the emitting surface both, in the low and in the high state. An intuitive model is that of a rotating white dwarf with an accretion–heated pole cap, as shown in Fig. 3.4. In principle, spectral fits with that model to the phase–resolved observations can reveal details of the temperature distribution. In reality, however, even the representation of this temperature distribution by a simplified two–component model with a lower temperature T_{wd} of the underlying white dwarf and a higher temperature T_{spot} of the heated pole cap meets with difficulties: the limited accuracy of the data does not permit a unique solution.

I decided, therefore, to represent the individual spectra by two parameters, a mean effective temperature and a solid angle $(R/d)^2$. The resulting parameters will then be a function of the orbital phase and have to be interpreted as a *flux–weighted mean temperature* and *mean source radius* of the emitting surface $A = \pi R^2$ at a given distance d. I adopted a distance of $90\,\mathrm{pc}$ (Sect. 3.5.4.1) and a surface gravity of $\log g = 8$, equivalent to a $0.6\,M_\odot$ white dwarf (Hamada & Salpeter 1961).

Fitting *IUE* observations of single white dwarfs with model spectra has been applied with remarkable success to both the ultraviolet continuum (Finley et al. 1990) and to the Lyα absorption profile (Holberg et al. 1986). A detailed description of these methods as well as a discussion of the problems arising from uncertainties in the *IUE* flux calibration and the degradation of the cameras can be found in these references. As there are few SWP and LWP/R[6]

---

[6]LWP = Long Wave Prime camera; LWR = Long Wave Redundant camera
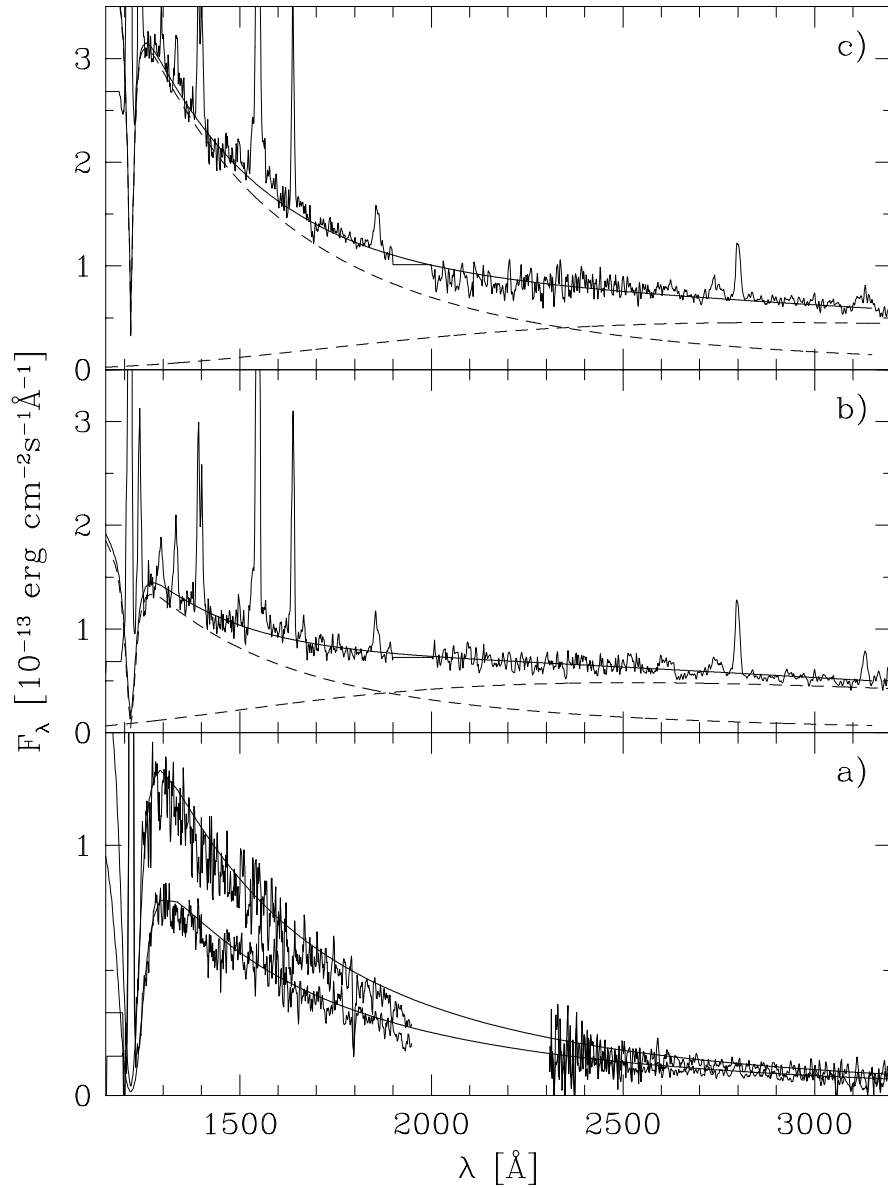
Figure 3.6: The ultraviolet spectrum of AM Herculis during the low state and the high state. *Upper two panels:* average high–state spectra for orbital maximum (c) and orbital minimum (b). The spectra can be described by the sum of a white dwarf model atmosphere and a blackbody which approximates the contribution of the accretion stream. *Lower panel:* low–state spectra at orbital maximum and orbital minimum along with the best–fit white dwarf models. See Fig. 3.7 for an enlarged display of the Lyα region.

spectra of AM Her which agree in phase, I decided to fit only the observed Lyα profile and the maximum flux in order to determine the temperature and the solid angle, respectively. The usable wavelength range is restricted to the red wing of Lyα, as the core is blended by geocoro-
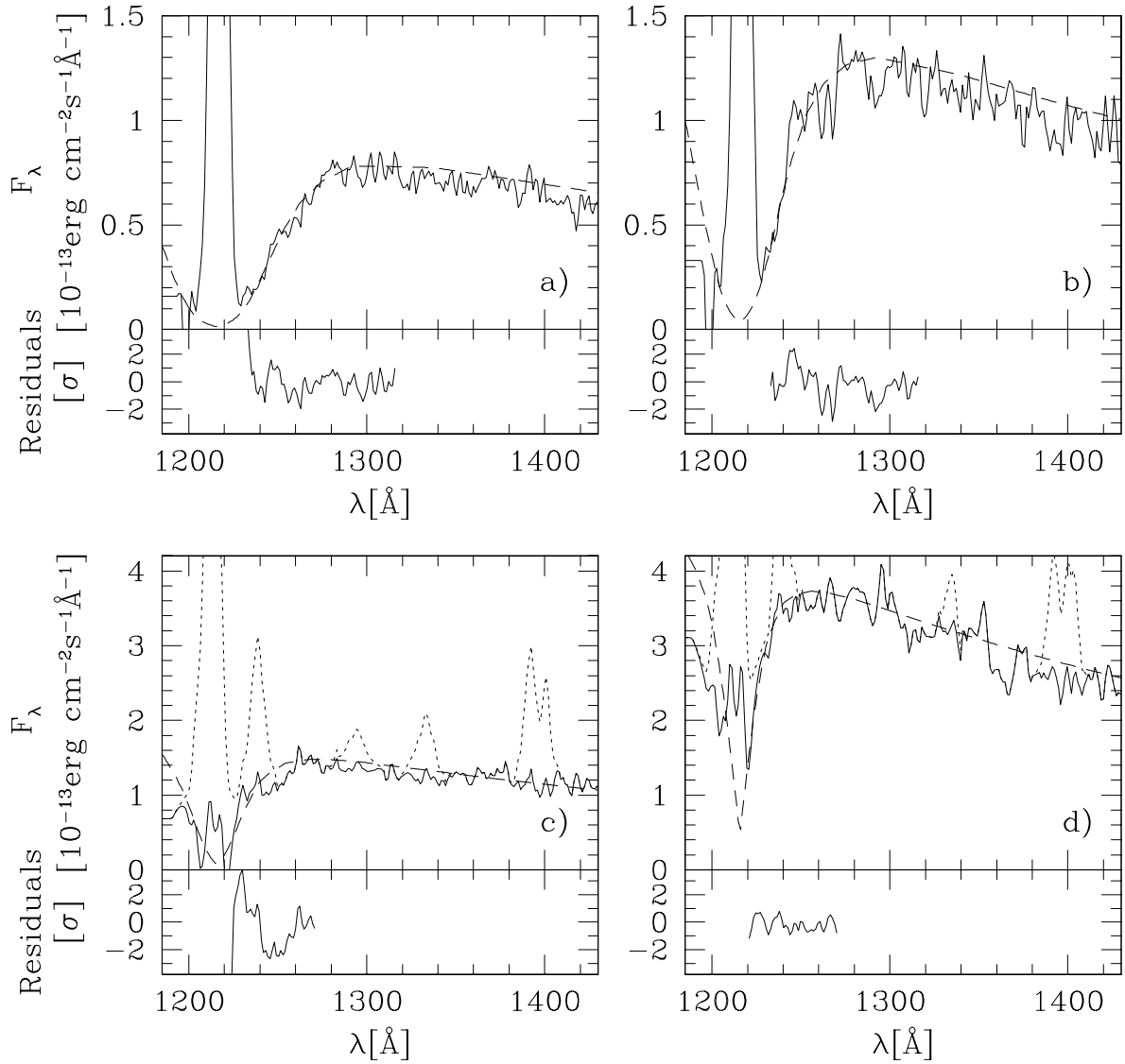
Figure 3.7: Selected *IUE* spectra of AM Herculis. *Top two panels:* low–state orbital minimum (a: SWP39671L) and maximum (b: SWP39670L). *Bottom two panels:* high–state orbital minimum (c: average of SWP41359L, SWP41362L and SWP41372L) and maximum (d: SWP41363L). The original observed high–state data are shown as dotted lines; the solid curves represent the spectra after subtraction of the emission lines. The best–fit white dwarf model spectra are shown as dashed lines, with effective temperatures 20 000 K (a), 23 000 K (b), 28 000 K (c) and 35 000 K (d)

ϕ_{mag}	N v 1240 Å	Si iv 1393 Å	1403 Å	C iv 1550 Å	He ii 1640 Å
0.08	15.7	10.0	8.3	68.9	17.2
0.25	9.6	12.2	7.6	57.3	13.5
0.38	7.6	3.2	6.5	33.8	11.2
0.42	5.8	3.2	7.2	34.3	10.5
0.55	3.3	3.8	6.1	29.4	6.6
0.59	4.2	4.6	6.8	37.4	8.9
0.75	5.5	4.0	6.8	36.2	9.5
0.95	12.0	11.1	11.8	54.2	14.4
mean	6.9	6.5	7.2	43.9	11.5

Table 3.4: Equivalent widths (Å) of the high–state emission lines.

nal emission and the sensitivity of the SWP camera is too low shortward of 1200 Å to provide reliable flux measurements.

The low–state spectra (Fig. 3.6) are as a whole compatible with my white dwarf models with no obvious additional radiation component. The high–state spectra of AM Her can be described by the sum of three components:

(1) The SWP spectra are dominated by high–excitation emission lines of N v λ 1240, Si iii λ 1300, C ii λ 1335, Si iv λλ 1393, 1403, C iv λ 1550 and He ii λ 1640, due to photoionization of the cold material in the accretion stream. In order to analyse the high–state data, the emission lines were fitted with Gaussians and subtracted from the spectrum (Fig. 3.7).

(2) A significant contribution to the continuum flux is present in the LWP range, which is almost independent of the orbital phase and which I ascribe to emission from the accretion stream. It can be represented by a blackbody of 10 000 K, ($\phi_{mag} = 0.6$) and 11 500 K, ($\phi_{mag} = 0.1$). The implied optical fluxes are consistent with quasi–simultaneous photometry (Beuermann et al. 1991b).

(3) The (heated) white dwarf dominates the continuum shortward of ~ 1400 Å, justifying the fit of white dwarf model spectra to the observed Lyα profile. Fig. 3.6 shows the fits to the two continuum components.

Strong irradiation of an atmospheres by hard X–rays may result in a temperature inversion (van Teeseling et al. 1994). Part of the emission lines could, therefore, be of photospheric/chromospheric origin. Inspection of the best–exposed high–resolution spectrum SWP25330 reveals a possible sharp (FWHM $\simeq 1.5$ Å) component of N v λ 1240 which, however, is contaminated by a hot pixel. Narrow components in *IUE* high–resolution spectra have also been reported by Raymond et al. (1979) for Si iv λλ 1393, 1403, C iv λ 1550 and He ii λ 1640, but in the spectrum SWP25330 these lines are broad with FWHM $\simeq 3.0$ Å, 4.6 Å,

5.6 Å and 3.0 Å, respectively. The equivalent widths of the strong lines N v, C iv and He ii measured from the low–resolution data set (Table 3.4) show a maximum at $\phi_{\mathrm{mag}} \simeq 0.1$ when the accreting pole is partially self–eclipsed and the projected area of the stream is maximal. Concluding, I remark that the observations are compatible with the bulk of the emission lines originating in the accretion stream but I cannot exclude additional narrow photospheric components. The quality of the available high–resolution spectra does not permit a definitive answer to overcome this uncertainty, making it a project worthy of the capabilities of the *Hubble Space Telescopy* (*HST*).

The results for the low–state and high–state data are summarized in Fig. 3.8 and Fig. 3.9, respectively, where the solid angle is represented by the equivalent radius *R* of a circular emitting disk at $d = 90$ pc. Figs. 3.6 and 3.7 show selected *IUE* spectra of AM Her along with the best–fit models.

3.5.3.3 Errors and uncertainties

Error analysis: I used χ^2 minimization to determine the best–fit models, considering only the statistical flux errors. For this purpose, each individual spectrum was filtered with a broad ($\sigma \sim 30$ Å) Gaussian in the interval 1400–1900 Å. In the absence of significant features in the continuum, this results in a smooth average spectrum. The deviations of the observed flux from that mean curve were plotted in an amplitude histogram. As expected for purely statistical noise, this histogram had a Gaussian shape and the mean flux error is then given by the standard deviation of this Gaussian. The values for the reduced χ^2 of the model fits to the *IUE* spectra ranged from 1.5 to 4.5 for 33 to 75 degrees of freedom. These rather large values are not surprising as my one–temperature pure–hydrogen model spectra may not be the adequate description for the photosphere of AM Her. However, Holberg et al. (1985) find that also fitting single (and, hence, undisturbed) DA white dwarfs can result in rather large values for the reduced χ^2, indicating that additional uncertainties exist outside the model atmospheres.

Surface gravity: The width of the Lyα absorption line increases with atmospheric pressure and, hence, with higher surface gravity. It decreases with rising effective temperature due to a higher degree of ionization. The suggested white dwarf masses of AM Her, $\simeq 0.4\,M_\odot$ (Young & Schneider 1981a) to $\simeq 0.9\,M_\odot$ (Sion 1991), correspond to $\log g \simeq 7.5$ to 8.5, which yield temperatures higher ($\log g = 8.5$) or lower ($\log g = 7.5$) by $\sim 1000 - 2000$ K. The principle shape of the orbital temperature variation remains unaffected.

Zeeman–broadening: In non–magnetic white dwarf atmospheres, the hydrogen lines are pressure–broadened by the linear Stark effect. Since the white dwarf in AM Her is magnetic, the additional broadening by the Zeeman effect should be taken into account (Szkody et al. 1982). At a field strength of $B = 14.5$ MG (Bailey et al. 1991), Lyα is still in the regime of the linear Zeeman effect (Wunner 1987). Hence, the separation of the σ^+ and σ^- components from the central π component is given by

$$\Delta\lambda = \frac{e}{4\pi m_e c^2}\lambda^2 B \qquad (3.4)$$
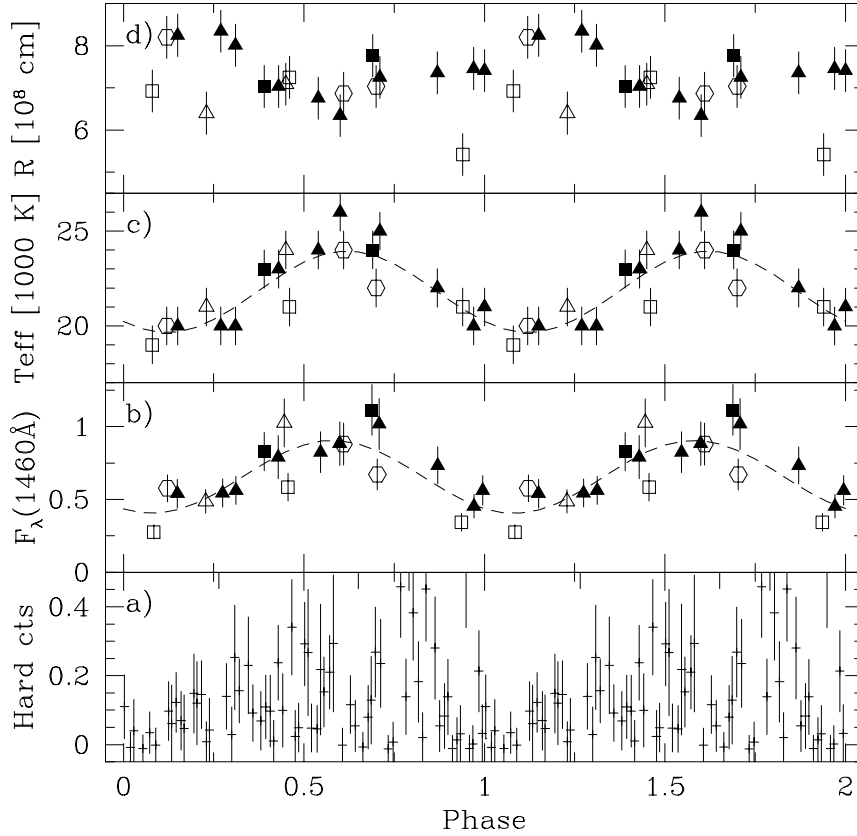
Figure 3.8: AM Her in low state. (a) Hard X–ray light curve (0.5–2.4 keV) from the *ROSAT* all sky survey. (b) *IUE* light curve of AM Her for several low states: (■), Sept. 1980 (△), Nov. 1983 (□), Sept. 1990 (○) and June 1992 (▲). The flux is given in $10^{-13} \mathrm{erg\, cm^{-2} s^{-1} \mathring{A}^{-1}}$, averaged over the interval 1420–1500 Å. (c) Effective temperatures derived from fitting white dwarf models to the observed Lyα profile. (d) Radius of the emitting area at $d = 90$ pc. Magnetic phases (eq. 3.3) are used.

For AM Her, $\Delta\lambda \simeq 10\,\mathring{A}$. This value can be considered as an upper limit for the additional magnetic broadening as the Stark broadening of each single Zeeman component is reduced substantially in the presence of a magnetic field (Jordan 1992). In order to investigate the importance of this effect, I simulated the additional broadening by shifting the Lyα profiles of my models 10 Å redwards, thereby assuming that only the width of the profile increases while its shape stays unchanged. Fitting the observed Lyα absorption with these models led to a similar orbital temperature variation as shown in Fig. 3.8, but with a slightly higher ($\sim$ 1000 K) amplitude and higher mean value ($\sim$ 2500 K). Hence, the systematic error in the derived temperatures due to the neglect of the Zeeman effect is likely to be $\leq 10\%$.

Limb darkening: The white dwarf model spectra used for the spectral fits are angle–averaged over the whole stellar surface. As the viewing angle of the accretion region changes with or-
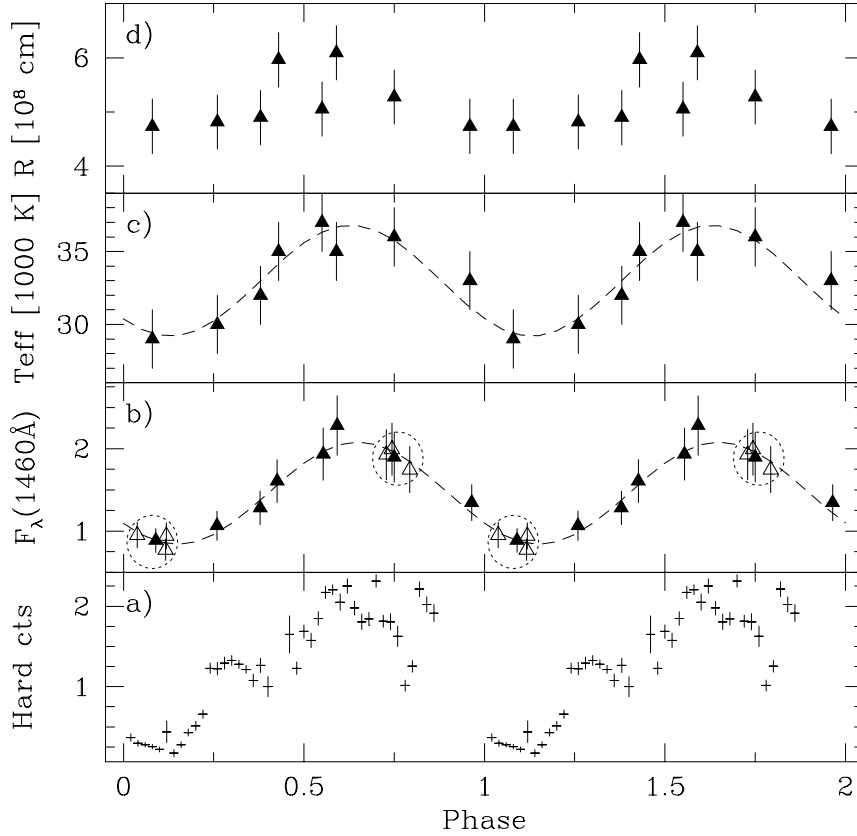
Figure 3.9: AM Her in high state, April 1991. (a) Hard X–ray light curve (0.5–2.4 keV) from pointed *ROSAT* observations. (b) Ultraviolet flux in $10^{-13}\,\mathrm{erg\,cm^{-2}s^{-1}\mathring{A}^{-1}}$. At $\phi_{\mathrm{mag}} \sim 0.1$ and $\phi_{\mathrm{mag}} \sim 0.75$, I have averaged three spectra each (open triangles) to obtain a higher S/N ratio. The co–added spectra (filled triangles) were then used in the further analysis. Panels (c) and (d) as in Fig. 3.8. Magnetic phases (eq. 3.3) are used.

bital phase, limb darkening may affect the emitted spectrum. However, spectra calculated for individual directions do not show a strong dependence of the Lyα line profile on viewing angle. The reason is that the Lyα profile is formed primarily in the outermost layers of the atmosphere where the temperature in LTE models is constant. I think, therefore, that limb darkening does not cause serious errors in the derived parameters.

Irradiation of the atmosphere: Below, I interpret the observed temperature variation by irradiation of part of the white dwarf with cyclotron (and bremsstrahlung) photons. Heating would cause a flatter temperature gradient in the atmosphere and a narrower Lyα profile. The derived temperatures may, therefore, be on the high side. In the absence of appropriate calculations it is difficult to quantify this effect.
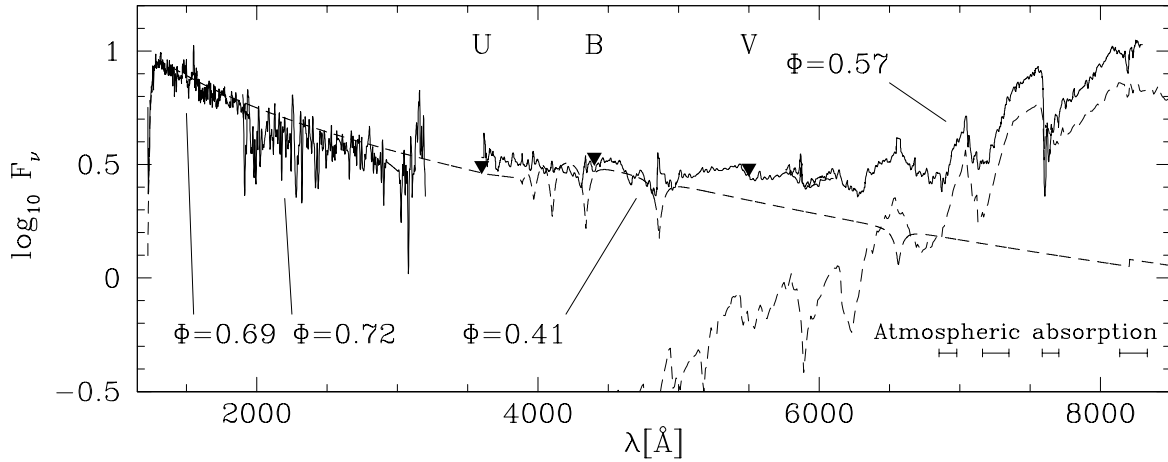
Figure 3.10: Ultraviolet and optical flux distribution of AM Her. Shown are the *IUE* spectra (SWP9343L, LWR8153L of June 22 and 30, 1980) and two optical spectra from Schmidt et al. (1981) (July 18–20, 1980). All spectra were taken near orbital (ultraviolet) maximum. Magnetic phases are indicated. Dashed: best–fit white dwarf model ($T_{\text{eff}} = 24\,000$ K), dM4–spectrum (GL273).

3.5.4 Results

3.5.4.1 The distance of AM Her

The distance of AM Her is an essential parameter in the interpretation of the observations. Previous estimates range from 71 ± 18 pc (Young & Schneider 1981b) to $108 \pm {}^{41}_{28}$ pc (Dahn et al. 1982). I reexamined the distance of AM Her using the K–band surface–brightness method of Bailey (1981), updated by Ramseyer (1994). The optical spectrum of AM Her in quiescence taken by Schmidt et al. (1981) can be described by the sum of the white dwarf and the late–type M–dwarf (Fig. 3.10). I scaled the red part of their spectrum down by a factor of 0.9 which is within the quoted uncertainty and is necessary for consistency with the blue part and with the low–state photometry of Szkody et al. (1982). After subtracting the (non–magnetic) white dwarf model the residual spectrum is consistent with that of a late M dwarf without any additional contribution from cyclotron emission (at $\lambda \leq 8000$ Å). Using a sequence of M–star spectra, I find that this spectrum is best fitted by a dM4+ (in the system of Boeshaar 1976) star within an uncertainty of 0.25 spectral classes, consistent with the spectral classification of Young & Schneider (1981b). This fit yields $R_J = 15.23 \pm 0.10$. With $R_J - K = 3.38 \pm 0.13$ for the adopted spectral type, I find $K = 11.86 \pm 0.17$ which agrees with $K = 11.83$ as derived by Bailey et al. (1988). The radius of the secondary star in AM Her, R_2, is given by Roche geometry (Patterson 1984): With the orbital period in units of four hours, $P_{4h} = 0.774$, the resulting radius is $R_2/R_\odot = 0.324 \pm {}^{0.015}_{0.020}$. The error is due to the uncertainty in the used ZAMS mass–radius relation (Eq. 4 of Patterson 1984). The corresponding masses of the secondary range from $0.22\,M_\odot$ to $0.28\,M_\odot$.

Using $S_K = 4.66 \pm 0.10$, applicable for a dM4+ star with $V - K = 5.2 \pm 0.2$ (Ramseyer 1994), I obtain a distance of $d = 91 \pm {}^{18}_{15}$ pc. The error in the distance is mainly due to the error in S_K and to a lesser degree to those in $R_2/R_\odot$ and K. Within the uncertainties, the distance of 91 pc is compatible with the values derived previously. With the presently available data the accuracy on d can not be further improved.

3.5.4.2 Low state

The derived effective temperature (Fig. 3.8c) varies in phase with the ultraviolet– and hard X–ray fluxes. As mentioned above, this temperature has to be understood as a flux–weighted mean value over the emitting surface. The minimum of a sinusoidal fitted to the low–state temperature variation thus translates into an *upper* limit to the temperature of the undisturbed non–accreting white dwarf. Correspondingly, the maximum gives a *lower* limit for the temperature of the heated pole cap (Table 3.5).

The effective source radius R in Fig. 3.8(d), valid for $d = 90$ pc, seems to vary in antiphase with the temperature. The maximum value of R of 8.5×10^8 cm is a lower limit to $R_{\rm wd}$ at this distance and suggests $R_{\rm wd} \le 0.6 M_\odot$. At the lower and upper distance limits of 75 and 109 pc, I have $R_{\rm wd} > 7 \times 10^8$ cm, $R_{\rm wd} < 0.8 M_\odot$ and $R_{\rm wd} > 1.0 \times 10^9$ cm, $R_{\rm wd} < 0.43 M_\odot$, respectively. The minimum value of R of $\sim 6 \times 10^8$ cm represents an upper limit to the radius of the hot spot (Fig. 3.8, Table 3.5). With $T_{\rm wd} = 20\,000$ K and $T_{\rm spot} = 27\,000$ K I find $R_{\rm pole} \simeq 3.3 \times 10^8$ cm. This value can be considered as a lower limit for the spot size as the observed Lyα profiles exclude spots much smaller and hotter than determined by the model fits. It has to be stressed that the model of a single–temperature 'hot spot' is only a crude estimate, in reality a temperature gradient will be present over the white dwarf surface. In any case, the 'spot' covers a substantial fraction of the white dwarf of the order of $f \sim 0.1$, similar to the model depicted in Fig. 3.4.

Heise & Verbunt (1988) suggested that AM Her does not show a single well defined low state. This statement was based on the different temperatures derived by these authors for the November 1983 data (20 000 K) and by Szkody et al. (1982) for the 1980 low state (50 000 K, see also Table 3.1). My analysis shows that there are, in fact, slight differences in flux between the individual low states but practically no differences in the derived temperatures. The temperatures for four observed low states all follow an orbital variation of quasi–sinusoidal form with a scatter of only ~ 1500 K. The times the system has spent in a low state before these individual observations range from a few days (June 1992)[7] to 150 days (September 1990). On the basis of these data, there is no evidence for a systematic cooling of the white dwarf following a preceding high state. Judging from the Nov 1983 observations which followed a prolonged high state, the timescale in which the accretion-heated pole cap cools from $\sim 37\,000$ K to $\sim 24\,000$ K must be shorter than ~ 25 days. This cooling timescale will be discussed further in Sect. 5. Finally, I note that AM Her has never been observed without X–ray emission (Sect. 3.5.2). The integrated accretion–induced low–state flux of about 7×10^{-11} erg cm^{-2}s^{-1} (Table 3.5) corresponds to an

---

[7]However, the high state in April/May 1992 was very short, reaching only $V \simeq 13.5$ and was preceeded by a long low state.

accretion rate of $\sim 10^{-11} M_\odot \mathrm{yr}^{-1}$ for an $0.6\,M_\odot$ white dwarf at a distance of 90 pc. This value is in agreement with the level of accretion expected if angular momentum loss is driven only by gravitational radiation. It seems that AM Her does not drop substantially below this level, in agreement with the standard evolutionary scenario (Sect. 2.1).

3.5.4.3 High state

In the high state, the temperature stays above the maximum value observed in the low state throughout the orbital cycle (Fig. 3.8 and 3.9). The effective source radius rather tends to vary in phase with the temperature, suggesting that this variation is due to the varying aspect of the spot. The maximum radius would then be a lower limit to the spot size. I conclude that both, in the high and the low state, the spot radius is $\sim 5 \times 10^8$ cm at $d = 90$ pc, implying $f \sim 0.08$. That a comparatively large fraction of the white dwarf is heated is suggested also by the fact that the orbital modulation in the ultraviolet is less pronounced than that in hard X–rays. The derived source radius confirms the suggestion by Heise & Verbunt (1988) of a large, moderately heated accretion region to explain the ultraviolet spectrum of AM Her during the high state.

3.5.4.4 Energy balance

In the "classical" reprocessing model (see Sect. 3.2), a shock stands low above the white dwarf surface, heating a small area by irradiation with hard X–ray and cyclotron radiation to temperatures of a few 10^5 K . The presence of a substantial ultraviolet flux in the low–state and high–state spectra, emitted by large regions of moderate temperature can not be understood in this picture. The interpretation of the high–state ultraviolet flux as the tail of the soft X–ray emission was previously questioned by Heise & Verbunt (1988) because the orbital variation of the ultraviolet emission stays in phase with that of the hard X–ray flux also when the system accretes in the reversed mode, i.e. there originates no obvious ultraviolet emission from the second pole. Examining the energy balance of hard X–ray, cyclotron and ultraviolet radiation, I find that, in contrast to eq. 3.2 the balance

$$L_{\mathrm{UV}} \simeq L_{\mathrm{tb}} + L_{\mathrm{cyc}} \tag{3.5}$$

holds for both, the low state and the high state (see Table 3.5). Here L_{UV} is the total integrated luminosity (including the FUV contribution taken from the model spectrum) in excess of the assumed underlying white dwarf with an adopted $T_{\mathrm{eff}} \simeq 20\,000$ K (Fig. 3.11) and L_{tb} is the integrated thermal bremsstrahlung luminosity derived from the hard X–ray data. The soft X–ray flux does not enter this energy balance. The situation for both states is as follows.

Low state: The white dwarf model spectra predict no substantial flux below the Lyman edge and examination of low–state LWP spectra shows that the orbital variation is small at 3200 Å. The resulting peak–to–peak modulation of the total ultraviolet flux due to heating then is 3.6×10^{-11} erg cm^{-2}s^{-1}, calculated by integrating the difference of the model spectra for orbital maximum and orbital minimum in the interval $900 < \lambda < 3200$ Å. Assuming a

	low states 1980–92	high state 1991
Flux [erg cm^{-2}s^{-1}]		
UV	3.6×10^{-11}	2.4×10^{-10}
Thermal bremsstr.	0.8×10^{-11}	1.3×10^{-10}
Cyclotron	1.8×10^{-11}	1.1×10^{-10}
Temperature [K]		
White dwarf	$\leq 20\,000$	-
Pole cap	$\geq 24\,000$	$\geq 37\,000$
Radius [10^8cm]		
White dwarf	≥ 8.5	-
Pole cap	≤ 6	~ 5

Table 3.5: Physical parameters of the white dwarf and the accretion spot in AM Her. Radius, temperature and ultraviolet flux have been derived by white dwarf model fits, the unabsorbed integrated bremsstrahlung flux has been calculated assuming $kT_{tb} = 20\,\mathrm{keV}$. The cyclotron fluxes are estimates according to Bailey et al. (1988) and Priedhorsky et al. (1978).

20 keV thermal bremsstrahlung spectrum and a hydrogen column density $N_H = 9 \times 10^{19}$cm^{-2} (van Teeseling et al. 1994), the *RASS* mean hard X–ray count rate at orbital maximum of 0.18 cts s^{-1} (September 1990) corresponds to a total flux of 0.8×10^{-11} erg cm^{-2}s^{-1}. The total low–state cyclotron flux was derived by Bailey et al. (1988) to be 1.8×10^{-11} erg cm^{-2}s^{-1}. The implication is that heating by hard X–rays and cyclotron radiation approximately accounts for the observed orbital modulation of the ultraviolet flux. It should be noted that the cyclotron component was not measured simultaneously and that the low–state hard X–ray flux is known to be variable (the *ROSAT* low–state observations of September 1991 showed a count rate higher by a factor ~ 3.5).

The maximum contribution of a soft X–ray blackbody component, limited by the non–detection in the *ROSAT PSPC* (< 0.02 cts s^{-1} in the $0.1 - 2.4$ kev band due to the blackbody emission) and by the observed deep Lyα profile ($F_{bb} \leq 2 \times 10^{-14}$ erg cm^{-2}s^{-1} at 1230 Å, see Fig. 3.7b), is 3.3×10^{-10} erg cm^{-2}s^{-1} at $kT_{bb} = 10$ eV, about five times the sum of the ultraviolet excess, the thermal bremsstrahlung and the cyclotron radiation fluxes. This hypothetical low–state soft X–ray component does not enter the energy balance of reprocessing. However, I can not exclude that during the low state the luminosity is still dominated by soft X–rays.

High state: I correct for the assumed underlying white dwarf with $T_{eff} = 20\,000$ K by subtracting the low–state model spectrum at orbital minimum from the high–state model spectrum at orbital maximum. Integrating this difference spectrum yields a total ultraviolet flux in excess of the white dwarf of 2.4×10^{-10} erg cm^{-2}s^{-1}. The simultaneous *ROSAT* observa-
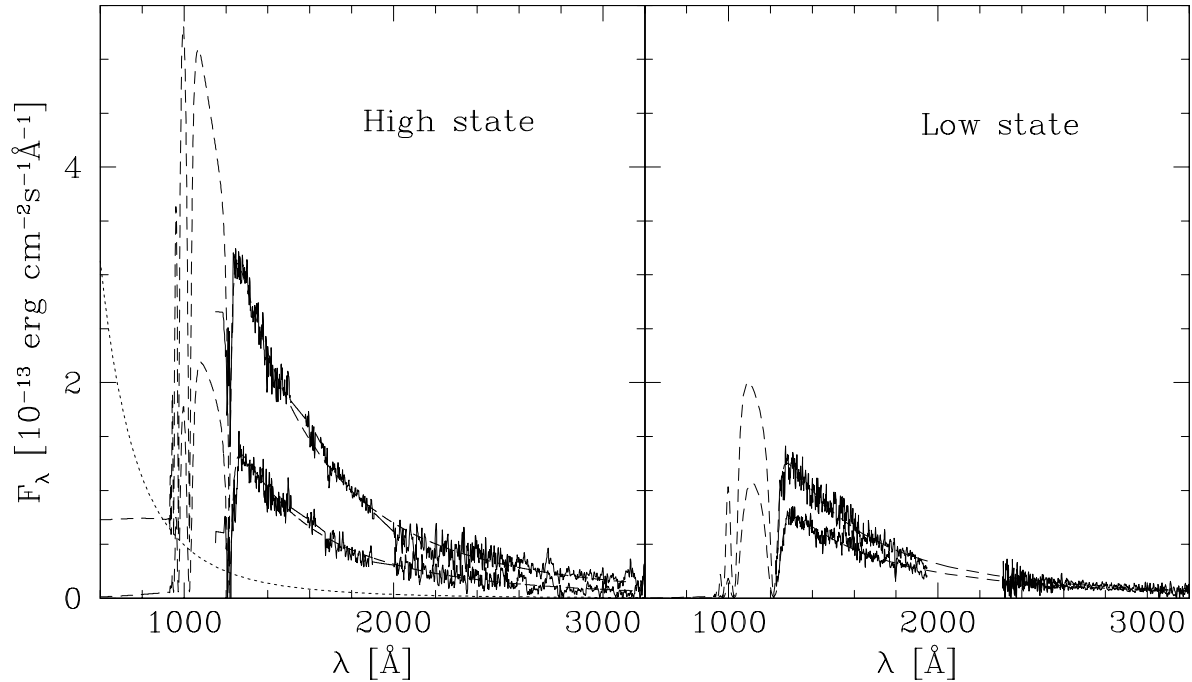
Figure 3.11: Soft X–ray vs. ultraviolet emission: Shown are emission line subtracted high–state spectra at orbital minimum and maximum, corrected for the contribution of the accretion stream (Fig. 3.6), along with the best–fit white dwarf model spectra (dashed). Also shown is a blackbody representation ($kT_{bb} = 29$ eV) of the observed soft X–ray emission.

tions yield a hard count rate of $2 \, \mathrm{cts \, s^{-1}}$ which corresponds, assuming again a $20 \, \mathrm{keV}$ thermal bremsstrahlung spectrum, to an integrated flux of $1.3 \times 10^{-10} \, \mathrm{erg \, cm^{-2} s^{-1}}$. The high–state cyclotron flux is estimated as follows. Bailey et al. (1988) quote a total high–state IR/optical flux at orbital maximum corrected for the photospheric contributions of $2.8 \times 10^{-10} \, \mathrm{erg \, cm^{-2} s^{-1}}$. At this time, AM Her was at $V = 12.2$. From his flux value I subtract an estimated contribution due to the accretion stream (Priedhorsky et al. 1978) and obtain a cyclotron flux of $1.8 \times 10^{-10} \, \mathrm{erg \, cm^{-2} s^{-1}}$. At the time of the April 1991 *IUE/ROSAT* observations, AM Her was at $V = 12.7$ at orbital maximum (Beuermann et al. 1991b) which corresponds to an estimated cyclotron flux of $1.1 \times 10^{-10} \, \mathrm{erg \, cm^{-2} s^{-1}}$. Again, the energy balance suggests an origin of the ultraviolet flux from heating by X–rays and cyclotron radiation (Table 3.5). The best blackbody fit to the April 1991 *ROSAT* data results in $kT_{bb} = 29$ eV, $N_H = 8.9 \times 10^{19} \, \mathrm{cm^{-2}}$ and $F_{bb} = 1.5 \times 10^{-9} \, \mathrm{erg \, cm^{-2} s^{-1}}$. In the 'classical' reprocessing picture this corresponds to a soft X–ray excess $(F_{bb} + F_{UV})/(F_{tb} + F_{cyc}) \sim 7.3$. The contribution of this soft X–ray component to the flux at $1300 \, \text{Å}$ is $1.6 \times 10^{-14} \, \mathrm{erg \, cm^{-2} s^{-1} Å^{-1}}$ (Fig. 3.11). The blackbody assumption is prone to large uncertainties: Studies of the new class of *super soft X–ray sources* (Heise et al. 1994) demonstrate that fitting *ROSAT PSPC* spectra with model atmospheres instead of blackbodies yields substantially smaller fluxes in the ultraviolet (and EUV). Since the same argument

probably applies to AM Her stars, I consider it justified to neglect the ultraviolet contribution of the soft X–ray component.

The temperature estimate of $20\,\mathrm{keV}$ for the thermal bremsstrahlung may be on the high side, but even with $kT_{\mathrm{tb}} \leq 13.5\,\mathrm{keV}$ for the flux absorbed in the photosphere as suggested by Beardmore et al. (1995a) my conclusions do not change substantially.

I have demonstrated that reprocessing of bremsstrahlung and cyclotron radiation can energetically account for the observed ultraviolet emission. The large area of the ultraviolet emitting region implies that the atmosphere is irradiated by a source which can reach some 0.1 of the white dwarf surface, e.g. because it is located at a height of $\sim 0.1 R_{\mathrm{wd}}$. There is no direct evidence that either bremsstrahlung or cyclotron emission occur this high above the photosphere, but the observations do not exclude this. The shock height obtained from simple 1–D hydrodynamics and cooling by bremsstrahlung (Aizu 1973) can be expressed as $h = 5.5 \times 10^5 v_{1000}^3 \dot{m}^{-1}$, where v_{1000} is the free–fall velocity in units of $1000\,\mathrm{km\,s^{-1}}$ and $\dot{m}$ is the mass–flow rate in $\mathrm{g\,cm^{-2}s^{-1}}$. This estimate is low because of the decreasing density in a funnel geometry, but high because of the additional cyclotron cooling. For the present purpose it is probably adequate. With $v_{\mathrm{ff}} = 4 \times 10^8\,\mathrm{cm\,s^{-1}}$ I have $h = 10^8\,\mathrm{cm}$ at $\dot{m} \simeq 0.4\,\mathrm{g\,cm^{-2}s^{-1}}$. Cyclotron emission (bremsstrahlung) will be characterized by a lower (higher) $\dot{m}$ and a larger (smaller) stand–off distance. With $R \simeq 8.5 \times 10^8\,\mathrm{cm}$, $h \simeq 10^8\,\mathrm{cm}$ implying $f \sim 0.06$, essentially as observed. Hence, heating of a large fraction of the white dwarf surface by bremsstrahlung and cyclotron radiation appears entirely plausible. As already mentioned in Sect. 3.2, cyclotron radiation is beamed perpendicular to the magnetic field and, therefore, parallel to the surface of the star which adds to distribute irradiation over a large area. Any finite lateral extent of the primary emission region further spreads irradiation.

In this picture, the soft X–ray flux does not enter the energy balance of the reprocessed radiation. It might be due to the physically separate mechanism of *blobby* accretion (see Sect. 3.2), where blobs of sufficiently high density penetrate into the photosphere, locally heating small areas to high temperatures. The fractional size of the soft X–ray emitting region implied by $T_{\mathrm{bb}} = 29\,\mathrm{eV}$ and $d = 90\,\mathrm{pc}$ is $f \simeq 7 \times 10^{-5}$ which is three orders of magnitude smaller than the size of the ultraviolet emitting area. This scenario explains also the fact that the ultraviolet and hard X–ray orbital flux variations stay in phase also in the reversed accretion mode, provided that the anomalous X–ray emission from the second pole is soft and dominated by *blobby* accretion.

Short timescale fluctuation studies of soft and hard X–rays indicate that the soft and hard X–ray emission are not correlated (e.g. Beuermann et al. 1991a for the case of EF Eri and Stella et al. 1986 for AM Her) which argues against an origin of the soft X–rays from reprocessing of the *observed* hard X–ray component. On the other hand, van Teeseling et al. (1994) showed that the *EXOSAT* grating spectrum of AM Her is not consistent with an undisturbed hot LTE white dwarf atmosphere, but is much better fitted by an irradiated atmosphere or an atmosphere heated by more diffuse blobs which disperse their energy at small optical depths. In any case, blobs of matter entering the atmosphere will produce shocks. These shocks may be covered up by infalling material and the associated hard radiation may *not be observed* but instead be
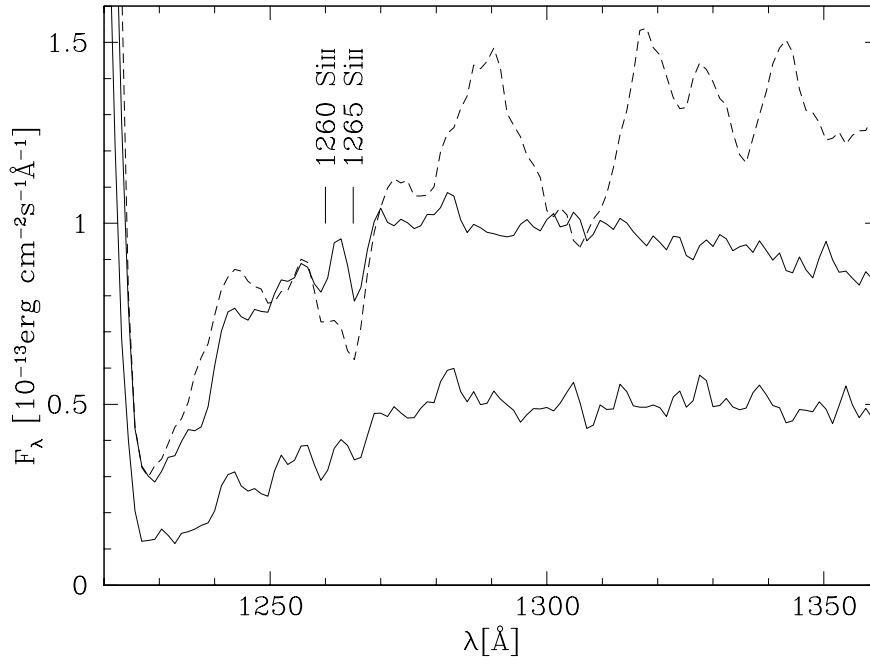
Figure 3.12: Absorption lines of heavy elements in the ultraviolet spectra of AM Her and VW Hyi. Solid: co–added SWP low–state spectra of AM Her during orbital minimum (lower curve) and maximum (upper curve). Dotted: average SWP spectrum of VW Hyi in quiescence.

reprocessed into soft X–ray emission. Hence, the hydrodynamics and the radiative transfer are certainly more complex than suggested by the original picture of Kuijpers & Pringle (1982).

For completeness, I note that heating the photosphere from below by energy carried deep into the white dwarf and distributed by circulation might be a process which competes with irradiation. I estimate the depth in which the penetrating material gets decoupled from the magnetic field ($P_{mag} = P_{gas}$) as 50–100 km[8]. It is unlikely that an area at the surface much larger than this dimension can be heated. Hence, irradiation from a high standing shock seems a more plausible mechanism.

3.5.4.5 Heavy elements in the atmosphere of AM Her?

Ultraviolet spectroscopy of non–magnetic accreting white dwarfs, e.g. in dwarf novae, revealed strong absorption lines by heavy elements (Gänsicke 1993; Long et al. 1993; Sion et al. 1990, 1995a; see also Chapter 4). In contrast to this, no metal abundances have yet been reported for the magnetic white dwarfs in polars, mainly due to the low S/N of the ultraviolet spectra available so far.

---

[8]In AM Her, $B^2/(8\pi) = 7.8 \times 10^{12}\,\mathrm{dyn\,cm^{-2}}$. A $T_{eff} = 20\,000\,\mathrm{K}$ model atmosphere computed with the code described on p. 18 shows that P_{gas} reaches this value at a depth of $\sim 60\,\mathrm{km}$.

However, close inspection of the residuals of the spectral fits in Sect. 3.5.3.2 revealed a double–peaked absorption–like structure near 1260 Å in nine out of the eleven low–state spectra gathered in 1980–1990. The 1992 data were not included in this sample because of their low S/N ratio. I corrected small (~ 1Å) deviations in the wavelength calibration between the individual spectra. Co–added spectra for the orbital minimum and maximum (Fig. 3.12) display several other weaker features in common. The position of the two strong absorption–like features closely coincides with the Si II $\lambda\lambda$ 1260,1265 doublet. The total equivalent width for the Si II doublet is ~ 2 Å and ~ 1.3 Å for the orbital minimum and maximum spectra, respectively. Whether the strength of the observed features depends on orbital phase and/or on the time spent in quiescence can not be determined from the present small dataset. I use the results of Mauche et al. (1988) with a hydrogen column density of $N_H = 9 \times 10^{19}$cm^{-2} (van Teeseling et al. 1994) to estimate the interstellar equivalent width of this Si II doublet as ~ 0.4 Å. This low value strongly supports the assumption of intrinsic absorption. Furthermore, the line Si II λ 1265 is caused by a transition from an excited level of Si II which is usually not populated in the interstellar medium.

For comparison, I show an average *IUE* spectrum of the dwarf nova VW Hyi in quiescence which also clearly shows the Si doublet, as well as a broad, unresolved trough of Si III $\lambda\lambda$ 1295–1303, Si II $\lambda\lambda$ 1304,1309 and O I λ 1302. The latter features can not be discerned in the spectrum of AM Her, which may be due to the generally lower equivalent widths compared to VW Hyi. Also high $\log g$ model spectra calculated for solar abundances by Hubeny (1994, private communication) result in a higher equivalent width for the Si II doublet of ~ 6 Å. Inspection of the available *IUE* high–resolution data did not provide further information; even the best–exposed spectrum (SWP25330L with 372 min. exposure time) is too noisy.

I conclude that there is some evidence for heavy elements in the accretion spot of AM Her; the Si II features can not be due to interstellar absorption. This is not unexpected as the accreting material from the late–type secondary should have approximately solar abundances. The low equivalent widths of the absorption lines suggest either a lower concentration of metals throughout the atmosphere or enrichment of only a small part of the white dwarf surface. The latter seems more likely as the accretion spot of AM Her is small and as it is not clear whether the accreted matter can spread perpendicular to the magnetic field lines over the white dwarf surface. Hence, the large irradiated but non–accreting hot region should have almost pure DA properties.

3.6 Further evidence of accretion–heated magnetic white dwarfs from Lyα absorption profiles

Encouraged by the results obtained for AM Her, I initiated two *IUE* programs in order to (a) obtain ultraviolet spectroscopy for previously unobserved polars in order to determine reliable effective temperatures of their accreting magnetic white dwarfs, and, if possible, to derive the temperature distribution over the white dwarf surface, and to (b) monitor at ultraviolet wavelengths the prototype AM Her in order to obtain a time series of spectra during the transition from a high state to low state. With these data, the cooling timescale of the accretion heated pole cap should have been determined. Unfortunately, due to the loss of *IUE's* 5th gyro in March 1996, both programs were terminated prematurely. *IUE* spectra were obtained for AR UMa, QQ Vul and the new, *ROSAT*–discovered polars RX J0153–59 and RX J1313–32 (Beuermann & Thomas 1993; Beuermann & Burwitz 1995).

These spectra were complemented with all archive *IUE* and *HST* data of polars available in spring 1996. The SWP spectra used for my analysis have been reprocessed with the *IUE* Final Archive procedures (*NEWSIPS*), yielding a better flux calibration and a better S/N, especially for underexposed spectra. The complete dataset contains ~ 550 ultraviolet observations for 28 polars.

In order to determine reliable white dwarf temperatures, I restricted the analysis to the systems which clearly display a Lyα absorption profile as the continuum slope alone is a poor indicator of both, the white dwarf temperature and its contribution to the ultraviolet flux. The remaining sample contains, apart from AM Her, the following six systems: BY Cam, V834 Cen, DP Leo, AR UMa, QQ Vul and RX J1313–32. All observations are average spectra over the binary orbit, except for DP Leo and QQ Vul, where phase–resolved spectra exist. BY Cam, V834 Cen, DP Leo, AR UMa and RX J1313–32 were observed in the low state (Table 3.6) while QQ Vul was observed in a high state (Table 3.7).

Using neutral hydrogen column densities derived from X–ray data, I checked for all six systems the possible contribution to the photospheric Lyα profile by interstellar and/or intrinsic absorption and find that it is negligible in all cases.

3.6.1 BY Camelopardalis

BY Cam ($P_{\mathrm{orb}} = 202\,\mathrm{min}$) is a peculiar member of the polar family: (a) It is slightly (($P_{\mathrm{orb}} - P_{\mathrm{wd}})/P_{\mathrm{orb}} = 1 - 2\%$) asynchronous; the white dwarf is rotating somewhat faster than once per orbital period (Silber et al. 1992). The only polar known before to be asynchronous was V1500 Cyg, which is also the only confirmed AM Her system to have undergone a classical nova outburst (Stockman et al. 1988). (b) BY Cam shows unusual ultraviolet emission line ratios with extremely strong N v λ 1240 emission while C IV λ 1550 is almost absent. These line ratios are untypical for cataclysmic variables in general. They are, however, observed in recurrent novae after outburst (Bonnet–Bidaud & Mouchet 1987). Taken together, these two charac-

Dataset	Obs. date	Exp. time	Instrument	Ref.
BY Cam:				
SWP35576L	17 Feb 1989	265	IUE	1
V834 Cen:				
SWP19359L	01 Mar 1983	168	IUE	2
LWP01817L	01 Mar 1983	100	IUE	2
DP Leo:				
Y0PS0201T	30 Oct 1991	25	HST	3
Y0PS0301T	31 Oct 1991	37	HST	3
Y0PS0401T	31 Oct 1991	29	HST	3
AR UMa:				
SWP56296L	15 Dec 1995	116	IUE	4
SWP56589L	18 Jan 1996	116	IUE	
RX J1313–32:				
SWP56879L	02 Mar 1996	230	IUE	
LWP32069L	06 Mar 1996	35	IUE	

(1) Szkody et al. 1990; (2) Maraschi et al. 1984; (3) Stockman et al. 1994; (4) Schmidt et al. 1996.

Table 3.6: Ultraviolet low–state observations of BY Cam, V834 Cen, DP Leo, AR UMa and RX J1313–32. Listed are the *IUE* frame number, the observation date, the exposure time and the instrument. The data for AR UMa and RX J1313–32 are from my own *IUE* programs, while the other spectra were retrieved from the archives.

teristics suggest that BY Cam may have undergone "recently" (i.e. within the last ~ 1000 yrs) an unnoticed nova explosion[9].

The only *IUE* low–state spectrum (Table 3.6) was analysed by Szkody et al. (1990) who set a lower limit to the white dwarf temperature of 70 000 K from the absence of any Lyα absorption line. However, reprocessing of the same data with the *NEWSIPS* software yields a higher S/N, revealing clearly the photospheric Lyα absorption of the white dwarf. A fit with single temperature white dwarf model spectra yields $T_{\rm wd} = 22\,000$ K. Using $E_{B-V} = 0.05$ (Bonnet–Bidaud & Mouchet 1987), the white dwarf is expected to have $V \simeq 17.8$, which is consistent with $V = 17.5$ observed simultaneously to the *IUE* spectrum. The distance of BY Cam can be estimated from the scaling factor between the observed spectrum and the model spectrum as this factor is proportional to $R_{\rm wd}^2/d^2$. Assuming a white dwarf radius of 8×10^8 cm, the implied distance is $d \simeq 250$ pc. An independent value for the distance of BY Cam was derived

---

[9]If the system underwent a nova eruption, the white dwarf will synchronize with the orbital period due to magnetic torques between the two stars. In V1500 Cyg, the spin period of the white dwarf is decreasing since the 1975 nova outburst, the estimated timescale for resynchronization of the system is ~ 170 yrs (Schmidt et al. 1995).
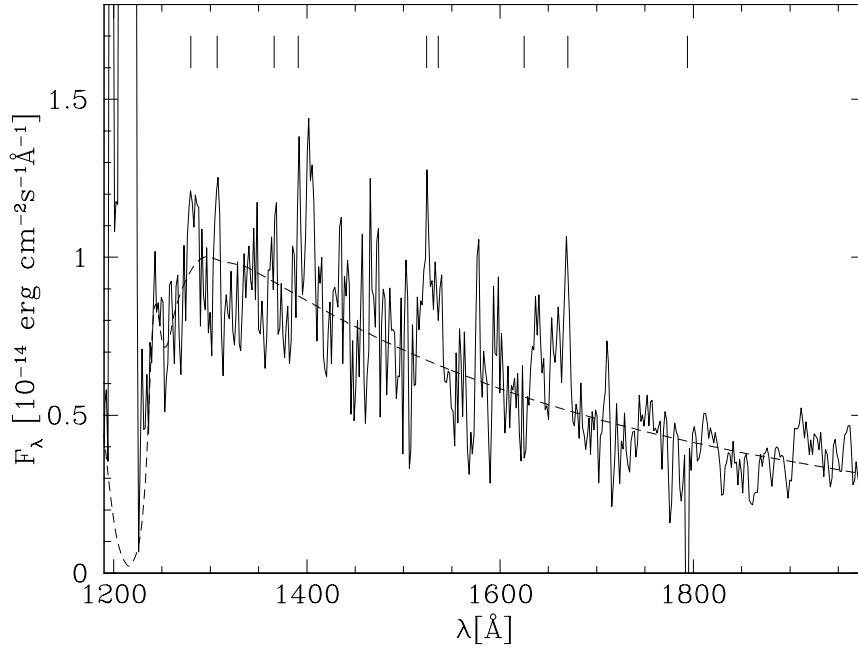
Figure 3.13: Low–state *IUE* spectrum of BY Cam, along with the best–fit white dwarf model ($T_{\rm wd}$=22 000 K). Due to the long exposure time (265 min), the spectrum is strongly affected by cosmic hits. Tick marks show the position of identified cosmic hits and reseaux marks.

by Szkody et al. (1990) from the observed low–state *J* magnitude, being a measure for the emission from the secondary. The authors estimated the distance of BY Cam to be about 2.5 times that of AM Her, i.e. $d_{\rm BY\,Cam} \sim 225$ pc with $d_{\rm AM\,Her} = 90$ as derived in Sect. 3.5.4.1. This estimate supports my interpretation of to the *IUE* low–state spectrum.

From the present observations, it is not possible to judge whether a heated region on the white dwarf in BY Cam exists or not. However, as the *IUE* data cover more than a binary orbit (Table 3.6), a hypothetic hot spot could have contributed to the observed spectrum. The fact that the spectrum can be fitted with a single–temperature white dwarf model indicates that an accretion heated spot, if present, can not be much hotter than the underlying white dwarf photosphere (compare V834 Cen, next Sect.).

3.6.2 V834 Centauri

Simultaneous optical and *IUE* low–state spectroscopy of V834 Cen ($P_{\rm orb} = 102$ min) was presented by Maraschi et al. (1984). The authors fitted the overall continuum with the sum of two blackbodies representing the photospheric emission of the two stellar components, finding $T_{\rm wd} = 26\,500$ K. They note, however, that the white dwarf interpretation of the ultraviolet continuum is somewhat ambiguous, as no broad Lyα absorption is observed.
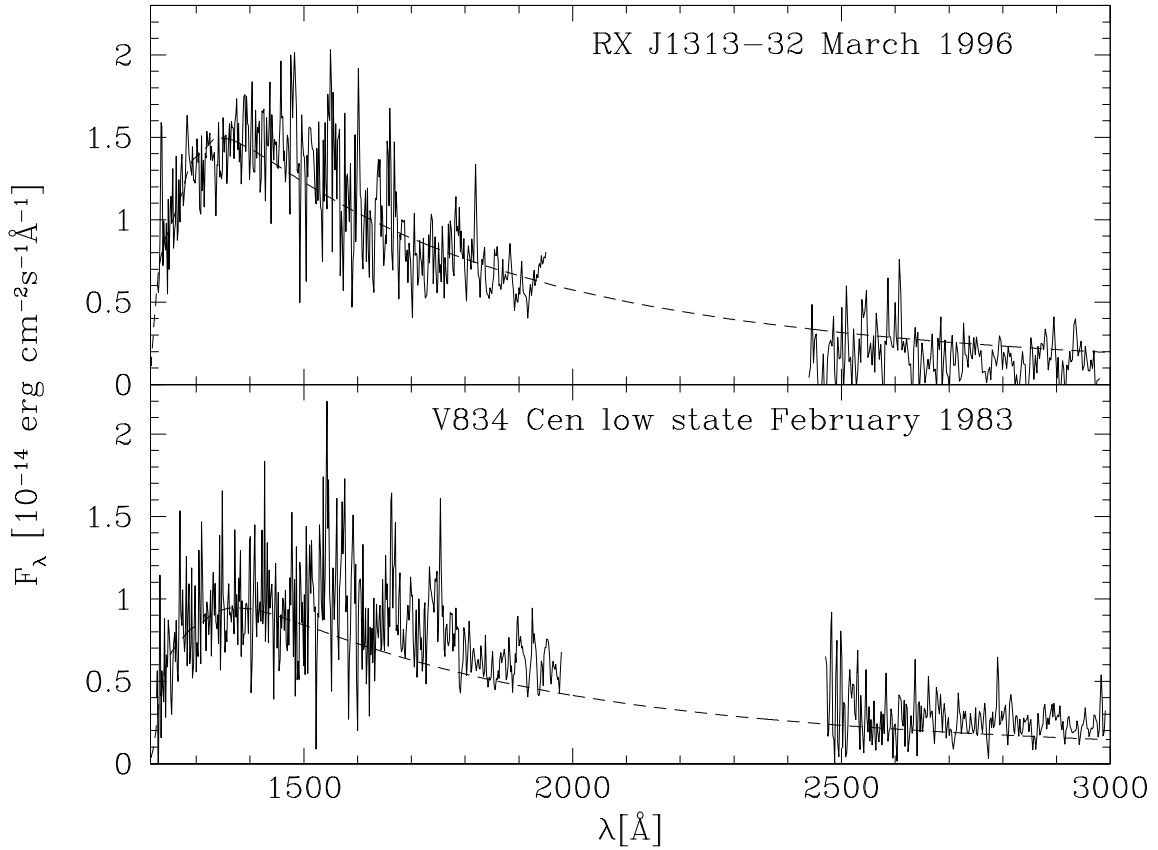
Figure 3.14: *IUE* low–state spectra of RX J1313–32 and V834 Cen, along with two–temperature white dwarf model spectra.

Further optical low–state spectroscopy and photometry was reported by Ferrario et al. (1992) and Schwope (1990). Interestingly, both papers suggest a two–temperature model for the white dwarf to fit the observations. Ferrario et al. (1992) show a very smooth, quasisinusoidal blue light curve (their Fig. 5), which they interpret as a hot spot of $T_{\rm spot} \simeq 50\,000$ K on a $T_{\rm wd} = 15\,000 - 20\,000$ K white dwarf. Schwope (1990) shows that fitting low–state spectroscopy of V834 Cen with a single–temperature magnetic white dwarf model yields to inconsistencies with the field strength derived from cyclotron spectroscopy. He concludes that a hotter ($T \simeq 30\,000$ K) contribution is necessary to achieve agreement between the results from Zeeman and cyclotron spectroscopy.

Fig. 3.14 shows the *IUE* low–state spectrum of V834 Cen reported by Maraschi et al. (1984), reprocessed with the *NEWSIPS* software. A clear flux turnover below ~ 1400 Å is observed, indicative of the photospheric Lyα absorption profile. However, the observed spectrum can not be fitted with a single–temperature white dwarf model[10].

_____

[10]So far (Sect. 3.5, 3.6.1), single–temperature models were a satisfactory description of the observations, indi-
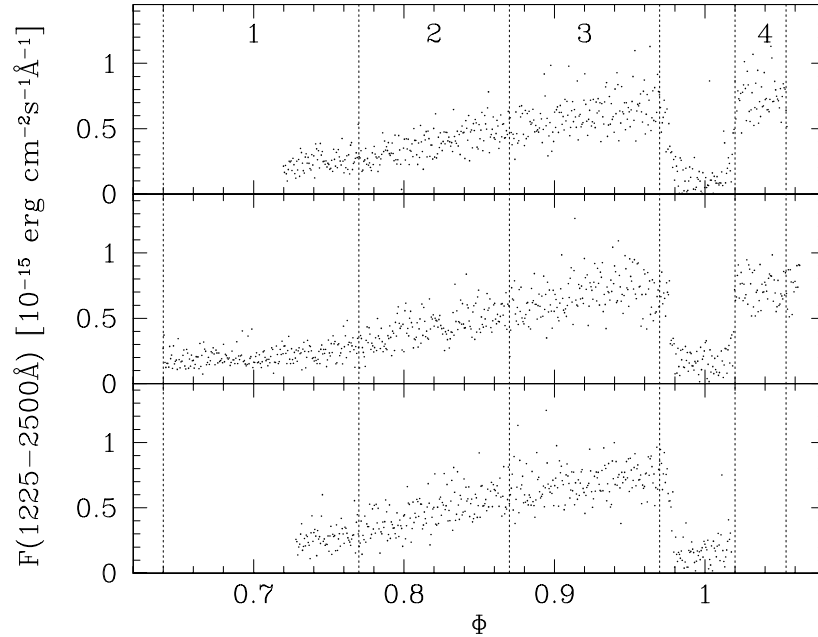
Figure 3.15: *HST/FOS* light curve of DP Leo. Co–added spectra for the phase intervals 1–4 are displayed in Fig. 3.17

I therefore adopted a two–temperature model (white dwarf plus heated pole cap), resulting in four free parameters: the white dwarf temperature T_{wd}, the spot temperature T_{spot} and the scaling factors of both components, R_{wd}^2/d^2 and R_{spot}^2/d^2. This two–temperature model fits the observations well with $T_{wd} = 14\,000$ K and $T_{spot} = 28\,000$ K (Fig. 3.14). The hot component is responsible for the rather narrow core of Lyα but drops rapidly towards longer wavelengths where the cool white dwarf dominates the emission. The fractional area of the spot is $f \simeq 0.015$ of the white dwarf surface. The optical magnitude of the model, $V = 17.3$, is consistent with the observed low–state brightness of the system (e.g. Ferrario et al. 1992). Assuming a white dwarf radius of $R_{wd} = 8 \times 10^8$ cm, the implied distance is $d \simeq 140$ pc, which is in reasonable agreement with distance estimates derived from the spectrum of the secondary star.

It is important to notice that the spot parameters are *orbital mean* values only. From the single phase–averaged *IUE* spectrum no conclusions can be drawn concerning the real size and the location of the hot spot on the white dwarf surface.

3.6.3 DP Leonis

DP Leo ($P_{orb} = 90$ min) was the first eclipsing AM Her system discovered (Biermann et al. 1985). Eclipsing systems offer a good opportunity to reliably determine the geometry (e.g.

---

cating that the temperature gradient over the (visible) white dwarf surface is not too large.
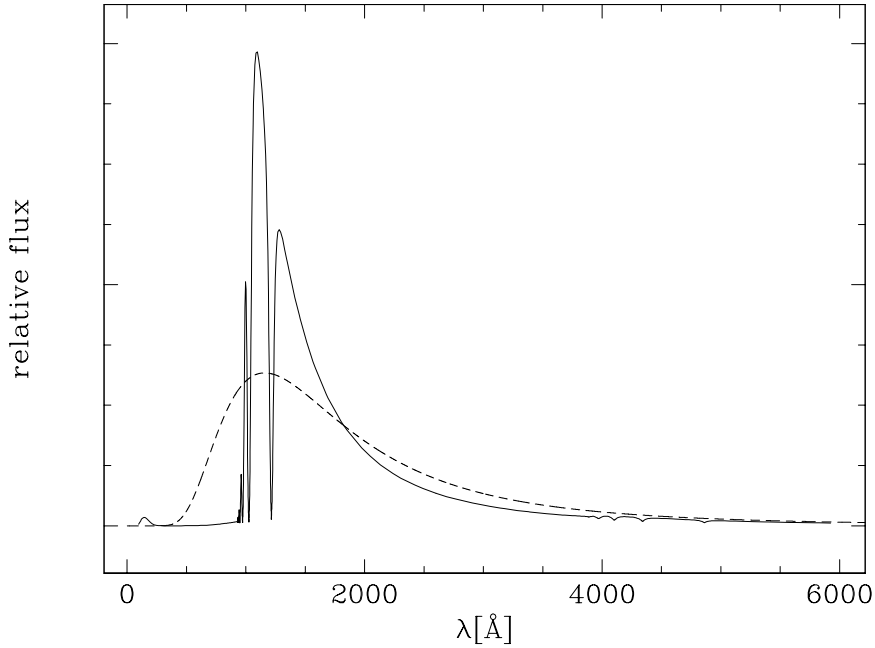
Figure 3.16: White dwarfs are not blackbodies: comparison between a white dwarf model spectrum (full line) and a blackbody (dashed line) for $T_{\text{eff}} = 25\,000\,\text{K}$.

inclination, colatitude of the accretion spot) and the stellar parameters (radius and mass of both components). Alas, the faintness of DP Leo ($V \sim 19$ in the low state) prevented detailed studies. The only *IUE* observation yielded a very weak spectrum with no emission lines (Szkody et al. 1985). It was clear that a large ultraviolet spectrograph had to be awaited before a study of the white dwarf in DP Leo could be attempted.

In October 1991, time–resolved ultraviolet spectroscopy of DP Leo was obtained with the *Faint Object Spectrograph*[11] (*FOS*) onboard *HST* during three satellite orbits (Stockman et al. 1994). As the binary period is very close to the orbital period of *HST*, they managed to cover three consecutive eclipses. During the observations, DP Leo was in a low state. Fig. 3.15 shows clearly the flux modulation as the accretion–heated spot moves into sight until the white dwarf is eclipsed by the secondary at $\phi = 1.0$. Stockman et al. (1994) estimated from the pre–egress spectrum $T_{\text{wd}} \simeq 16\,000\,\text{K}$. Their main argument for this temperature is the observed flux decline below $1400\,\text{Å}$, which they ascribe to the absorption by quasi–molecular hydrogen H_2^+.

It is interesting to note that none of the cool magnetic white dwarfs in polars analysed here, i.e. V834 Cen, DP Leo and RX J1313–32 (Sect. 3.6.6), clearly shows the quasi–molecular absorption[12] of H_2^+ at $1400\,\text{Å}$ which is in fact a strong feature in cool ($T_{\text{wd}} \leq 19\,000\,\text{K}$)

---

[11]for a description of the instrument see Keys (1995).

[12]The broad Lyα absorption arises through absorption by neutral hydrogen atoms perturbed by collisions with electrons, called *pressure broadening*. Perturbation by a proton (H^+) results in a *satellite* line at $\sim 1400\,\text{Å}$, called quasi–molecular H_2^+ absorption; while perturbation by a neutral hydrogen atom results in a satellite at $\sim 1600\,\text{Å}$,
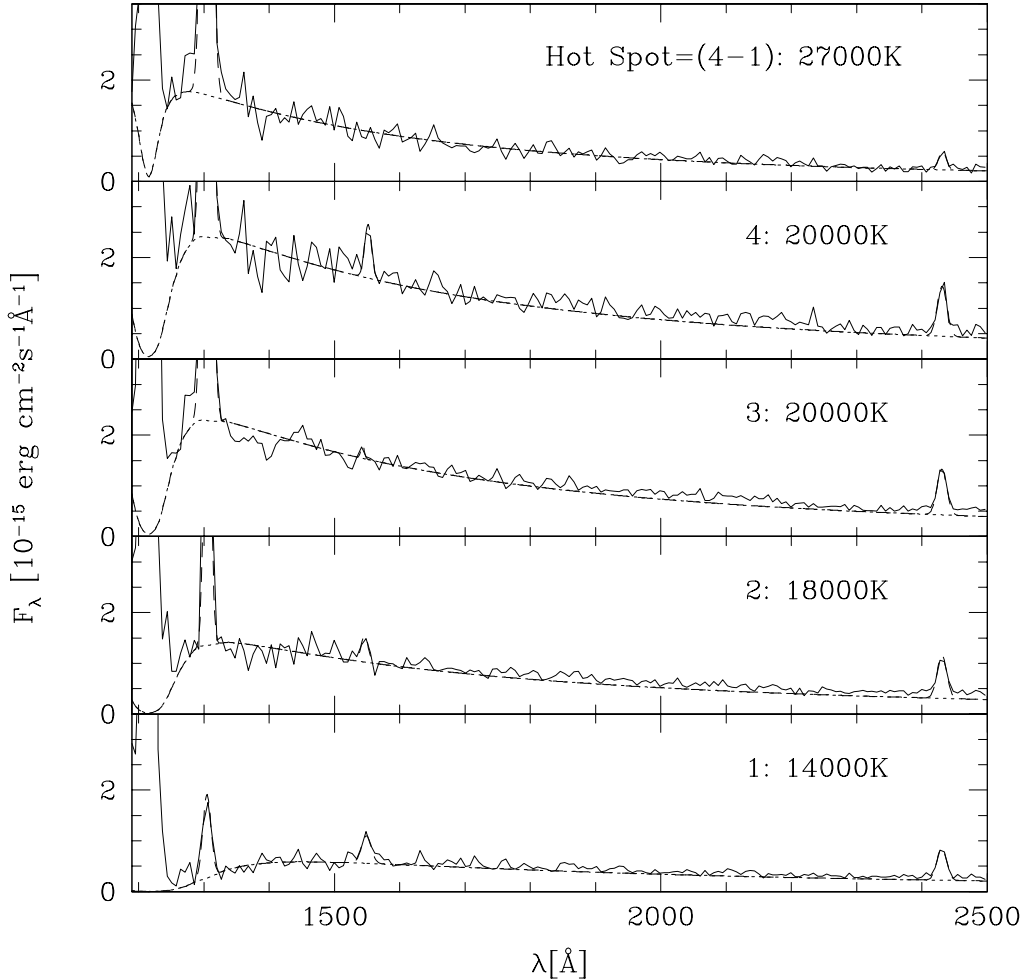
Figure 3.17: Phase–resolved *HST/FOS* spectra of DP Leo in a low state. The four bottom panels show the *FOS* spectra co–added in the phase intervals shown in Fig. 3.15, the top–most panel shows the likely spectrum of the hot spot, i.e. the difference of bright phase spectrum (4) and pre–egress spectrum (1). The emission lines at 1306 Å and 2430 Å are of geocoronal nature, O I and second–order Lyα, respectively. The best–fit single temperature white dwarf models are plotted as dashed lines.

non–magnetic white dwarfs (Koester 1985). Comparing the *IUE* spectra of V834 Cen and RX J1313–32 (Fig. 3.14) to observations of the non–magnetic single white dwarf Wolf 485a ($T_{\rm wd} = 14\,600\,{\rm K}$; Gänsicke 1993) indicates that the 1400 Å feature should be detectable even in the low S/N spectra of the two polars, if present. However, no theory exists so far predicting the

---

called quasi–molecular H_2. The 1400 Å and 1600 Å features were detected in early *IUE* observations of DA white dwarfs, seriously puzzling the white dwarf community. Their nature as H_2^+ and H_2 satellite lines was identified by Koester et al. (1985) and Nelan & Wegner (1985).

strength of this feature in strongly magnetic atmospheres. It may, hence, be that the equivalent width of the H_2^+ absorption is reduced in the presence of a strong magnetic field.

Stockman et al. (1994) extracted the assumed spectrum of the hot spot in DP Leo from the *HST/FOS* observations by subtracting the pre–egress spectrum from the bright phase spectrum. From a blackbody fit to this spectrum, they derived a spot temperature of $T_{spot} \simeq 50\,000\,K$ and a spot area of $f \sim 0.006$ of the white dwarf surface. However, blackbody spectra deviate substantially from white dwarf model spectra for temperatures below $\simeq 50\,000\,K$, having a much flatter continuum slope in the ultraviolet. Hence, the spot temperature derived by Stockman & Schmidt (1994) is likely to be on the high side. As I showed for AM Her (sect 3.5), low–state observations of polars are entirely consistent with standard white dwarf models (with a caveat to the Zeeman splitting of the Lyα profile, see Sect. 3.5.3.3). Therfore, I have fitted the *FOS* co–added spectra shown in Fig. 3.17 using single–temperature white dwarf models as described in Sect. 3.5.3.2, and find $T_{wd} \simeq 14\,000\,K$, in agreement with the value by Stockman et al. (1994). The distance derived from the fit, again assuming $R_{wd} = 8 \times 10^8\,cm$, $d = 390\,pc$, is in good agreement with the distance estimate by Biermann et al. (1985). The white dwarf model spectrum has $V \simeq 19.5$, which is consistent with the observed low–state magnitude of DP Leo.

As expected, the hot spot in my model is cooler, $T_{spot} \simeq 27\,000$, and, hence, occupies a larger fraction ($f \simeq 0.03$) of the white dwarf surface than that of Stockman et al. (1994). These results are similar to what was obtained for AM Her in Sect. 3.5.

3.6.4   AR Ursae Majoris

AR UMa ($P_{orb} = 116\,min$) is probably the most exciting polar in the sample presented here. Detected as strong and variable soft X–ray source (1 ES 1113+432) during the *Einstein slew survey* and identified with the semi–regular variable AR UMa, this object turned out to be a bright ($V \simeq 16.5$ in the low state) and near ($d \simeq 88\,pc$) AM Her star (Remillard et al. 1994). In contrast to most other polars, AR UMa spends only $\sim 10\,\%$ of the time in the high state, during the remaining 90% it appears as an unspectacular blue object without noticeable X–ray emission (it was not detected during the *RASS*).

However, among the polars, AR UMa is one of the brightest systems even in the low state, and I, therefore, obtained two *IUE* spectra of AR UMa (Table 3.6) as part of my project to extend the temperature scale of white dwarfs in polars. The unusual absorption near $1300\,\text{Å}$ shown in these spectra, along with the moderately strong circular polarization observed in the optical during the low state, was interpreted by Schmidt et al. (1996) as evidence for a high magnetic field of $B \sim 230\,MG$.

Thus, AR UMa is the long–sought example of a polar with a high–field magnetic white dwarf. Hitherto, all analysed polars contained white dwarfs with $B < 100\,MG$, a puzzling fact as single magnetic white dwarfs with B up to $1000\,MG$ are known (Schmidt & Smith 1995; see also Fig. 4 of Beuermann 1997). Fig. 3.18 shows a fit of a magnetic white dwarf model spectrum (Stefan Jordan, private communication) to the *IUE* data, yielding $B = 190\,MG$ and
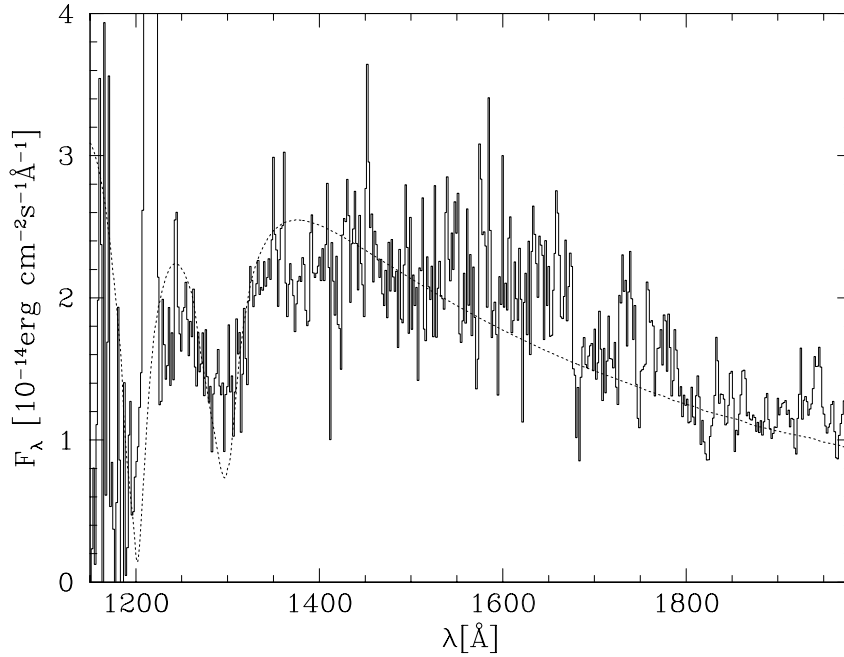
Figure 3.18: Low–state *IUE* spectrum of AR UMa with the best–fit magnetic white dwarf model for $B = 190\,\mathrm{MG}$ and T_{wd}=25 000 K. (model spectrum provided by S. Jordan). The absorption feature at 1300 Å is interpreted as σ^+ component of Lyα in a strong magnetic field (Schmidt et al. 1996).

$T_{\mathrm{wd}} = 25\,000\,\mathrm{K}$. However, these values should be regarded as preliminary as the *IUE* spectrum is an orbital average, smearing out any information about the field geometry.

Surprisingly, in AR UMa the *continuum* flux level does not increase during the high state (Schmidt et al. 1996). Furthermore, there is no compelling evidence for the emission of cyclotron radiation (Schmidt el al. 1996) or of thermal bremsstrahlung (Remillard et al. 1994) during the high state. However, once the accretion is switched on, AR UMa *is* a very strong source of soft X–ray emission (Remillard et al. 1994). All these observational findings may fit together as follows: for the high field strength in AR UMa, cyclotron cooling is so efficient that the stand–off shock collapses and is eventually buried in the white dwarf photosphere. Radiation transfer then reprocesses the primary thermal bremsstrahlung and cyclotron radiation into the observed strong soft X–ray emission. Thus, in contrast to the other polars discussed here, it is not possible to heat a larger region of the white dwarf surface by irradiation from the accretion column, and, hence, no increase of the ultraviolet continuum flux is expected for the high state. An additional/alternative model is that due to the high magnetic field, the accretion stream gets threaded already at the L_1 point, yielding a small accretion area and, hence, a high local mass flow rate which will again result in deep buried shocks (Schmidt et al. 1996).

Frame No.	Obs. date	ϕ_{mag}	Δ_{ϕ}
SWP57104L	11 May 96	0.560	0.157
SWP57110L	12 May 96	0.905	0.270
SWP57114L	12 May 96	0.701	0.270
SWP57120L	13 May 96	0.209	0.270
SWP57127L	14 May 96	0.001	0.270
SWP57131L	14 May 96	0.799	0.270
SWP57150L	16 May 96	0.804	0.270
SWP57154L	16 May 96	0.606	0.270
SWP57161L	17 May 96	0.502	0.270
SWP57164L	17 May 96	0.080	0.270
SWP57171L	18 May 96	0.807	0.270
SWP57175L	18 May 96	0.804	0.270
SWP57180L	19 May 96	0.522	0.270
SWP57184L	19 May 96	0.307	0.270
SWP57190L	20 May 96	0.711	0.202
SWP57191L	20 May 96	0.134	0.270
SWP57214L	22 May 96	0.625	0.270
SWP57218L	22 May 96	0.408	0.270
SWP57224L	23 May 96	0.113	0.270
SWP57228L	23 May 96	0.212	0.270
SWP57233L	24 May 96	0.308	0.270
SWP57234L	24 May 96	0.906	0.270

Table 3.7: *IUE* high–state observations of QQ Vul. Listed are the *IUE* frame number, the observation date, the orbital phase at the middle of the observation and the phase interval of the exposure.

3.6.5 QQ Vulpeculae

Even though already discovered in 1984 (Nousek et al. 1984), QQ Vul ($P_{\mathrm{orb}} = 222\,\mathrm{min}$) is still one of the more controversial polars. The soft X–ray light curve observed with *EXOSAT* and *ROSAT* switches between two very different shapes which was interpreted as the change from one–pole accretion to two–pole accretion (Osborne et al. 1987; Beardmore 1995b), similar to the change between the "normal" and "reversed" mode observed in AM Her (Heise et al. 1985; Sect. 3.5). However, the X–ray light curve in the suggested two–pole accretion mode is not yet fully understood. For a comprehensive discussion of the accretion geometry see Schwope (1991). Another intriguing point is the distance of QQ Vul. Mukai & Charles (1986) detected the secondary star in QQ Vul and derived a distance limit of 215 pc using the method of Bailey (1981). However, Mukai et al. (1988) discovered a close optical companion of QQ Vul and re–estimated the distanced to $d \geq 321\,\mathrm{pc}$. Schwope (1991) pointed out an error in the value of the surface brightness S_K used in both of these papers and re–evaluates the distance to be
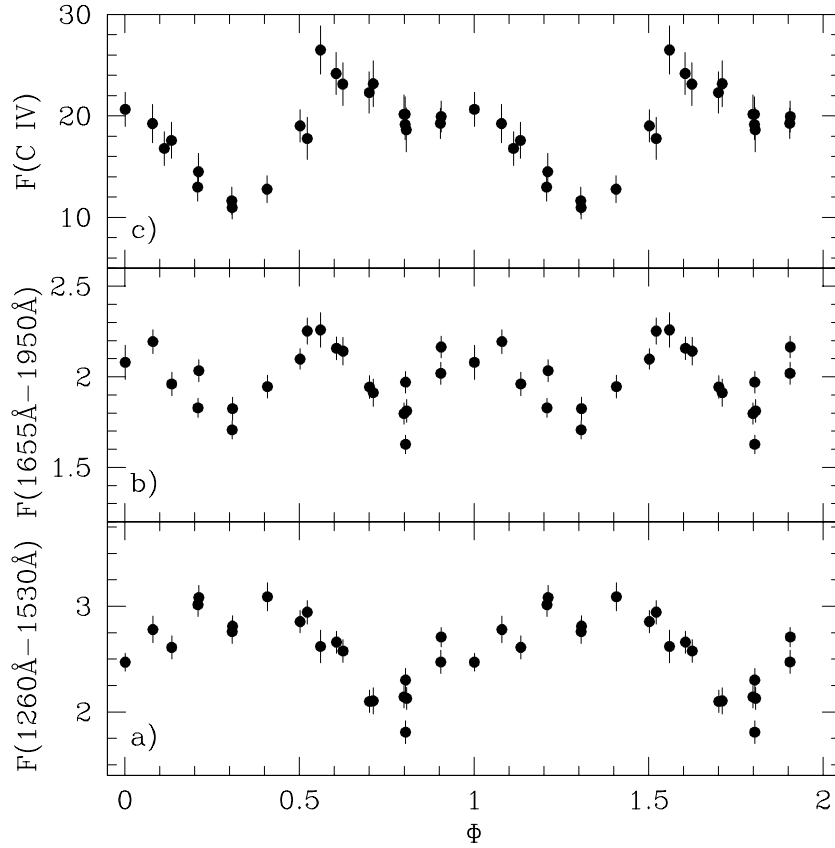
Figure 3.19: Ultraviolet light curves of QQ Vul in a high state: (a) far ultraviolet continuum, (b) near ultraviolet continuum and (c) line flux in C IV λ 1550. Continuum fluxes are in 10^{-14} erg cm^{-2}s^{-1}Å^{-1}, the line fluxes are in 10^{-13} erg cm^{-2}s^{-1}.

$d \geq 500$ pc. However, considering the low galactic latitude of QQ Vul ($b_{\mathrm{II}} = 5°$), the reported interstellar hydrogen column density of $N_{\mathrm{H}} \simeq 5 \times 10^{19}$cm^{-2} (Osborne et al. 1986, Beardmore et al. 1995b) seems rather low for $d \geq 500$ pc, even considering the fact that QQ Vul is located in an interarm region in the local interstellar space (e.g. Paresce 1984).

After the failure of the 5th gyro in March 1996, *IUE* continued observations in an one–gyro operation mode with very restricted pointing capabilities. The only polar observable in this mode was QQ Vul, of which a large set of phase–resolved spectroscopy was secured during a high state (Table 3.7). The orbital phases were computed using the ephemeris given by Osborne et al. (1987, based on private communication by Cropper),

$$\mathrm{HJD}(\phi_{\mathrm{mag}} = 0) = 2445234.8364(4) + 0.15452105(6)\mathrm{E} \tag{3.6}$$

where $\phi_{\mathrm{mag}} = 0$ is defined as the middle of the linear polarization pulse, i.e. when the accretion column is viewed almost perpendicular (however, see Schwope 1991 for a discussion on the ephemeris).
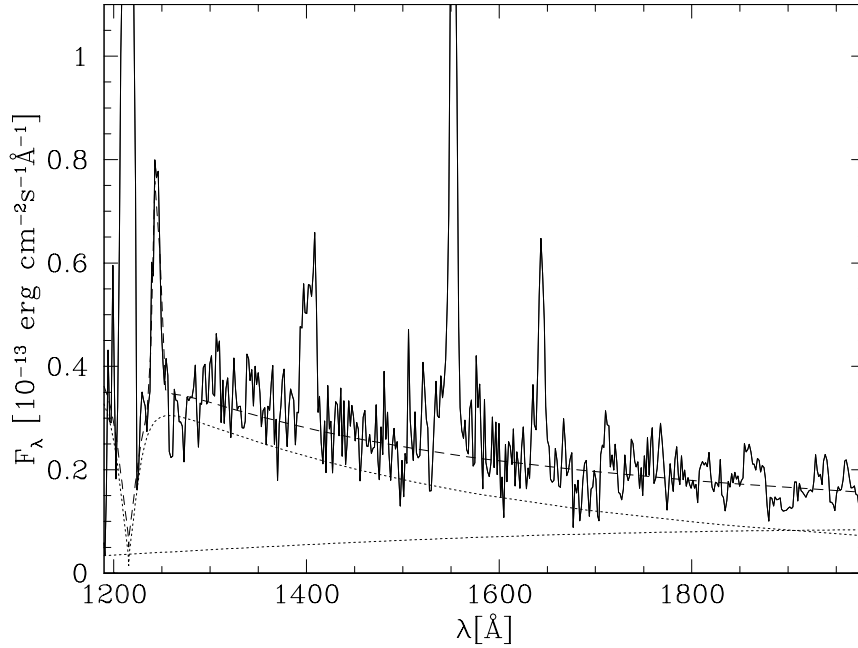
Figure 3.20: Bright–phase *IUE* spectrum of QQ Vul in high state. Also plotted are the contribution by the hot spot and the accretion stream (dotted) as well as the sum of the two models (dashed). The sum includes a Gaussian fit to N v λ 1240.

The ultraviolet light curves of QQ Vul are rather similar to those of AM Her. The far ultraviolet continuum (Fig 3.19a) shows a single–humped quasi–sinusoidal modulation, which I will interpret below as a hot spot on the white dwarf surface rotating in and out of view. The near ultraviolet (Fig 3.19b) and the emission of C IV λ 1550 (Fig. 3.19c) show a double–humped modulation with the primary minimum occurring at the maximum of the far ultraviolet flux. The near ultraviolet flux and the emission lines originate very likely in the illuminated accretion stream. The light curves can be understood as follows. At the phase of maximum far ultraviolet flux ($\phi_{mag} \sim 0.30$), the hot spot is viewed most directly; at the same time the line of sight is parallel to the accretion stream (at least to the part which couples to the magnetic field line) and the unilluminated backside of the stream is seen. At $\phi_{mag} \sim 0.55$, the stream is viewed from the side, and, hence, has the maximum projected area, yielding the flux maximum in the near ultraviolet and C IV λ 1550 emission. At $\phi_{mag} \sim 0.8$, the far ultraviolet flux has its minimum, the accretion spot is maximally obscured by the white dwarf; simultaneously the illuminated front side of the accretion stream is seen. This explains that the secondary minimum (Fig. 3.19c) is less deep. It is interesting to not that the scatter in the continuum flux is largest at this phase (covered with four SWP spectra). Finally, at $\phi_{mag} \sim 0.05$ the accretion stream is again viewed from the side, resulting in the second maximum in the near ultraviolet and C IV light curves[13].

---

[13]A similar double–humped light curve is observed for high–inclination systems in the infrared where it is due to the varying aspect of the Roche–lobe filling, deformed secondary star (ellipsoidal modulation)

The phase–resolved *IUE* spectra of QQ Vul allow to discern the Lyα absorption of the white dwarf/hot spot (Fig. 3.20). However, the contribution of the accretion stream to the ultraviolet flux is much stronger than e.g. in AM Her, hampering a clear separation of the fluxes from the white dwarf, the hot spot and the stream. I analysed the *IUE* data with the same methods as described for AM Her (Sect. 3.5.3.2), using a two–component model composed of a white dwarf model spectrum and a blackbody to account for the white dwarf and the stream emission, respectively. The resulting parameters are $T_{wd} \simeq 20\,000 - 25\,000$ K and $T_{spot} \sim 30\,000 - 40\,000$ K. To account for the observed modulation of the far ultraviolet flux, the heated region must be, as in AM Her, of the order of 10% of the white dwarf surface. The derived values are, however, less reliable than those of AM Her due (a) to the larger contribution of the accretion stream; (b) to the fact that no low state has been observed, and, hence, the temperature of the underlying white dwarf can not be derived independently from the high–state data; and, (c) to the unknown distance. In fact, the far ultraviolet flux can be due to the photospheric emission of the white dwarf/hot spot only for a distance $\lesssim 250 - 300$ pc, otherwise the white dwarf radius implied from the fit becomes to large. A check on the distance of QQ Vul is, therefore, mandatory.

Despite the caveat with respect to the distance, the above interpretation of the *IUE* data is appealing because of the similarities to the well–defined test case AM Her. A concluding remark concerns the small dip observed in the far ultraviolet light curve (Fig. 3.20) at $\phi_{mag} = 0.30$. This phase has been covered twice during the observation run, and both spectra display a somewhat lower flux compared to the spectra at $\phi_{mag} = 0.20, 0.40$. The phase of this far ultraviolet dip coincides with a short ($\Delta\phi \sim 0.07$) but total eclipse of the soft X–rays during the accretion mode defined by Osborne et al. 1987 as "complex", which the authors ascribe to two–pole activity. Also observed by *ROSAT*, this dip seems to be a rather stable feature in the soft X–ray light curve (Beardmore et al. 1995b). With the interpretation of the ultraviolet light curves given above, this dip should be due to the eclipse of part of the accretion–heated white dwarf surface by the accretion column. In this picture, the sum of inclination and colatitude of the accretion spot must exceed 90° in QQ Vul, as also suggested by Schwope (1991), based on polarization measurements.

3.6.6   RX J1313.2−3259

RX J1313.2−3259, henceforth RX J1313–32, is a long period ($P_{orb} = 252$ min) discovered from the *RASS* (Beuermann & Thomas 1993). I obtained a pair of SWP and LWP spectra of RX J1313–32 in March 1996 when the system was apparently in a low state. Despite the large difference in orbital periods, V834 Cen and RX J1313–32 show almost identical ultraviolet spectra in the low state (Fig. 3.14).

I have, therefore, fitted the *IUE* SWP spectrum with a two–temperature model as described in Sect. 3.6.2. The best fit is achieved for a white dwarf of $T_{wd} = 15\,000$ K plus a hot spot of $T_{spot} = 30\,000$ K covering $f \simeq 0.015$ of the white dwarf surface. Again assuming a white dwarf radius $R_{wd} = 8 \times 10^8$ cm, the implied distance is $d \simeq 140$ pc.

Fig 3.21 shows the *IUE* spectra along with an optical low–state spectrum obtained by K.
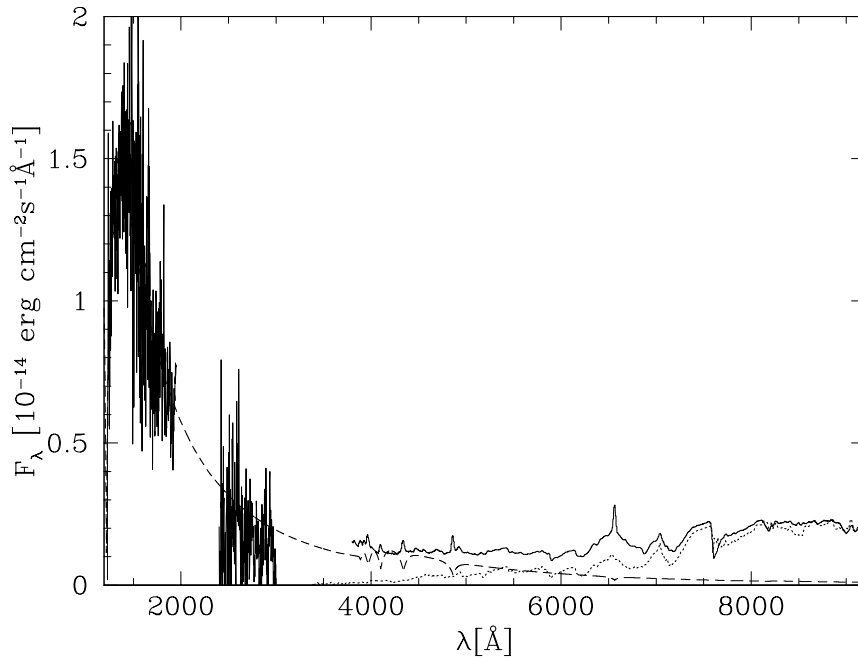
Figure 3.21:   *IUE* and optical low–state spectroscopy of RX J1313–32 (taken by K. Reinsch). The best–fit to the ultraviolet data is shown dashed, an appropriately scaled M4–dwarf (GL273) is shown dotted.

Reinsch. I fitted the emission of the secondary with the M4–dwarf GL273 and find $V = 17.18$ and $K = 12.22$. Following the methods described in Sect. 3.5.4.1, I find $S_K = 4.46$ and $R_2/R_\odot = 0.450 \pm 0.015$, yielding a distance estimate of $d \simeq 160\,\mathrm{pc}$. A somewhat later spectral type of the secondary, as may be more appropriate for the orbital period of RX J1313-32, would reduce the distance. Concluding, I note that the distance derived from the optical low–state spectrum entirely supports my fit to the ultraviolet spectrum.

3.7   Discussion, part I

3.7.1   The reprocessed component identified

Orbital phase–resolved *IUE* spectroscopy of AM Herculis in its high and low state revealed a strong orbital modulation of the far ultraviolet flux in phase with the X–ray emission from the main accreting pole. This flux modulation is accompanied by a change of the spectral shape, both in the continuum and in the Lyα absorption profile. I showed that these observational findings can be explained by a large, moderately hot spot on the white dwarf surface. I derived the effective temperatures and sizes of this accretion–heated pole cap in the low state and in the high state, as well as the effective temperature of the unheated white dwarf photosphere.

Comparing the ultraviolet excess flux with the observed cyclotron and hard X–ray fluxes indicated that irradiation from the accretion column is likely to cause the heating of that large spot. Identifying the ultraviolet emission of this hot spot as the reprocessed post–shock radiation solves, at least in the case of AM Her, the long–standing *soft X–ray puzzle*: $L_{UV} = L_{tb} + L_{cyc}$ instead of $L_{SX} = L_{tb} + L_{cyc}$, as originally suggested by Lamb & Masters (1979). In this picture, the observed intense soft X–ray flux of AM Her *must* originate through an accretion mode in which the primary bremsstrahlung is unseen, i.e. totally reprocessed. A viable hypothesis is heating of the photosphere by "blobby" accretion (Kuijpers & Pringle 1982), i.e. the accretion of dense blobs of matter which penetrate deep into the atmosphere, resulting in shocks covered by optically thick material.

Analysing all polars which clearly exhibit their white dwarf primary at ultraviolet wavelengths through a broad Lyα absorption profile, I found that four additional systems (Table 3.8) show strong evidence for the presence of rather large moderately hot spots. Recent work based on *HST/FOS* spectroscopy points to large ultraviolet spots also in ST LMi and UZ For (Stockman & Schmidt 1996) as well as in QS Tel (de Martino et al. 1997), even though the Lyα absorption of the white dwarf can not be discerned in these observations due to the very broad geocoronal Lyα emission. Especially interesting is the case of QS Tel. De Martino et al. (1997) find that the ultraviolet flux emitted by the hot spot of $\sim 45\,000\,K$ is of the same order of magnitude as the observed cyclotron flux. However, whereas in AM Her the fluxes of thermal bremsstrahlung and of cyclotron radiation are of the same order of magnitude, in QS Tel $F_{cyc}/F_{tb} \simeq 3$. This fits nicely into the picture for moderate accretion rates, as outlayed in Sect. 3.2, where an increasing magnetic field strength suppresses the thermal bremsstrahlung in favour of emission of cyclotron radiation.

The comparison between AM Her and QS Tel also gives a hint on the so far unanswered question: is the heating of the pole cap on the white dwarf caused by irradiation with cyclotron emission, thermal bremsstrahlung or both? The energy balance summarized in Table 3.5 is unlikely to be more accurate than a factor of ~ 2, hence no definite conclusion is possible. However, the observations of QS Tel point to a dominant rôle of cyclotron radiation, as thermal bremsstrahlung is not sufficient to power the ultraviolet excess observed in this system. Alas, few detailed models of irradiated white dwarf atmospheres have been computed so far. Test calculations with the code described by van Teeseling et al. (1994; 1996) show that the reflection albedo for hard X–ray photons is very high in the case of a pure hydrogen atmosphere due to Compton scattering (van Teeseling, private communication). Enrichment of the atmosphere with accreted metals may lower the reflection albedo; however, the *IUE* observations indicate rather low abundances (Sect. 3.5.4.5).

Based on these considerations, a self–consistent treatment of the radiation transfer in atmospheres irradiated by cyclotron radiation is a highly desirable exercise for the near future. However, a few preliminary conclusions can be drawn already from the present observational material.

(a) In the low state, the ultraviolet observations of polars can be described in all cases with model spectra of undisturbed white dwarfs. The observed Lyα absorption profiles (Figs. 3.7; 3.13;

System	P_{orb}[min]	B [MG]	T_{wd}[K]	T_{spot}[K]	f	Quality
DP Leo	90	31	16 000	27 000	0.030	A
V834 Cen	102	23	14 000	28 000	0.015	A
AR UMa	116	230	25 000	–	–	B
AM Her	186	14	20 000	24 000[1] 37 000[2]	0.10	A
BY Cam	202	28	22 000	–	–	B
QQ Vul	222	31:	22 500:[2]	37 000:[2]	0.10:	C
RX J1313–32	252	42	15 000	30 000	0.015	A

[1]: low state, [2]: high state

Table 3.8: Photospheric temperatures (T_{wd}) of white dwarfs in polars, as derived in Sect. 3.5 and Sect. 3.6. All systems but BY Cam and AR UMa show evidence for a moderately heated spot of T_{spot} covering a fraction f of the white dwarf surface. All temperatures are derived from low–state observations unless indicated otherwise. The magnetic field strengths are taken from the compilation by Beuermann (1997). A "quality" flag for the temperatures with the definition as in Table 3.1 is included.

3.14; 3.17) are almost 100 % modulated, indicating that the actual temperature stratifications in the white dwarf atmospheres do not deviate too much from those of undisturbed, i.e. non–irradiated ones.

(b) Irradiation generally causes the temperature profile of the white dwarf atmosphere to become flatter until, for high fluxes directed inwards, a temperature inversion is formed[14]. Subsequently, increasing the irradiating flux will gradually fill in the absorption lines and eventually result in the formation of emission lines. In the high state, the photospheric Lyα profile will generally be narrower due to the increased temperature. Hence, in the available *IUE* and *HST/FOS* observations, the geocoronal Lyα emission largely blends with the white dwarf photospheric absorption profile (Figs. 3.7c/d; 3.20). From these data it is, therefore, not possible to judge whether Lyα is filled in by emission or not. The far ultraviolet spectrum (900 Å ≲ λ ≲ 1200 Å) taken of AM Her in a high state with the *ORFEUS* experiment shows no strong Lyman absorption lines (Lyβ or higher members of the series), which would be expected from an undisturbed white dwarf photosphere (Raymond et al. 1995). Zeeman–splitting of the higher Lyman lines is larger than for Lyα, and may, therefore, hamper a clear detection of the various components in the low S/N *ORFEUS* spectra. Nevertheless, taken at face value, the *ORFEUS* spectra indicate that strong irradiation during the high state causes deviations from the temperature stratification of an unirradiated model, resulting in a flatter temperature gradient within the white dwarf atmosphere. A substantial temperature inversion, however, seems unlikely as no strong Lyγ or Lyδ emission is observed (Lyβ is blended with emission of O IV). However, the two spectra *do* show a clear modulation of the continuum flux with the orbital phase, consistent with that observed with *IUE*. The authors suggest that this modulation of the continuum is caused by a hot spot,

---

[14]see e.g. Brett & Smith (1993) for the case of irradiated M–dwarfs; van Teeseling et al. (1996) for irradiated hot white dwarfs.

supporting the results derived in Sect. 3.5.

A concluding remark concerns the derived areas of the accretion–heated spots: The size of the heated region depends sensitively on the height of the shock, on the inclination of the magnetic field lines in the accretion region and on the lateral extent of the accretion column. At present, the latter two parameters depend themselves heavily on observed properties of the system, so that I will not further discuss them here. However, bearing in mind the accretion scenarios of Sect. 3.2, predictions can be made for the shock height: higher field strengths will reduce the shock height and should, therefore, result in smaller and possibly hotter ultraviolet spots. Even though the observational evidence is meagre so far (Table 3.8), it agrees with the expected trend: apart from QQ Vul, where the derived parameters are still uncertain, AM Her has the lowest field strength and the largest hot spot while the other systems with higher fields display smaller spots. For very high fields, the shock may be totally buried or the accretion stream may be largely threaded into compact "blobs", so that no heating by irradiation is possible[15]. This is supported by the fact that in AR UMa no change of the ultraviolet continuum flux is observed during the transition between the high state and the low state and, hence, no additional heating of the white dwarf surface occurs during the high state.

3.7.2   The photospheric temperatures of white dwarfs in polars

I have derived photospheric temperatures of the white dwarfs in seven polars in an uniform way by fitting their ultraviolet spectra with white dwarf models. Including previously published values, I present here the so far largest set of photospheric white dwarf temperatures for polars (Table 3.1, 3.8). The values of T_{wd} are plotted against the orbital period in Fig. 3.22. The individual systems were assigned different symbols according to the reliability of the temperature estimate for their white dwarf. Inspection of the plot yield the following conclusions.

(a) All white dwarfs in polars are colder[16] than 30 000 K. The hottest system in the sample is V2301 Oph (T_{wd}=27 500 K), with a rather uncertain temperature estimate[17]. The systems with the best–determined temperatures cluster in the range T_{wd}=15 000–20 000 K. For non–magnetic white dwarfs in dwarf novae, much hotter photospheric temperatures are reported, e.g. U Gem with T_{wd}=30 000 K (Long et al. 1993) or TT Ari with $T_{wd} \simeq 50 000$ K (Shafter et al. 1985). It seems, hence, that the magnetic accreting white dwarfs are less heated than the non–magnetic ones. Possible reasons include a lower white dwarf mass or a lower mean accretion rate.

---

[15]However, a shock buried in the atmosphere *does* heat a very small area of the white dwarf to high temperatures of $\gtrsim 10^5$ K. In fact, the idea of "blobby" accretion (Kuijpers & Pringle 1982; Litchfield & King 1990) yields many individual buried shocks, one for each blob. These hot accretion spots emit in the soft X–ray regime and are thought to be the source of the large observed soft X–ray luminosity.

[16]V1500 Cyg has been excluded in this plot as its white dwarf was heated to $\sim 300 000$ K when nuclear burning started on its surface during the 1975 nova outburst. The white dwarf is, therefore, out of its secular thermal equilibrium.

[17]Szkody & Silber fitted white dwarf model spectra to an *IUE* high–state spectrum, their fits do not agree very well with the observed spectrum in the SWP wavelength range. Furthermore, the flux of a typical $0.6 M_\odot$ white dwarf would by far exceed the observed flux for the distance adopted by them.
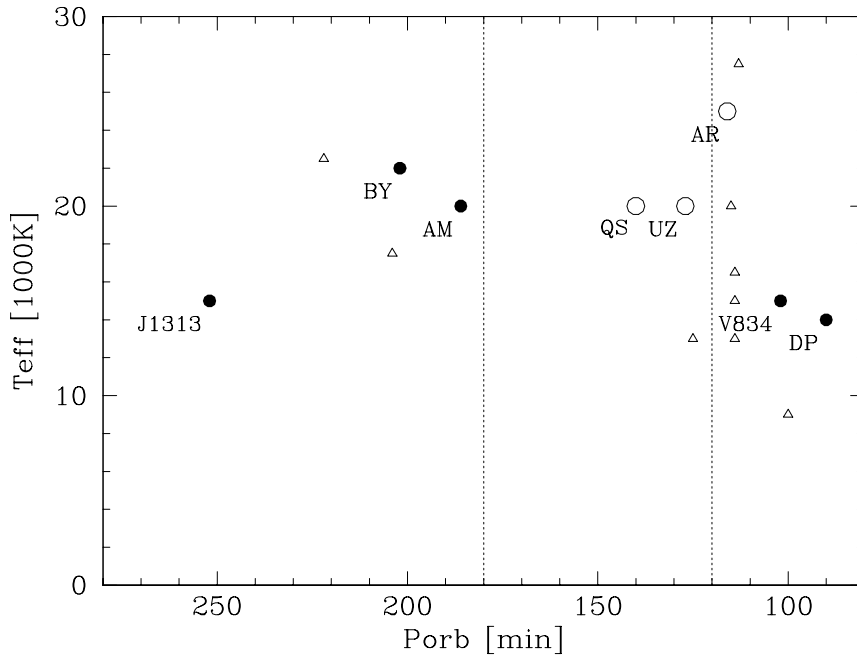
Figure 3.22: Photospheric temperatures of the white dwarfs in polars plotted against the orbital period. The orbital period gap is marked by dotted lines at two and three hours. Values are from Tables 3.1, 3.8. Symbols are defined according to the "quality" flag listed in the tables, (●) = A, (○) = B, and (△) = C. If several C–values are listed, an average temperature is plotted.

(b) Sion (1991) argued that the coolest accreting white dwarfs are found in polars. This may be partly due to a selection effect. The emission of polars during a low state is almost entirely dominated by emission from the two stellar photospheres. In dwarf novae, the hot spot on the disc rim and possibly the disc itself continuously remain sources of emission even if accretion stops, possibly outshining a rather cold white dwarf. In addition, inspecting Fig. 3.22 shows that the very low white dwarf temperatures reported for some polars fall in the less reliable category. The lowest reliable temperatures are $T_{\mathrm{wd}} \simeq 15\,000\,\mathrm{K}$ which is of the same order as for dwarf novae, e.g. WZ Sge (Sion et al. 1995a).

(c) Polars below the period gap contain somewhat colder white dwarfs than those above the gap. This is in agreement with the standard evolutionary scenario for cataclysmic variables which predicts that systems below the gap are in general older (age $> 10^9$ yrs) than systems above the gap (age $\sim 10^8$ yrs) and, hence, had time to cool down to lower temperatures. This also confirms the work of Sion (1991) who shows a similar plot, reproduced in Fig. 2.4, including all subtypes of cataclysmic variables. However, the sample is yet too small to derive any firm conclusions.

(d) RX J1313–32 is the first cataclysmic variable above the period gap ($P_{\mathrm{orb}} = 252\,\mathrm{min}$) containing a rather cool white dwarf. In Fig. 2.4 (from Sion 1991), RX J1313–32 falls far out of

the temperature range of long–period cataclysmic variables. It may be that this system expe-
riences a prolonged episode of low accretion activity below the secular mean for the magnetic
braking regime, causing cooling of the white dwarf. The existence of long–term ($\tau \gtrsim 100$ yrs)
oscillations of the accretion rate around the secular mean is suggested by the large spread in
observed mass transfer rates (Patterson 1984). King et al. (1995) suggested that irradiation of
the secondary star by the hot, accreting white dwarf may cause cyclic fluctuations of the mass
loss rate. The fact that RX J1313–32 undergoes a period of low mass transfer rate may be sup-
ported by the fact that it was hitherto always encountered at a rather low level of activity (K.
Reinsch & V. Burwitz, private communication). However, the system is known only since a few
years, so that this conclusion may be premature. Another possibility to explain the cold white
dwarf in RX J1313–32 is that that system is a rather young cataclysmic variable, i.e. it just
"recently" evolved into the semi–detached state, starting the mass transfer, but may have spent
a sufficiently long time before in the detached ($\dot{M} = 0$) pre–cataclysmic variable configuration.
In that case, the white dwarf had the chance to cool during that period just as his single relatives
do. Inspection of Fig. 2.2 gives for an $0.6 \, M_\odot$ single white dwarf of $T_{\mathrm{wd}} = 15\,000$ K an age of
2×10^8 years. Future mass transfer may heat up the white dwarf in RX J1313–32 again to a
typical accretion–induced temperature of $20\,000$–$30\,000$ K .

Chapter 4

Dwarf Novae

4.1 Overview

4.1.1 Disc accretion

In the absence of a strong magnetic field on the accreting white dwarf, the accretion stream flowing from the L_1–nose of the secondary star will follow a free–fall trajectory and, hence, stay within the orbital plane[1]. For the sake of angular momentum conservation, the stream can not hit the white dwarf but is slung back by the gravity of the compact star, and finally impinges onto itself close to the L_1 point, dissipating some of its kinetic energy. As the mass loss from the secondary continues, a ring of matter will form within the Roche–lobe of the white dwarf, rotating at Keplerian velocity. Viscous dissipation between radii of slightly different rotational velocity will heat the material, and the ring will spread towards the white dwarf[2]: an accretion disc is born. The actual mechanisms of angular momentum transfer within the disc are still debated, as is, hence, the very structure of the accretion disc. A very elegant theoretical formulation of the radial structure was developed by Shakura & Sunyaev (1973), parameterising all the unknown physics concerning the viscosity within the disc in a single parameter α which connects the tangential component of the viscous stress to the gas pressure[3]. Even though much work was invested in accretion disc modelling, many (or most) models still incorporate somewhere the α parameter.

Eventually, when the inner radius of the disc reaches the white dwarf, disc matter rotating at Keplerian velocities will be decelerated to the rotational velocity of the white dwarf. Following

---

[1]Actually, recent investigations have shown that part of the accretion stream hitting the disc rim may *spray* over the disc on a ballistic trajectory, possibly falling down close to the white dwarf (Armitage & Livio 1996; Hessman 1997)

[2]However, angular momentum conservation requires that at the same time some amount of matter is ejected *outwards*; this material is usually not considered any further by cataclysmic variable researchers

[3]In the original work by Shakura & Sunyaev (1973), the kinematic viscosity ν_k is expressed by $\nu_k = \alpha c_s H$, where c_s is the local sound velocity and H is the height of the disc.
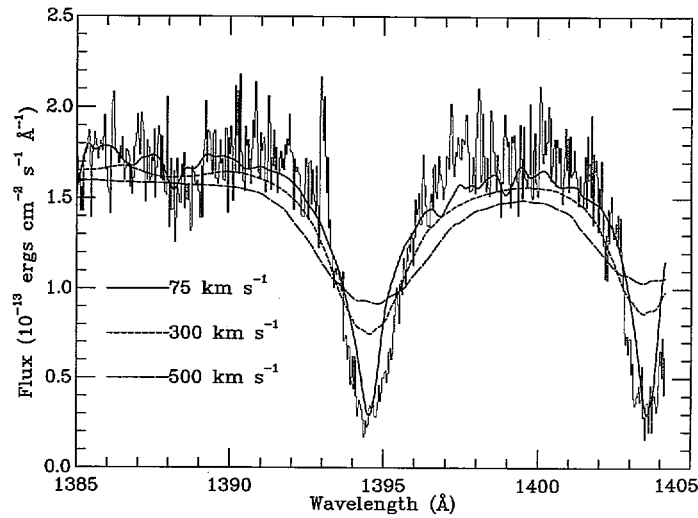
Figure 4.1: *HST/GHRS* spectrum of U Gem in quiescence (from Sion et al. 1994). The Si IV $\lambda\lambda$ 1394, 1403 doublet originates in the metal–enriched photosphere of the white dwarf. Shown are model spectra for a 35 000 K white dwarf with solar abundances rotating at three different velocities. The best fit is achieved for $v \sin i = 75 \, \mathrm{km \, s^{-1}}$.

the Virial theorem, only half of the available accretion energy has so far been dissipated in the disc and, hence, the same amount is available to heat up that geometrically small disc–star interface. The so–called *boundary layer* will thereby become a substantial source of EUV and X–ray emission and the following energy balance should hold:

$$L_{\mathrm{bl}} \simeq L_{\mathrm{disc}} \simeq \frac{1}{2} \frac{GR_{\mathrm{wd}}\dot{M}}{R_{\mathrm{wd}}} \tag{4.1}$$

However, in many systems the observed boundary layer luminosity is much lower than expected (e.g a factor 1/20 in VW Hyi; Mauche (1996)).

The energy range in which the emission will peak depends on the optical depth of the boundary layer. If the boundary layer is optically thin, which is probably the case for dwarf novae in quiescence, the emissivity of the material is low and the boundary layer will be heated up to $\sim 10^8$ K, radiating in the hard X–ray regime. In the optically thick case, as probably valid for dwarf novae during the outburst, the boundary layer temperature will reach only a few 10^5 K and will cool by blackbody emission in the EUV.

Modelling the structure and the spectrum of the boundary layer is even more complicated than it is for the accretion disc, as the physical processes relevant in mixing the accreting material into the white dwarf are largely unknown. I quote here only one parameter (obvious and relevant for this thesis) which possibly decreases the boundary layer luminosity: the angular velocity of the white dwarf[4]. In fact, if the white dwarf is rotating, the boundary layer luminosity

---

[4]It may be that the white dwarf is rotating differentially, being spun up to highest velocities at the equator by accretion of angular momentum.

is given by (e.g. Kley 1991)

$$L_{\rm bl} = \frac{1}{2} \frac{GR_{\rm wd}\dot{M}}{R_{\rm wd}} \left(1 - \frac{\Omega_{\rm wd}}{\Omega_{\rm K}(R_{\rm wd})} \right)^2 \qquad (4.2)$$

where $\Omega_{\rm wd}$ is the rotational velocity of the white dwarf and $\Omega_{\rm K}(R_{\rm wd}) = \sqrt{GR_{\rm wd}/R_{\rm wd}}$ is the Keplerian velocity at the white dwarf surface ($\sim 3000\,{\rm km\,s^{-1}}$ for a $0.6\,M_\odot$ white dwarf). So far, rotational velocities have been determined only for three dwarf novae, namely VW Hyi ($v\sin i \simeq 400\,{\rm km\,s^{-1}}$; Sion et al. 1997), U Gem ($v\sin i \simeq 75\,{\rm km\,s^{-1}}$; Sion et al. 1994; see Fig. 4.1) and WZ Sge ($v\sin i \simeq 1200\,{\rm km\,s^{-1}}$; Cheng et al. 1997). This large spread in the rotational velocities clearly indicates that neglecting this parameter may lead to large errors in both, modelling and interpreting the boundary layer emission of dwarf novae.

4.1.2   Dwarf nova outbursts

Dwarf novae acquired their name long before their nature was understood by the fact that they show more or less regularly sudden increases of their visual magnitude by $\Delta V \sim 2 - 6$, lasting for a few days to weeks. In contrast, the *real* novae usually have only one observed[5] outburst and brighten by $\Delta V \gtrsim 10$. A fundamental difference between these two classes is the physical engine powering the outburst: In novae, it is the sudden thermonuclear ignition of accreted hydrogen onto the surface of a white dwarf resulting in an explosive ejection of part of the white dwarf envelope. The outbursts in dwarf novae are due to a sudden increase of the mass flow through the disc and onto the white dwarf, hence, to the release of potential energy of matter falling in the gravitational well of the white dwarf.

Concerning the cause of the dwarf nova outbursts, two models have been proposed. (a) In the mass–transfer–burst model instabilities in the atmosphere of the secondary star cause unstable mass flow through the L_1 point (Bath 1973). (b) In the nowadays largely accepted disc–instability model the dwarf nova outbursts originate in the disc. The matter is stored in the accretion disc until a mode transition occurs which is associated with a sudden increase in the viscosity, a substantially larger mass flow rate through the disc, and, hence, a brightening of the disc and the boundary layer. Basically, the disc–instability mechanism is based on the sensible dependence of the opacity from the ionization fraction of hydrogen (somewhat similar to the κ mechanism which is based on the ionization equilibrium between He I and He II causing the pulsations in Cepheids). Observational evidence largely supports the disc–instability model. In the disc–instability model, the mass loss rate from the secondary is generally assumed to be

---

[5]As dwarf novae and novae both involve accreting white dwarfs, they refer to different phenomena on the same type of object: after $\sim 10^5$ dwarf nova outbursts, the accreted material may reach the condition for a thermonuclear runaway. However, the usual recurrence time is so long (several $1000\,{\rm y}$) that only one outburst per nova is observed. In addition, some novae show repetitive outbursts which may also be of thermonuclear nature and are, therefore, called *recurrent novae*. If so, these have to be systems with extremely high mass transfer rates and very massive white dwarfs. However, some recurrent novae may also be misidentified dwarf novae with extreme long outburst cycles (as e.g. WZ Sge).

constant. However, the long–term light curves of (discless) polars show that in these systems the mass loss rate of the secondary *does* vary significantly on timescales of $\sim$ months to years (Sect. 3.3; Fig. 3.5). Intuitively, there is no reason why the secondary star in dwarf novae should not follow the same behaviour. However, the accretion disc acts as a large reservoir of matter, probably ironing out any fluctuations of the mass loss rate of the secondary. For a recent review on dwarf nova outburst modelling see Osaki (1996).

Long–term monitoring by dedicated amateur astronomers resulted in detailed optical light curves of many dwarf novae, showing a variety of outburst morphologies. Similar to the development in particle physics during the 1960's and 70's where each new nuclear fragment found in collider experiments defined a new elementary particle, a large variety of non–magnetic cataclysmic variable subclasses was defined in order to account for the observed differences in the long–term variability. At present, a more unified classification scheme based on the value of the mass transfer rate is attempted (Warner 1997). I will define here only the systems encountered in the discussion below: U Gem systems display quasi-regular outbursts, the duration of the outbursts shows a bimodal behaviour. SU UMa dwarf novae are short period systems ($P_{\mathrm{orb}} \lesssim 2\,\mathrm{h}$) which show in addition to the normal outbursts brighter and much longer lasting superoutbursts[6]. WZ Sge stars, presently also called TOADs (Tremendous Outburst Amplitude Dwarf novae), have rather rare but very bright and long lasting outbursts and may also be grouped among the SU UMa stars. This characteristic led to the miss–classification of WZ Sge as a recurrent nova, as it had only three observed outbursts in this century.

4.1.3   Dirty white dwarfs

Even though the compact objects in dwarf novae were thought to be white dwarfs since long (e.g. Kraft et al. 1969) and first spectroscopic evidence for a white dwarf was found even earlier in WZ Sge (Greenstein 1957)[7], space–based ultraviolet observatories had to be awaited to convincingly confirm the white dwarf nature of the accreting primary. The first spectroscopical identifications of accreting white dwarfs in cataclysmic variables were broad Lyα absorption profiles detected in *IUE* spectra of the quiescent dwarf novae U Gem (Panek & Holm 1984) and VW Hyi (Mateo & Szkody 1984).

On theoretical grounds, Smak (1984) argued that the white dwarf should be the dominant source of ultraviolet emission in all quiescent dwarf novae and derived effective temperatures for the white dwarfs in 11 dwarf novae. Using published estimates for the white dwarf masses and the distances of the systems, Smak converted the effective temperatures in luminosities and found a clear correlation of the luminosities with the average mass transfer rates from Patterson

---

[6]These superoutbursts may be caused by a tidal interaction between an elliptical precessing disc and the secondary star, see Osaki (1996).

[7]However, at that time WZ Sge was considered a recurrent nova and not a dwarf novae. The identification of the white dwarf as source of the observed broad Balmer absorption lines was doubted later by Robinson et al. (1978), who argued that these lines originate in an optically thick accretion disc rotating at Keplerian velocities. Nowadays, the white dwarf case seems very likely again, based on *HST* observations of very broad Lyα profile typical of cool white dwarfs (Sion et al. 1995a).

(1984). However, Smak (1984) admitted that the errors in his derived temperatures are likely rather large[8].

In contrast to the accretion geometry in polars (Sect. 3.2), the white dwarfs in dwarf novae accrete over a rather large equatorial belt. In the absence of a strong magnetic field, the accreted material (with bona–fide solar abundances) may spread over the white dwarf surface, leading to a photosphere largely enriched by heavy elements. In general, the outburst period is short compared to the diffusion timescale so that metal lines should contribute significantly to the ultraviolet opacity. The first direct evidence of heavy elements in the photospheres of the accreting white dwarfs in cataclysmic variables was found in U Gem by Panek & Holm (1984), who noted that the observed ultraviolet spectrum resembles that of early B–stars, with the difference of the much broader Lyα absorption profile in U Gem. Observations of U Gem with the *Hopkins Ultraviolet Telescope* (*HUT*) and with *HST* confirmed roughly solar abundances in the photosphere of the white dwarf in U Gem (Long et al. 1993, 94, 95; Sion et al. 1994). Apart from U Gem, photospheric abundances were derived only for the white dwarfs in VW Hyi (Gänsicke 1993; Sion 1995b) and WZ Sge (Sion et al. 1990, 95a). In both systems, the abundances of several elements differ from solar values. A large overabundance of phosphorus observed in VW Hyi was interpreted by Sion et al. (1997) as being produced from proton capture by Si during a previous thermonuclear runaway. However, a general explanation for the different observed abundances does not exist so far.

4.2 Heating of the white dwarf by disc accretion

Patterson & Raymond (1985a,b) compared the large sample of X–ray observations of dwarf novae collected with the *Einstein* satellite with the theoretical predictions for the boundary layer emission. They pointed out that, for low $\dot{M}$, the white dwarfs in all (disc–accreting) cataclysmic variables should be heated substantially by hard X–ray emission from the optically thin boundary layer.

Using simple estimates for the scale height and for the luminosity of the boundary layer and assuming that all radiation intercepted by the white dwarf is thermalized, they computed the expected effective temperatures of what they called the *pseudo white dwarf* as a function of the accretion rate. Comparison with the observed white dwarf temperatures in 15 systems[9] led

---

[8]Smak obtained the white dwarf temperatures by comparing ultraviolet fluxes measured with the *IUE* and the *Astronomical Netherlands Satellite* (*ANS*) with published white dwarf model spectra (Wesemael et al. 1980). However, it appears today very doubtful whether the white dwarf dominates the ultraviolet emission in all dwarf novae during quiescence; in most cases there is few to no spectroscopic evidence for photospheric emission from the white dwarf (e.g. SS Cyg, WX Hyi). Other authors used recently a similar approach as Smak in order to derive white dwarf temperatures in dwarf novae (Hassall & La Dous 1996), these temperatures should be judged with the same precaution as those of Smak (1984).

[9]To my knowledge, the article given by Patterson & Raymond (1985) as reference for the temperature of YY Dra, Patterson et al. (1985) *in preparation*, never appeared. However, a temperature estimate ($T_{wd} \leq 30\,000$ K) for YY Dra, based *HST/FOS* observations, was published by Haswell et al. (1997).

the authors to the conclusion that, indeed, X-ray heating is a valuable hypothesis to explain the observed temperatures.

In the same year, Hassall et al. (1985) published *IUE* spectroscopy of the dwarf nova WX Hyi obtained during an outburst and throughout the following quiescence. The observations indicate that after the end of the outburst the SWP flux continues to gradually decrease for ~ 6 days. Similarly, a decline of the ultraviolet flux of $\sim 20 - 30\,\%$ throughout quiescence was observed in VW Hyi. This observed flux decline was interpreted by Pringle (1988) as the decreasing emission of a cooling white dwarf which was heated during the previous outburst. Another hint that the white dwarf in dwarf novae may be heated during the outburst came from U Gem, where the white dwarf was already clearly identified by its photospheric Lyα absorption profile: Kiplinger et al. (1991) presented a series of *IUE* spectra taken throughout one quiescent interval and concluded that the white dwarf cools from $\gtrsim 40\,000\,\mathrm{K}$ shortly after outburst to $\sim 30\,000\,\mathrm{K}$ in quiescence.

Summarized, there is some observational and theoretical evidence that the white dwarfs in disc–accretors are heated by accretion and that dwarf novae may offer the chance to quantify the amount of energy deposited in the white dwarf envelope thanks to their periodic on/off accretion phases. Before I will examine in detail the case of the dwarf nova VW Hyi in Sect 4.3 I introduce below the different approaches to model the heating of the white dwarf during dwarf nova outbursts which have been published so far.

4.2.1 Irradiation

Pringle (1988) suggested that the post–outburst decline of the ultraviolet flux observed in VW Hyi is due to cooling of the white dwarf heated during the outburst by irradiation from an optically thick hot boundary layer. He simulated the effect of irradiation semi–analytically by solving the envelope solution of a white dwarf atmosphere including a time dependent outer temperature boundary. Essentially, this equals putting the white dwarf into an infinite heat bath causing energy diffusion into the star. Pringle's calculations show that the white dwarf is heated down to a depth where its intrinsic temperature equals the temperature of the external heat bath. Heating and cooling occurs basically on the Kelvin–Helmholtz timescale of the mass of the envelope above that depth. To account for the ultraviolet flux decline observed in VW Hyi, a boundary layer temperature of the order of $10^6\,\mathrm{K}$ is needed. For lower temperatures only a thin layer is heated for which the cooling timescale is much too short compared to observation. Pringle simulated the different response of the white dwarf envelope to a normal and a super-outburst by varying the duration for which the external heat bath is in place. He found that a noticeable difference in the post–outburst cooling timescale occurs only for boundary layer temperatures above $10^6\,\mathrm{K}$, as only for temperatures this high the Kelvin–Helmholtz timescale of the envelope mass involved is longer than the duration of a normal outburst.

Recently, Popham (1997) evaluated the amount of emission intercepted by the white dwarf from the inner disc and from the boundary layer. He finds that for thin discs, as probably present in cataclysmic variables, the irradiation of the white dwarf by the disc is negligibly

small. However, the energy transferred from the boundary layer to the white dwarf may be as high as 25% of the total accretion luminosity. Estimating the timescale to reach thermal equilibrium between the boundary layer and the outer layers of the white dwarf, Popham finds that in a typical dwarf nova less than a day is necessary. He compares his findings with those of Pringle (1988) and concludes that heating by irradiation from the boundary layer is likely to be most important in dwarf novae with massive white dwarfs and/or extremely high accretion rates where high temperatures are reached at the bottom of the boundary layer.

4.2.2 Compression

Sion (1995) simulated the thermal response of a white dwarf to periodic compression by mass accretion during dwarf nova outbursts. He used a standard Henyey–type stellar evolution code, modified to allow for time–dependent mass accretion. The simulations were carried out through 15–55 consecutive dwarf nova outbursts, following the structure readjustment of the white dwarf in small time steps. The two simplifications of this model are radially symmetric accretion and neglect of radiative heating from the hot boundary layer. The results of Sion's simulations are (a) that the white dwarf is heated by cyclic mass deposition on its surface to an equilibrium temperature $\sim 10\,000 - 20\,000\,\mathrm{K}$ higher than its intrinsic ($\dot{M} = 0$) temperature and (b) that during a mass deposition episode ($=$ dwarf nova outburst) the actual photospheric temperature is raised by $\sim 5000 - 10\,000\,\mathrm{K}$ above the accretion–induced equilibrium temperature, followed by cooling on a timescale of weeks to months.

4.2.3 Viscous heating by a rapidly rotating accretion belt

A third possibility to heat the white dwarf due to disc accretion was discovered as a by–product of nova theory. In order to overcome the simplification of spherically symmetric accretion, Kippenhahn & Thomas (1978) studied the evolution of matter accreted in an equatorial belt on a white dwarf. They found that this belt will keep on rotating rapidly very long ($\geq 10^6$ years) if molecular viscosity is the only mechanism of friction between the belt and the white dwarf. Kutter & Sparks (1987) describe the accretion of matter transferring angular momentum onto an initially non–rotating white dwarf, largely based on the work of Kippenhahn & Thomas (1978). They include, however, an expression for turbulent mixing between the rotating belt and the white dwarf, reducing the timescale of spin–up of the outer layers of the white dwarf. They find that while the accreting material penetrates into the star and spreads towards the poles angular momentum is conserved but kinetic energy is gradually converted into heat. In an application of their model to a $1.0\,M_\odot$ initially non–rotating white dwarf accreting at $\dot{M} = 4.23 \times 10^{-10} M_\odot\,\mathrm{yr}^{-1}$ (Kutter & Sparks 1989), they find that heating due to shear mixing peaks after 3180 yrs with a luminosity of $0.152\,L_\odot$ (or $\sim 20\,\%$ of the rotational kinetic energy). While accretion goes on, heating due to shear mixing becomes less important as the outer layers of the white dwarf are spun up near to Keplerian velocities. It should be noted that this model was computed, like most nova models, for the case of a constant accretion rate. A detailed model of

the heating of the white dwarf due to shear mixing during a nova outburst is still missing. As an initial step, an explorative study for the cooling of the white dwarf in WZ Sge was presented by Sparks et al. (1993).

4.2.4   Ongoing heating by disc evaporation

A completely different explanation of the observed decline of the ultraviolet flux, if interpreted as a decrease of the white dwarf effective temperature, is to assume that the accretion rate is high enough to heat the white dwarf even after the end of the (optical) outburst. If a mechanism can be found that predicts the accretion rate to decline throughout the quiescent interval, the ultraviolet flux decline might be due to a decreasing *instantaneous* heating of the outermost atmosphere layers rather than to cooling (i.e. a decrease in internal energy of the white dwarf envelope).

Even though targeted at another aim[10], Meyer & Meyer–Hofmeister (1994) proposed such a model. They show that a cool accretion disc must lose mass to a hot corona situated on top of the disc; subsequently, the matter flows from this corona onto the white dwarf. The so–called *coronal syphon flow* is sustained by the fact that the corona heats the underlying disc and, thereby, evaporates the chromosphere of the disc. In this process, the inner disc regions vanish gradually as they get accreted on the white dwarf through the coronal syphon flow. The velocity at which the evaporation proceeds to larger disc radii decreases as does, hence, the accretion rate through the coronal flow.

---

[10]The model was primarily developed to explain the depletion of the inner disc in dwarf novae during quiescence. Such a "hole" is required to model the observed ultraviolet delay in some dwarf novae during outburst, i.e. the fact that the ultraviolet flux rises roughly a day later than the optical flux.

4.3 VW Hydri

4.3.1 Introduction

VW Hyi is a short–period ($P_{orb} = 107$ min) dwarf nova of the SU UMa type. It is one of the brightest dwarf novae ($V_{max} \simeq 8.5$) and shows frequent outbursts (normal outbursts every $\sim$ 27 d; superoutbursts every $\sim$ 180 d). These two characteristics made VW Hyi a favoured target for optical and ultraviolet studies, following the evolution of the system throughout several entire outbursts. A large multiwavelength campaign on VW Hyi was carried out in 1984 and is reported by Pringle et al. (1987), van Amerongen et al. (1987), Verbunt et al. (1987), Polidan & Holberg (1987), and van der Woerd & Heise (1987).

The *IUE* observations obtained during this campaign showed a decline of the ultraviolet flux throughout quiescence, both after a normal and after a superoutburst (Verbunt et al. 1987). The authors tried to confirm this trend using the available *IUE* archive data and found it to be less definitive when combining all spectra. They concluded that the interoutburst flux decline may be camouflaged by orbital variations and by non–uniform exposures (i.e. instrumental effects). However, Verbunt et al. (1987) plotted the ultraviolet fluxes over an interoutburst phase, thus normalising the time between two outbursts. As I will show below, this scrambled the trend of the interoutburst flux decline. Verbunt et al. (1987) and Pringle et al. (1987) showed that the origin of the SWP flux may be a 20 000 K white dwarf or a cool ($T \lesssim 13\,000$ K) accretion disc, without drawing a firm conclusion. However, using *HST* spectroscopy, Sion et al. (1995b,c) confirmed the identification of the flux turnover at $\lambda \lesssim 1400$ Å as pressure–broadened Lyα absorption in the white dwarf photosphere, first suggested by Mateo & Szkody (1984).

An earlier version of this section has been published in Gänsicke & Beuermann (1996).

4.3.2 Observations

IUE has observed VW Hyi 13 times between 1979–1990, yielding a total of 86 low–resolution SWP spectra of which 28 where obtained during late decline and quiescence (Table 4.1). All spectra were taken through the large aperture, resulting in a spectral resolution of $\sim$ 6 Å. I used spectra reprocessed with the recent *IUESIPS* procedures in order to obtain a coherent wavelength and flux calibration. I restricted my analysis to the SWP data as only few LWP/LWR spectra of sufficient quality are available. Description of the data obtained up to 1984 was given by Bath et al. (1980), Hassall et al. (1983), Mateo & Szkody (1984), Schwarzenberg-Czerny et al. (1985), and Verbunt et al. (1987). I determined the time elapsed since the last outburst (days past outburst=d.p.o.) from the long–term photometric database of the variable star section of the Royal Astronomical Society of New Zealand (VSS RASNZ), defining $t = 0$ when V drops below 12.0. This is about two days after the begin of decline from maximum. I chose this definition because it is more accurate (± 0.5 days) than the time when the system reaches optical quiescence. I find that the ultraviolet flux shows an exponential decline with time which decreases markedly faster after a normal outburst than after a superoutburst (Fig. 4.4a).
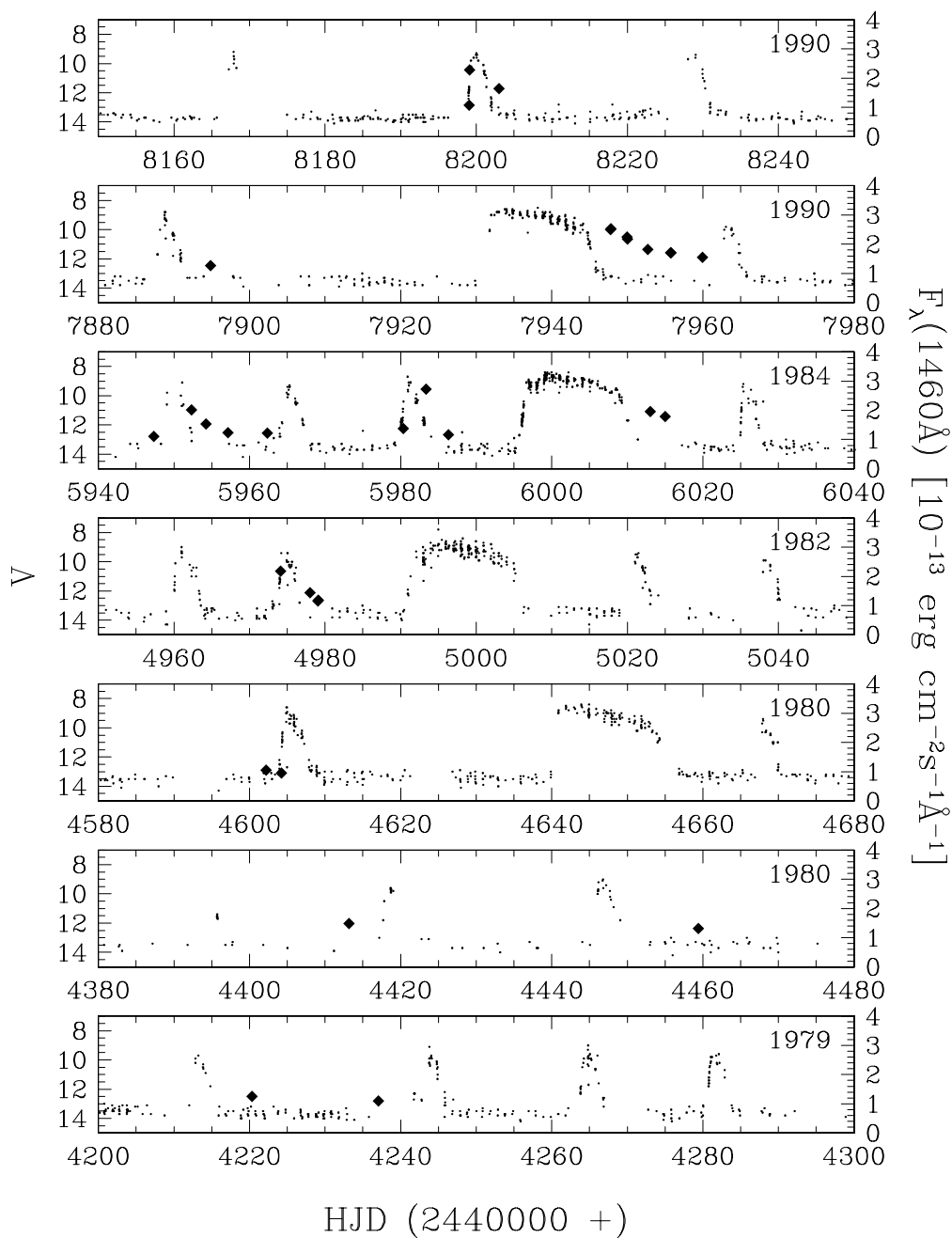
Figure 4.2: Long–term optical light curve of VW Hyi. Diamonds mark ultraviolet fluxes measured by *IUE*, plotted linearly to better demonstrate the interoutburst flux decrease following the outbursts (very nice e.g. after the superoutburst on HJD = 2 447 940). The optical data shown here have kindly been provided by F. Bateson

Frame No.	HJD $-2\,440\,000$	t.p.o.	d.p.o	Frame No.	HJD $-2\,440\,000$	t.p.o.	d.p.o
SWP07380L	4220.33	N	5.1	SWP24157L	5983.36	N	0.4
SWP07498L	4237.08	N	21.9	SWP24166L	5986.34	N	3.3
SWP09345L[n]	4413.18	N	17.3	SWP24415L	6013.05	S	2.7
SWP09726L	4459.40	N	10.3	SWP24435L	6015.02	S	4.4
SWP10911L	4602.20	N	41.1	SWP37943L	7894.84	N	4.0
SWP10928L[n]	4604.22	N	43.1	SWP38251L	7947.77	S	2.0
SWP15952L	4974.11	N[1]	-2.3	SWP38252L	7947.84	S	2.0
SWP15988L	4978.04	N	1.7	SWP38263L	7949.94	S	4.1
SWP16000L	4979.07	N	2.7	SWP38264L	7950.02	S	4.4
SWP16001L	4979.12	N	2.8	SWP38283L	7952.71	S	6.9
SWP23865L	5947.35	N	22.0	SWP38304L	7955.71	S	9.9
SWP23905L	5952.32	N	0.6	SWP38305L	7955.78	S	10.0
SWP23923L	5954.26	N	2.5	SWP38324L	7959.92	S	14.1
SWP23951L	5957.17	N	5.4	SWP40028L	8199.06	N[1]	-2.4
SWP23999L	5962.34	N	10.5	SWP40029L	8199.12	N[1]	-2.4
SWP24131L	5980.36	N[1]	-2.6	SWP40073L	8203.03	N	1.5

t.p.o.: type of previous outburst. N=normal, S=super;

d.p.o.: days past previous outburst.

[1] on the rise to the next outburst; [n] very noisy

Table 4.1: *IUE* observations of VW Hyi during quiescence

The evolution of the ultraviolet spectrum of VW Hyi following normal (N) and superoutbursts (S) is shown in Fig. 4.3. Except for the depth of the N v λ 1240, Si IV λ 1400 and C IV λ 1549 absorption lines, the overall spectral shape remains unchanged while the flux drops by a factor of ~ 50. In an approximate way, the spectral appearance of VW Hyi can be characterized by three components:

(1) A disc remnant displaying a very blue spectrum with strong absorption lines of N v λ 1240, Si IV λ 1400 and C IV λ 1549 as well as broad undulations longward of 1600 Å.

(2) An optically thin emission–line component. Particularly strong is C IV λ 1549. Weaker emission of N v λ 1240 and Si IV λ 1400 is detected in several spectra. The emission lines are particularly strong following a superoutburst with the line strength decreasing throughout the interoutburst period. Spectra taken deep in quiescence do not show any line emission anymore (Fig 4.3).

(3) The white dwarf with its characteristic broad photospheric Lyα absorption profile (Mateo & Szkody 1984; Sion et al. 1995b) superimposed by strong absorption troughs of Si II λ 1260, Si III $\lambda\lambda$ 1295–1310 and C II λ 1335. The white dwarf may itself have a composite spectrum due to variations of temperature and composition over its surface.

From optical spectroscopy obtained during quiescence in January 1989 I derive a temperature of the hot spot of 10 000 K which agrees with the previous estimate of Mateo & Szkody (1984). The contribution of this component to the SWP flux is less than 6% at 1600 Å. During and close to outburst maximum, the ultraviolet spectrum is dominated by the accretion disc. The white dwarf and the emission lines appear ~ 0.4 days after the outburst. Spectra taken 22 and 41 days after a normal outburst show no further evolution.

4.3.3   Analysis

In order to derive the variation of the flux contribution of the white dwarf and of its photospheric temperature, I decomposed the 28 *IUE* spectra taken during late decline and quiescence, starting 0.4 days after outburst (Fig. 4.3) when the spectrum is still disc dominated. In order to account for the three spectral contributions described above I use the following components:

(1) Considering the large uncertainties in current accretion–disc model spectra, I chose to describe the contribution of the (remnant) accretion disc by an average *observed* ultraviolet spectrum of VW Hyi near maximum, when the contribution of the white dwarf is negligible.

(2) Considering the large number of metal absorption lines superimposed on the Lyα profile (Gänsicke 1993; Sion et al. 1995b), it is obvious that a reliable determination of the white dwarf photospheric temperature is not possible using the pure–hydrogen models described on p. 18. Therefore, I used for the white dwarf contribution a grid ($\log g = 8.0$ and $11\,000\,\mathrm{K} \leq T_{\mathrm{eff}} \leq 30\,000\,\mathrm{K}$) of model spectra calculated for solar abundances kindly provided by I. Hubeny. The models have been convolved with a Gaussian of 6 Å FWHM to match the *IUE* wavelength resolution. From the observations, there is no sign for additional broadening due to rotation of the white dwarf. Given the $1200\,\mathrm{km\,s^{-1}}$ velocity resolution of *IUE*, this is consistent with the measured rotational velocity of $v\sin i \lesssim 600\,\mathrm{km\,s^{-1}}$ (Sion et al. 1995b). The use of solar–abundance models is justified as I am mainly interested in the white dwarf temperature and as the metal abundances do not significantly affect the temperature structure of the white dwarf atmosphere. The most prominent (at *IUE* resolution) deviation from solar abundances is found in the two Si II doublets (1260,65 Å, 1527,33 Å) which are without exception stronger in the models than in the observed spectra. I, therefore, excluded these two regions from the fit. I will discuss the possibly inhomogeneous distribution of metals over the white dwarf surface below.

(3) The optically thin component was represented by Gaussian emission lines of N V λ 1240, Si IV λ 1400 and C IV λ 1549. The lines were restricted to be entered within ± 3 Å of the rest wavelengths and to have $2\,\text{Å} \leq \mathrm{FWHM} \leq 12\,\text{Å}$. I neglected the corresponding optically thin continuum.

The fits were performed using an evolution strategy algorithm (Rechenberg 1994) with six free parameters (the scaling factors for all five components and the white dwarf temperature) and six semi–free parameters (the line centres and FWHM). The employed code turned out to be a versatile tool for such multidimensional optimisation problem; a brief overview of the algorithm is given in Appendix B. As *IUE* is not a photon–counting instrument it is difficult to assess the random error in the observed flux. In principle, the statistical error can be deduced
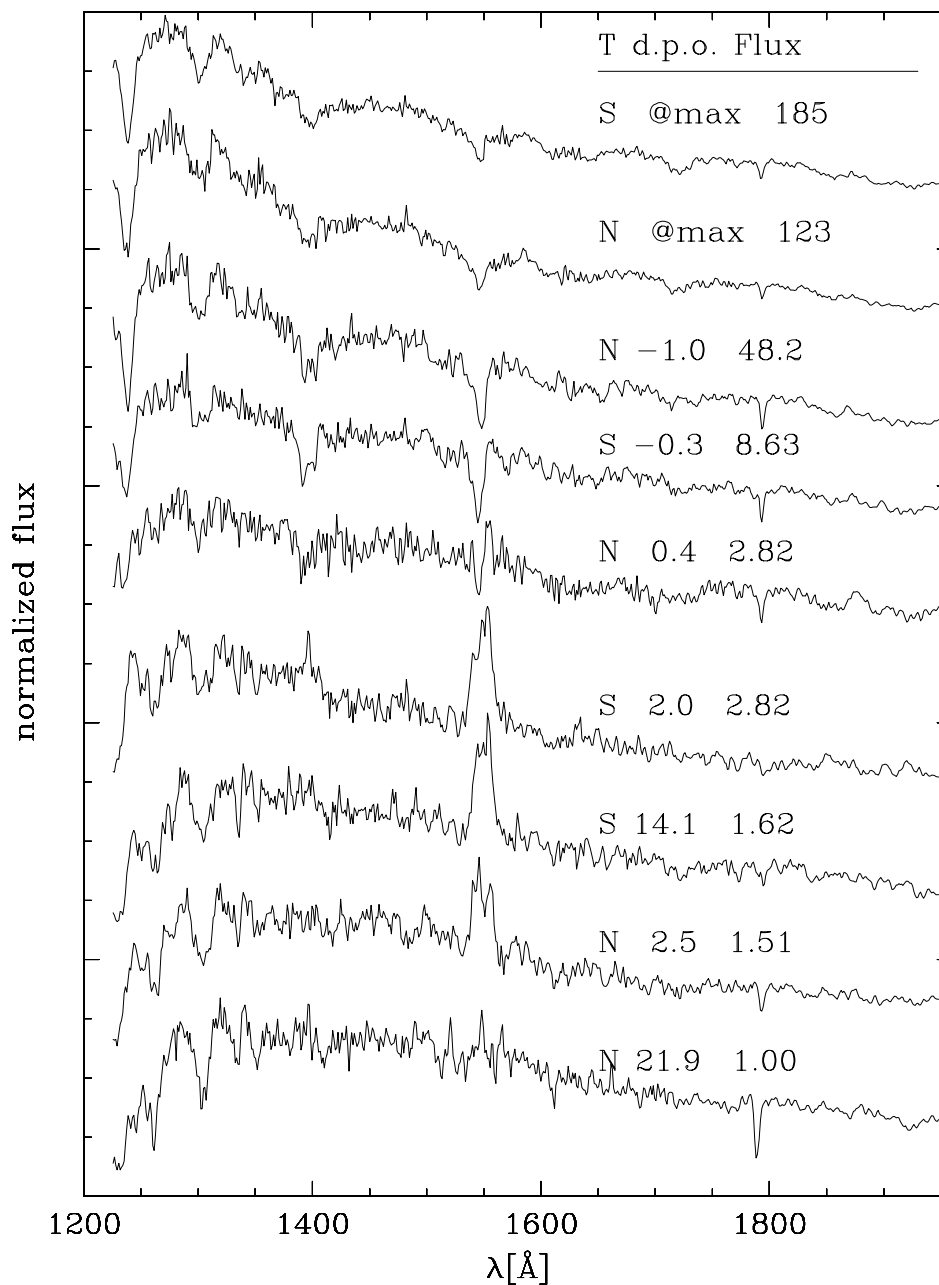
Figure 4.3: Evolution of the ultraviolet spectrum of VW Hyi during the decline from the outburst. Given are the type of the previous outburst (S=super, N=normal), the days elapsed after the outburst (d.p.o.) and the integrated SWP flux level, normalised to the flux of the bottom spectrum. The two top spectra were obtained at the maximum of a normal and a superoutburst.
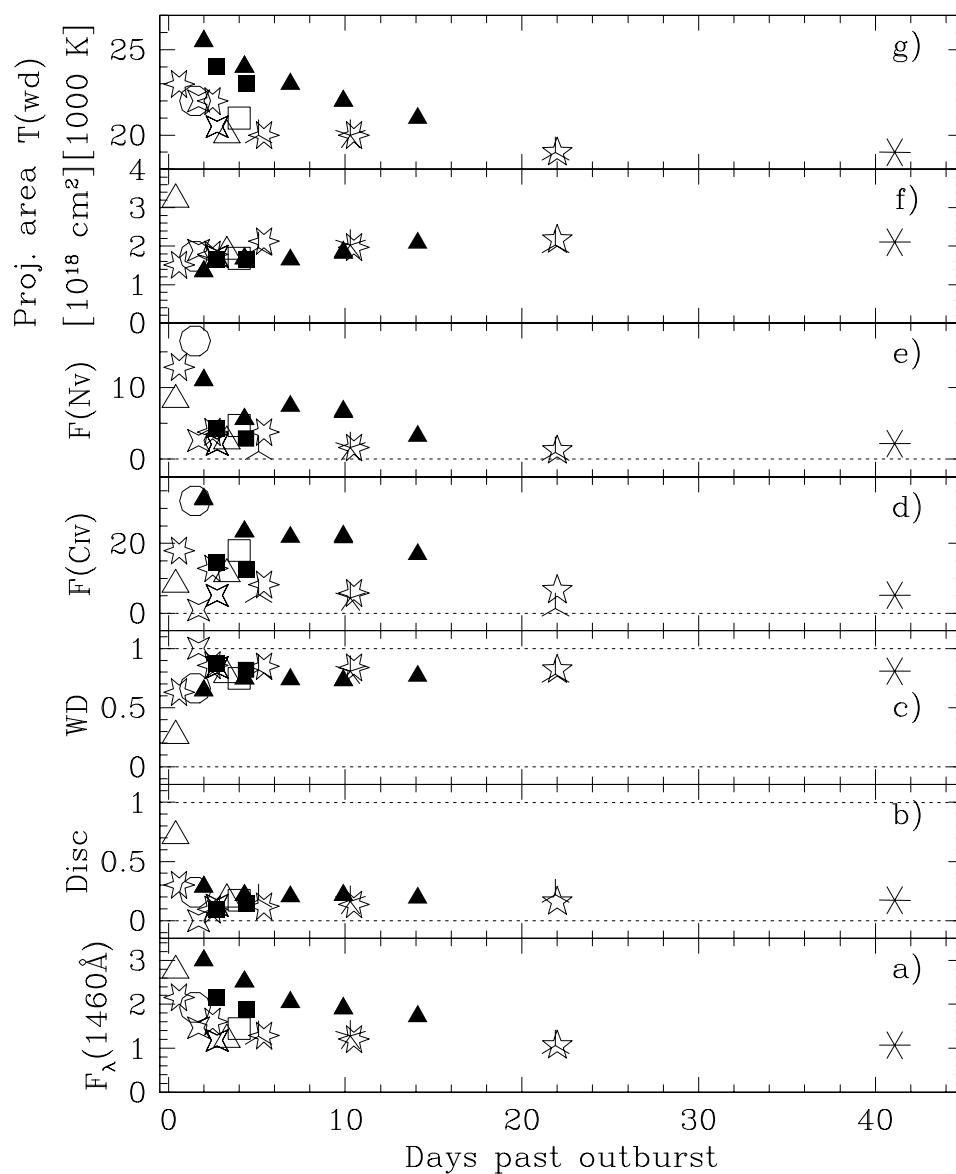
Figure 4.4: Interoutburst characteristics of VW Hyi: Data taken after normal and superoutbursts are indicated by open and filled symbols, respectively (1979: λ, 1980: $\times$, $\star$ $*$, 1982: ϖ, 1984: $\star$, $\star$, $\triangle$, $\blacksquare$, 1990: $\square$, $\blacktriangle$, $\circ$). (a) observed ultraviolet flux in 10^{-13} erg cm^{-2}s^{-1}Å^{-1}. (b) and (c) relative contributions of the disc–remnant and the white dwarf to the SWP flux, respectively. (d) and (e) line fluxes in 10^{-13} erg cm^{-2}s^{-1}. (f) Effective area of the white dwarf at $d = 65$ pc. (g) mean white dwarf temperature.
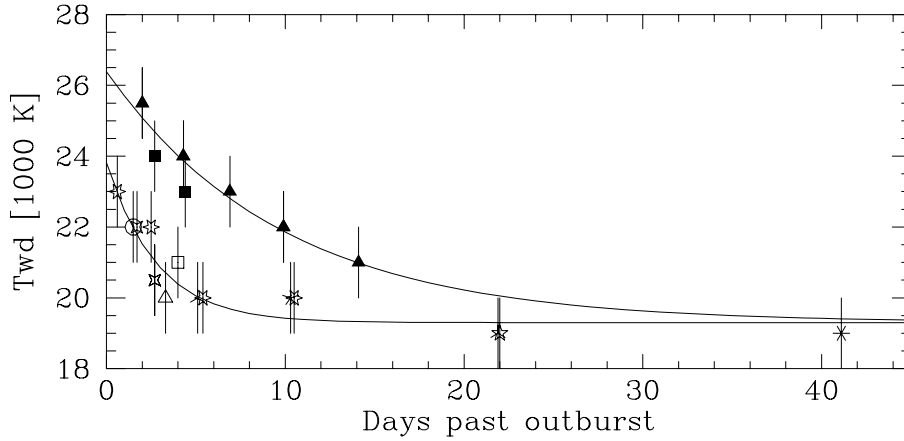
Figure 4.5: Cooling of the white dwarf in VW Hyi, symbols as in Fig. 4.4. The cooling time is significantly longer after superoutburst than after normal outburst. The temperature is a mean value over the visible surface of the white dwarf.

from the spectrum if part of the observed continuum is intrinsically flat (Sect. 3.5.3.3). In the case of VW Hyi it is, however, by no means clear which of the observed structures are due to unrecognized absorption by heavy elements and which are not. I, therefore, decided not to apply χ^2-statistics, and not to quote formal errors for the fit. Nevertheless, I am confident that the error of the derived temperature is less than 1 000 K, except for the first spectrum (0.4 d.p.o., see Fig. 4.3) which yields still uncertain white dwarf parameters as the flux contribution of the white dwarf is only $\sim 25\%$.

The results are displayed in Fig. 4.4. From bottom to top, the panels give the observed spectral flux (averaged over 1420–1500 Å), the relative contributions of disc and white dwarf, the fluxes of two prominent lines, and the derived projected emitting area (at 65 pc, Warner 1987) and temperature of the white dwarf. Interpreting the area in terms of the white dwarf radius is complicated by the possible obstruction of the white dwarf surface by the inner accretion disc.

The temperatures shown in the top panel of Fig. 4.4 clearly demonstrate that the white dwarf cools after outbursts. After a superoutburst, the white dwarf is hotter and cools more slowly than after a normal outburst. The observed temperatures can be represented by

$$T_{\text{exc}}(t) = T_{\text{wd}} - T_{\text{int}} = T_{\text{exc}}(0) \exp(-t/\tau) \tag{4.3}$$

where the white dwarf is taken to have an initial temperature excess $T_{\text{exc}}(0)$ over its intrinsic temperature T_{int}. After a normal outburst, I find $T_{\text{int}} = 19\,300 \pm 250$ K, $\tau_N = 2.8 \pm^{1.0}_{0.5}$ days and $T_{\text{exc}}(0) = 4\,520 \pm 680$ K. I adopt $T_{\text{int}} = 19\,300$ K also for the post–superoutburst data and find $\tau_S = 9.8 \pm^{1.4}_{1.1}$ days and $T_{\text{exc}}(0) = 7\,090 \pm 430$ K (Fig. 4.5). Assuming that the whole white dwarf is visible ($R_{\text{wd}} = 0.6 M_\odot \Rightarrow R_{\text{wd}} = 8.4 \times 10^8$ cm), the temperatures of Fig. 4.5 correspond to $L(0) \simeq 1.6 \times 10^{32} \text{erg s}^{-1}$ and $2.4 \times 10^{32} \text{erg s}^{-1}$ for the normal and superoutburst, respectively, compared to a quiescent value of $0.7 \times 10^{32} \text{erg s}^{-1}$. From Fig. 4.5, the energy stored in the white dwarf is obtained by integrating the luminosity in excess of the intrinsic white dwarf

emission from the end of the outburst to the end of the quiescent interval, i.e.

$$L_{\text{stored}} = 4\pi R_{\text{wd}}^2 \sigma \int_0^{t_{\text{max}}} T^4(t) - T_{\text{int}}^4 dt \tag{4.4}$$

This yields 0.2×10^{38} ergs in the normal and 1.2×10^{38} ergs in the superoutburst which is of the order of 1% of the radiative energy ($\lambda > 912\,\text{Å}$) released in the outbursts[11]. Heating, obviously, reached deeper levels during superoutburst.

4.3.4   Results

4.3.4.1   Cooling timescale

Several mechanisms have been proposed for the observed cooling of the white dwarf in dwarf novae after outbursts: deep radiative heating from the dissipative hot boundary layer (Sect. 4.2.1), compressional heating of the white dwarf (Sect. 4.2.2), and viscous cooling of a rotating accretion belt (Sect. 4.2.3).

Pringle (1988) simulated the thermal effect of irradiation by the boundary layer for both types of outburst by placing the white dwarf into a heat bath with a temperature T_{peak} for a time interval equal to the outburst duration t_{ob}. The effect of the accreted mass on the internal constitution of the white dwarf was neglected. Radiative heating proceeds to greater depths for a longer outburst duration. Hence, the initial post–outburst luminosity $L(0)$ of the white dwarf and its decline rate both increase with t_{ob} and T_{peak}. Pringle's model requires a temperature of the heat bath $\geq 10^6$ K which could be identified with the temperature at the base of an optically thick dissipative boundary layer (the basic shortcoming of this model is discussed below in Sect. 4.5.1). In his model, my results for VW Hyi correspond to $T_{\text{peak}} \simeq 1.0 \times 10^6$ and 1.3×10^6 K, for the normal and the superoutburst, respectively.

Sion (1995) considered the compressional heating caused by the matter added onto the white dwarf during a dwarf nova outburst but neglected external radiative heating. Compressional heating affects the whole white dwarf, however, the effect is strongest for the outermost layers which have the desired short Kelvin–Helmholtz timescales. Sion's numerical results demonstrate that excess temperatures of several $1\,000$ K are reached for the accretion of some $10^{-10}\,M_\odot$ within 14 days, as may be typical of superoutbursts in VW Hyi. Although cooling takes place over long times, the initial drop in temperature can amount to 500 K per day, again comparable to what is observed in VW Hyi.

---

[11]Most dwarf novae emit a substantial amount of the accretion energy released during an outburst at wavelengths $\lambda \geq 912\,\text{Å}$ (e.g. Mauche et al. 1991; van Teeseling et al. 1993). I found that the ultraviolet/optical flux of dwarf novae in outburst scales with the visual magnitude as $\log F_{(\text{UV\&opt})} = -4.22V - 3.76$. Integrating over the optical light curve of an outburst, e.g. the AAVSO/VSS RASNZ data, then yields a lower limit to the energy radiated away during this outburst.
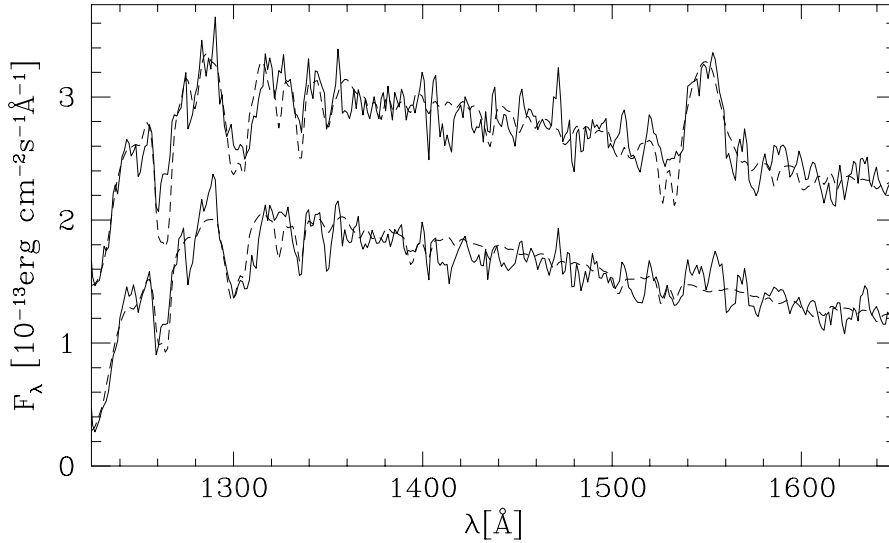
Figure 4.6: upper curve: observed spectrum (SWP24435L) of VW Hyi obtained 4.4 days after a superoutburst (solid line, offsetted by 1 unit) and five–component model (dashed line, white dwarf, disc–remnant and 3 emission lines.) Bottom: observed spectrum minus disc–remnant and emission lines (solid) and two–temperature white dwarf model (dashed, 16% by area 28 000 K solar component plus 84% by area 16 000 K pure hydrogen component.)

As a third possibility, dissipative processes in a rotating belt (Kippenhahn & Thomas 1978; Kutter & Sparks 1989) could extend beyond the cessation of accretion and produce the observed afterglow but no detailed model is available.

4.3.4.2 A white dwarf with inhomogeneous temperature and abundances distribution?

Since the white dwarf in a dwarf nova accretes in the equatorial plane it is likely to be hottest at the equator and coolest at the poles. Similarly, it seems possible that the chemical composition will vary over the surface, with highest abundances at the equator and lowest at the poles. The temperatures and areas derived here as well as the non–solar abundances derived by Sion (1995b) from *HST* spectra have, therefore, the character of *mean* values. An intuitive two–component model accounts for the polar region by a cool pure–hydrogen component and for the equatorial region by a hot component with solar composition (similar two–component approaches have been previously explored by Long et al. (1993) for U Gem and Huang et al. (1996) for VW Hyi). This model fits the observed white dwarf spectra (obtained by subtracting the disc and line contributions); the Lyα profile as well as the strongest metal lines (Si $\scriptstyle\rm II$ $\lambda\lambda$ 1260,65 & 1527,33) are well reproduced (Fig. 4.6). The best–fit temperatures are $T_{\rm pole} = 15\,000\,{\rm K}$ and $T_{\rm equator} = 28\,000 - 22\,000\,{\rm K}$, for the normal outburst and the last three superoutburst spectra. The hot component covers $\sim 20\%$ of the surface. Unfortunately, the quality of the *IUE* spectra is not sufficient to carry the analysis of such a model much further.

4.4   EK Triangulis Australis

4.4.1   Introduction

It has been suggested that the white dwarf in the poorly studied dwarf nova EK TrA ($P_{\rm orb} \simeq$ 92 min) is a dominant source of UV radiation during quiescence (Verbunt 1987). I have re–analysed the single available post–outburst ultraviolet spectrum and show that the remnant accretion disc or belt as well as the white dwarf contribute to the observed flux. I also show that EK TrA is rather similar to the well studied dwarf nova VW Hyi. However, as EK TrA has an extremely long outburst period, it may be better suited for studying the evolution of the white dwarf and the possible presence of a Kippenhahn–Thomas type accretion belt through the interoutburst period.

An earlier version of this section has been published in Gänsicke et al. (1997).

4.4.2   Observations

4.4.2.1   Ultraviolet spectroscopy

During the superoutburst of EK TrA in August 1980, four low–resolution *IUE* spectra (~ 6 Å, Table 4.2) were obtained, covering mid–outburst to late decline from the outburst (Hassall 1985). The SWP spectra used here have been recently reprocessed with the *IUE* Final Archive procedures (*NEWSIPS*), yielding a better flux calibration and a higher S/N. I find that in EK TrA the evolution of both, the ultraviolet spectrum and the flux throughout the outburst is very similar to that in VW Hyi (Sect. 4.3): at maximum light EK TrA shows a very blue continuum with strong absorption lines of N V λ 1240, Si IV λ 1400 and C IV λ 1549. This spectral shape remains unchanged throughout the early phase of decline. Approaching quiescence, the absorption lines become weaker and C IV develops a prominent P Cygni profile. The ratio of ultraviolet to optical fluxes at a given time during the outburst is the same in both systems. Fig. 4.7 compares two spectra of EK TrA taken at mid–outburst and during late decline with equivalent observations of VW Hyi selected from Sect. 4.3. The latest *IUE* spectrum of EK TrA (SWP09768L) was obtained at $V \simeq 15$, still ~ 1.5 mag above the quiescent level.

Fig. 1 of Hassall (1985) shows the VSS RASNZ outburst light curve along with the time of the *IUE* exposures. Unfortunately, there is some uncertainty about the flux levels during decline. The last two amateur detections of EK TrA show the system at flux levels which exceed the earlier *IUE* measurements represented by *Fine Error Sensor* (*FES*) magnitudes (admittedly somewhat uncertain for $V > 14$) and by the AB magnitudes derived from the SWP and LWR exposures (more reliable). As a secondary rise during decline would be quite unusual I consider the *IUE* derived magnitudes more reliable than the amateur visual estimates. I conclude that the flux level during the *IUE* observations was $V \simeq 15.0$. For a termination of the superoutburst plateau on August 12, 1980, the flux level of SWP09768L is consistent with the typical decline time of ~ 2 d. In the case of VW Hyi, an equivalent spectrum (SWP24157L) exists, capturing

Frame No.	V_{FES}	normalised SWP flux	comment
EK TrA			
SWP09705L	12.1	18.8	closest to maximum
SWP09725,28L	12.2	16.4	early decline
SWP09768L	$\simeq 15.0$	1.00	late decline
VW Hyi			
SWP24148L	10.7	16.6	early decline
SWP24157L	13.4	1.00	late decline
SWP07498L	$\simeq 14.2$	0.35	quiescence

Table 4.2: *IUE* observations of EK TrA and VW Hyi.

the turnover between disc and white dwarf dominated ultraviolet flux. This spectrum is a factor of ~ 3 above the quiescent level. By comparison, the same should be true for the presently discussed spectrum of EK TrA. In contrast to VW Hyi, no truly quiescent ultraviolet spectrum of EK TrA exists so far. Table 4.2 lists for both systems the *FES* magnitude and the integrated SWP flux, normalized to the late decline spectrum.

4.4.2.2 Optical spectroscopy

A low–resolution (FWHM ~ 25 Å) spectrum of EK TrA was obtained by H.–C. Thomas on July 18, 1996 (JD $= 2\,450\,282$) with the ESO/MPI 2.2 m telescope at La Silla. The spectrum was taken through thin clouds and yields $V = 17.4$. However, a CCD image taken during the previous night gave $V = 16.7$. Fig. 4.9a shows the spectrum adjusted to the CCD magnitude. The most recent outburst of EK TrA occurred on JD $= 2\,450\,078$, a short normal outburst with rise and fall times of one day (F. Bateson, private communication). Hence, at the time of the observations, the system was in quiescence since ~ 200 days. The optical spectrum of EK TrA in quiescence shows strong Balmer emission lines, weaker emission lines of He I and possibly of He II λ 4686. Line measurements are summarized in Table 4.3. The Balmer jump in emission indicates that optically thin material is a significant source of the continuum flux. No emission from the secondary star can be discerned in the spectrum.
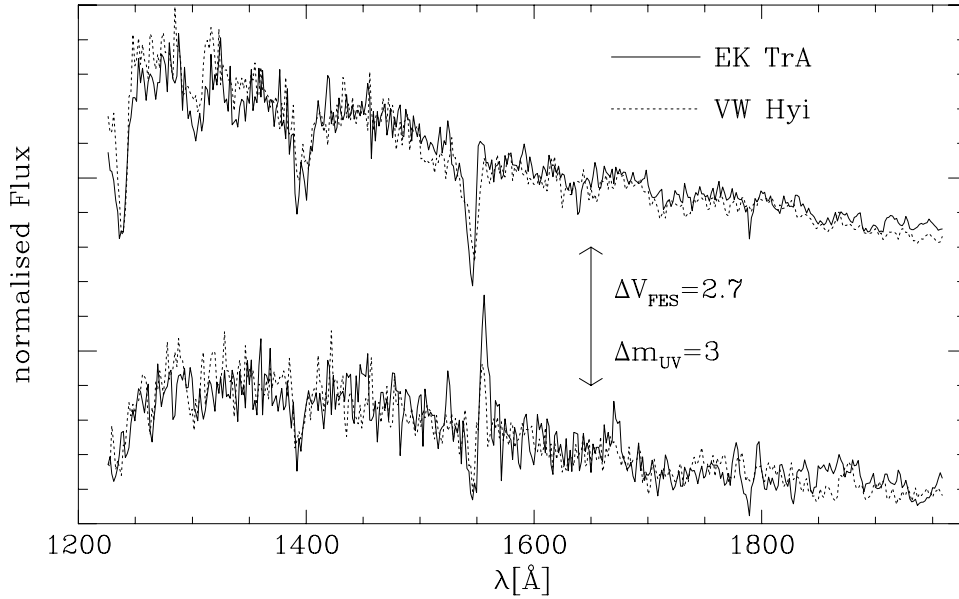
Figure 4.7: EK TrA and VW Hyi: spectroscopic twins. Top spectra: EK TrA and VW Hyi during early decline from the outburst maximum, SWP09725L and SWP24148L, respectively. Both systems show strong absorption lines of N v λ 1240, Si iv λ 1400 and C iv λ 1549. Bottom spectra: the two systems during late decline from the outburst (EK TrA: SWP09768L, VW Hyi: SWP24157L). The absorption lines become weaker, C iv shows a strong P Cygni profile, also the Si iv absorption is partly filled up by emission. The flux ratio between the maximum and minimum spectrum is the same for the two systems, both at ultraviolet and at optical wavelengths. Note that the *absolute* flux of VW Hyi is a factor ~ 8 higher than that of EK TrA.

4.4.3   Analysis

4.4.3.1   The white dwarf contribution to the ultraviolet flux

Verbunt (1987) has listed EK TrA among four short–period dwarf novae which show a drop in flux shortward of ~ 1400 Å during quiescence. However, considering that EK TrA had not yet reached its quiescent level when the *IUE* spectrum SWP09768L was taken, the interpretation of this drop in flux as the pressure–broadened Lyα absorption of the white dwarf is not straightforward. In order to determine the contribution of the white dwarf to the ultraviolet flux, I have decomposed the spectrum into accretion disc and white dwarf contribution following the method described in Sect. 4.3: I use the *observed* spectrum close to outburst maximum (SWP09705L) to describe the shape of the disc contribution and a grid ($11\,000\,\mathrm{K} \leq T_{\mathrm{wd}} \leq 30\,000\,\mathrm{K}$, solar abundances) of *calculated* model spectra provided by I. Hubeny for the white dwarf. As the present data do not allow to estimate the mass of the white dwarf in EK TrA, I assume $R_{\mathrm{wd}} = 0.6 M_{\odot}$, equivalent to $\log g = 8.0$, which is the mean mass of single white dwarfs (Bergeron et al. 1992). In cataclysmic variables, the mean white dwarf mass may somewhat differ

Line	λ [Å]	FWHM [Å][1]	E.W. [Å]	Flux[2]
		±4	±3	±5
He I	7065	47	17	86
He I	6678	39	21	109
Hα	6562	31	191	949
He I	5876	32	40	249
Fe II	5170	32	13	102
He I,Fe I	5016,18	37	12	95
He I	4922	36	10	81
Hβ	4861	25	86	731
He I	4471	25	11	109
Hγ	4340	23	53	541
Hδ	4102	23	43	459

[1] corrected for the instrumental resolution.
[2] in 10^{-16} erg cm^{-2}s^{-1}

Table 4.3: Emission–line measurements of EK TrA in quiescence

from that of single white dwarfs, for a discussion see Sect. 5. In the considered range of the white dwarf temperature in EK TrA, a lower mass ($R_{wd} = 0.4 M_\odot \Leftrightarrow \log g = 7.5$) or higher mass ($R_{wd} = 0.9 M_\odot \Leftrightarrow \log g = 8.5$) will yield temperatures lower or higher, respectively, by $\sim 1000 - 2000$ K. Following the experience with VW Hyi, I allow in the fit for Gaussian emission lines of N v λ 1240, Si IV λ 1400 and C IV λ 1549. The observed spectrum was then fitted with the sum of these components, using an evolution strategy algorithm like for VW Hyi. Reasonable fits to the observed ultraviolet spectrum are achieved for $T_{wd} = 16000 - 20000$ K, with the white dwarf and the accretion disc contributing $\sim$25% and $\sim$75% to the SWP flux, respectively. Fig. 4.8 shows a fit for $T_{wd} = 18000$ K. However, as the accretion disc still dominates the ultraviolet light, the derived white dwarf parameters remain presently somewhat uncertain. Comparison with VW Hyi tells us that the decline of the spectrum towards Lyα should not, at face value, be taken as a measure of the white dwarf contribution to the overall flux.

4.4.3.2 The distance of EK TrA

Assuming $R_{wd} = 0.6 M_\odot$, the scaling factors of the white dwarf models ($T_{wd} = 16000 - 20000$ K) yield a distance of $d = 130 - 200$ pc, 2–3 times that of VW Hyi. Allowing for $R_{wd} = 0.4 - 0.9 M_\odot$, this range extends to $d = 85 - 300$ pc. From the non–detection of the secondary and using the rather red M5+ dwarf Gl866 as a template, I set an approximate lower limit to the distance of $\sim$180 pc, consistent with the (uncertain) estimate of 200 pc derived by Warner (1987) from the assumed absolute magnitude of EK TrA. Any earlier M–dwarf template would yield a still larger distance. The distance of 68–86 pc as derived by Hassall (1985) from fits of model disc spectra is likely to be too low.
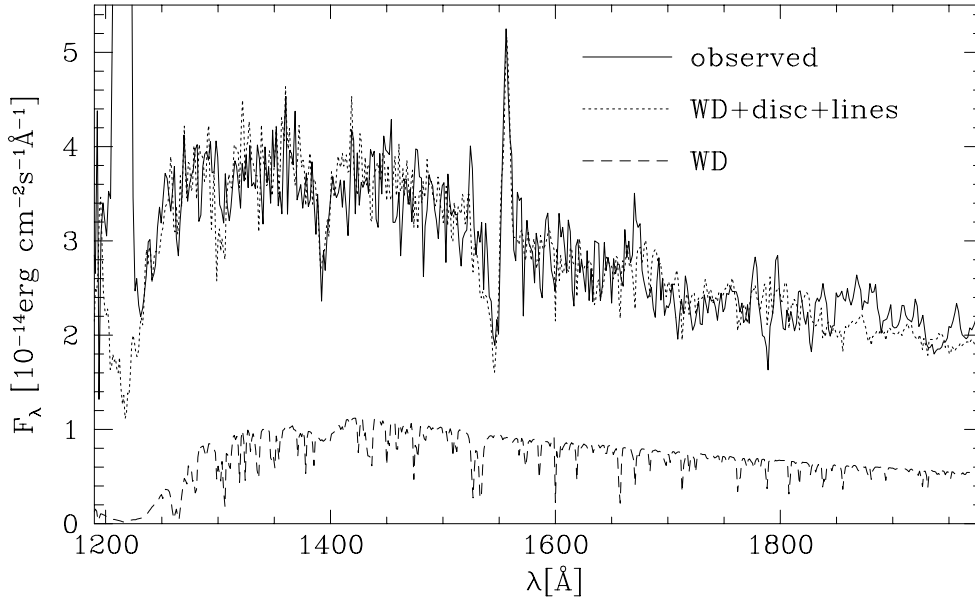
Figure 4.8: Best fit to the *IUE* spectrum of EK TrA obtained at $\Delta V \sim 1.5$ above quiescent level. The white dwarf with $T_{wd} = 18\,000$ K contributes $\sim 25\%$ to the observed ultraviolet flux. The strong observed Lyα emission is of geocoronal nature.

4.4.3.3   The optical spectrum in quiescence

The optical flux predicted from the UV–adjusted white dwarf spectrum is compatible with the observed flux (Fig. 4.9a). Considering that the white dwarf spectrum is derived from *IUE* observations very early in quiescence while the optical spectrum shows the system $\sim$200 days after an outburst and considering the post–outburst cooling rate of the white dwarf observed in VW Hyi (Sect. 4.3), the white dwarf contribution in quiescence is expected to decrease throughout the quiescence interval. Assuming that the post–outburst cooling of the white dwarf in EK TrA resembles that in VW Hyi, a quiescent white dwarf temperature of $\sim$14 000 K seems plausible. The corresponding optical flux is also shown in Fig. 4.9a. In order to interpret the excess optical flux over that of the white dwarf, presumably originating in the accretion disc, I have computed model spectra for an isothermal and isobaric slab according to

$$F_\nu = B_\nu(T)(1 - e^{-\tau_\nu})\Omega \tag{4.5}$$

where B_ν is the Planck function and Ω is the solid angle of the emitting surface of the slab. I have included in the computation of the optical depth τ_ν free–free and bound–free emission of hydrogen (taking into account H$^-$) as well as Balmer and Paschen line emission. Stark broadening was included in the calculation of the line profiles, but was found to be negligible in the considered parameter range. In the absence of detailed kinematic information, I grossly model the kinematic broadening by folding the spectrum with the *observed* FWHM of the Balmer
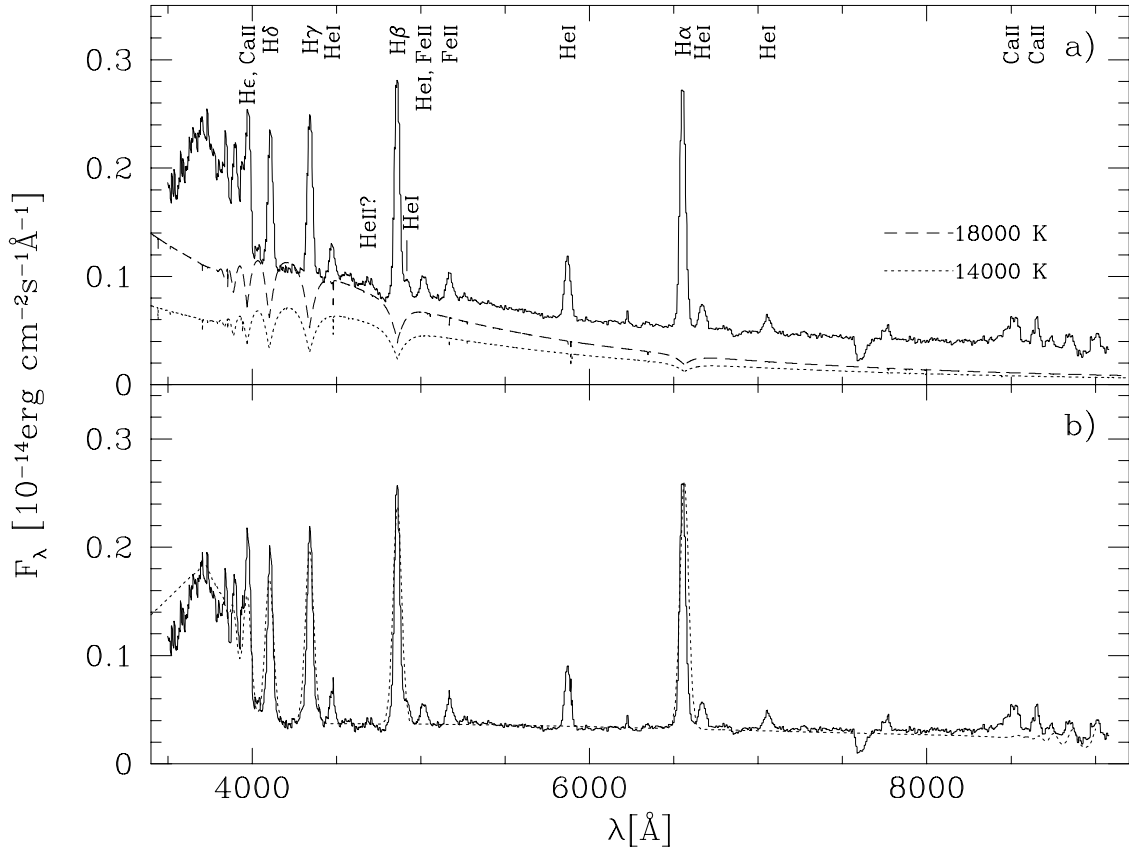
Figure 4.9: Optical spectrum of EK TrA in quiescence. Panel (a) shows the observed spectrum (full line) together with the optical contribution of the best–fit ($T_{wd} = 18\,000\,K$) white dwarf from Fig. 4.8 (dashed line). As the white dwarf is expected to cool during quiescence, a plausible model for $T_{wd} = 14\,000\,K$ is also shown (dotted line, see text for details). Major emission lines are identified. Panel (b) shows the difference of the observed quiescent spectrum and the 14 000 K white dwarf model (full line) along with the spectrum of an isothermal and isobaric plasma slab of $\rho = 3.7 \times 10^{-10}$ g/cm^3, $T = 6500\,K$ and $h = 1 \times 10^8$cm. The observed flux below 3 700 Å is uncertain due to the rapidly decreasing response of the detector.

lines, i.e. 25 Å. Input parameters for the code are the density ρ, the temperature T and the geometric depth h of the slab. After subtracting the $T_{wd} = 14\,000\,K$ white dwarf model spectrum, the remaining optical spectrum can be described by the emission of a slab with $T \simeq 6500\,K$ (Fig. 4.9b). Both, the continuum shape and the line strengths of Hα to Hδ fit the observations quite well. The excess flux observed in H$\epsilon\,\lambda\,3970$ is due to emission of Ca II K/H $\lambda\lambda\,3934,3969$. I should caution the reader, however, that this isothermal and isobaric slab should not to be taken as a disc model; it is merely a simple and successfull approach to represent the optical emission in terms of physical parameters. The flux ratios and equivalent widths of the Balmer

P_{orb} (min)	V_S	V_N	V_Q	f_S (days)	f_N (days)	T_{wd} (K)	d (pc)
EK TrA:							
92[2]	11.2[2]	12.1[3]	16.7[0]	487[3]	231[3]	18 000:[0]	68-86;[2] 200:;[4] 180[0]
VW Hyi:							
107[3]	8.5[3]	9.5[3]	13.5[3]	179[3]	27[3]	19 000[1]	65[4]

[0] This work; [1] Sect. 4.3; [2] Hassall (1985); [3] Ritter (1990); [4] Warner (1987)

Table 4.4: System parameters of EK TrA and VW Hyi. Listed are the visual brightness, the outburst frequency, the white dwarf temperature and the distance, with the indices S, N, and Q referring to superoutburst, normal outburst, and quiescence, respectively

lines and the strength of the Balmer jump define the temperature and the optical depth of this slab within narrow ranges. The resulting values are consistent with the accretion disc models of Williams (1980) which predict disc temperatures $T \simeq 6000$ K for low accretion rates. Although optically thin in the continuum, their discs are optically thick in the Balmer lines. Essentially, the fit determines the optical depth along the line of sight $\tau_v = h\rho\kappa_v/\cos i$ and the solid angle $\Omega = \pi R_d^2/(d^2\cos i)$ subtended by the slab, where h is the height of the slab, ρ its density, R_d its radius, κ_v the mass absorption coefficient throughout the slab, i the inclination and d the distance of the system.

I use $d = 180$ pc and choose $i \simeq 60°$ in analogy to the other dwarf novae showing a white dwarf spectrum at ultraviolet wavelengths during quiescence. Adopting $h \sim 10^8$ cm as a realistic height of the slab, I obtain $\rho \simeq 3.7 \times 10^{-10}$ g cm^{-3} and $R_d \simeq 3.1 \times 10^{10}$ cm. The derived density appears plausible for a tenuous disc. Taking $R_{wd} = 0.6 M_\odot$, $M_{sec} = 0.08 M_\odot$ and $P_{orb} = 1.53$ h, the Roche–lobe radius of the primary is $\simeq 2.9 \times 10^{10}$ cm. Hence, the emitting slab can possibly extend over much of the Roche–lobe of the white dwarf. The mass contained in the emitting volume is $\sim 10^{19} - 10^{20}$ g. Even at very low accretion rates of $\sim 10^{14}$ g s^{-1} this mass will be furnished by the secondary within a few days. It may, hence, be that the optical emission originates from a kind of corona located on top of a colder disc which is unobserved at optical wavelengths. Lack of spectral and orbital phase resolution prevents a more exact location of the emitting material within the binary system.

For completeness, I note that the luminosity of the slab is $L \simeq 1.5 \times 10^{31}$ erg s^{-1}. This compares with $L_{wd} = 1.8 \times 10^{31}$ erg s^{-1} (for $T_{wd} = 14000$ K) and a quiescent X–ray luminosity observed during the *Rosat All Sky Survey* of $L_x \sim 1.4 \times 10^{31}$ erg s^{-1} (0.19 *PSPC* cts s^{-1}, Voges et al. 1997). Considering the small solid angle subtended by the accretion disc as seen from the white dwarf, it is unlikely that the observed optical flux is solely due to reprocessing of ultraviolet or X–ray emission from the white dwarf/the boundary layer in the surface layer (chromosphere) of the disc. Energetically, the optical flux could be the result of ongoing accretion a low level as suggested by the observed X–ray flux. The observed quiescent *PSPC* count rate of 0.19 cts s^{-1} is consistent with the count rates of 1.26 and ~ 2 cts s^{-1} observed for VW Hyi in quiescence (Belloni et al. 1991 and Wheatley et al. 1996, respectively), considering

that the distance of EK TrA is about three times that of VW Hyi.

4.4.4 Results

Apart from the similarities of the ultraviolet spectra and their evolution during outburst, EK TrA and VW Hyi have further characteristics in common (Table 4.4). Both objects are short–period SU UMa type systems with comparable outburst amplitude ($\Delta V = 4 - 5$); the outburst duration in both systems is ~ 3 d and $10 - 14$ d for the normal and the superoutbursts, respectively. On the other hand, EK TrA and VW Hyi must differ in the mass transfer rate: as the systems match in size, spectral shape, outburst amplitude and duration, the total accretion–induced emitted energy will roughly scale with the fraction of time the systems spend in outburst (apart from possible differences in the outburst EUV/X–ray emission or wind losses). This yields for VW Hyi a transfer rate roughly 5 times higher than for EK TrA. With $\dot{M} \simeq 10^{-10} M_\odot \, \mathrm{yr}^{-1}$ for VW Hyi (Patterson 1984) this suggests a transfer rate of $\sim 2 \times 10^{-11} M_\odot \, \mathrm{yr}^{-1}$.

VW Hyi proved to be a key system for studying the interoutburst behaviour of dwarf novae as well as the properties of their white dwarf primary. This includes the cooling of the white dwarf following the heating during normal and superoutbursts (Sect. 4.3), its rotation rate and chemical abundances (Sion et al. 1995b,c) as well as the possible detection (Sect. 4.3, Sion et al. 1996) of the hot accretion belt predicted by Kippenhahn & Thomas (1978). The limitation of such studies imposed by VW Hyi is its short outburst cycle, raising the question whether the system ever reaches a truly quiescent level. With its long outburst period, EK TrA appears to be a viable candidate to advance the above studies.

4.5   Discussion, part II

4.5.1   The optical depth of the boundary layer

Heating of the white dwarf by an optically thick hot boundary layer provided a successful modelling of the post–outburst cooling time observed in VW Hyi (Pringle 1988). This model is appealingly simple, but proves to have some shortcomings when compared to the overall observational facts gathered for VW Hyi.

The main argument against the irradiation model proposed by Pringle (1988) is that hot ($T_{\mathrm{BL}} \geq 10^6$ K) boundary layers are generally not observed at X–ray wavelengths in dwarf novae. However, if the boundary layer is sufficiently optically thick, it may reach high temperatures at its bottom while the bulk of the emission is radiated from its surface in the ultraviolet/EUV. I will derive here a very simple estimate of the depth and the bottom temperature of the boundary layer in VW Hyi. The mass accretion rate given by Patterson (1984) is $10^{-10} M_\odot \, \mathrm{yr}^{-1}$. However, Patterson used a distance of ~ 150 pc, which is probably too large by a factor of ~ 2. Assuming $d = 65$ pc translates to $\dot{M} \simeq 2 \times 10^{-11} M_\odot \, \mathrm{yr}^{-1}$. VW Hyi has about 13 normal outbursts and two superoutbursts per year lasting four days and 12 days, respectively (see Table 4.4). Hence, VW Hyi spends about 76 days per year in outburst.

Neglecting that the optical magnitude during superoutbursts is somewhat higher than during the normal outbursts, and neglecting accretion during the quiescent intervals, the mass accreted during a normal outburst is $\sim 1.0 \times 10^{-12} M_\odot$ or $\sim 2.1 \times 10^{21}$ g. During the superoutburst, the corresponding number is $\sim 3.2 \times 10^{-12} M_\odot$ or $\sim 6.3 \times 10^{21}$ g. With a white dwarf radius of 8×10^8 cm, this material if dispersed over the whole white dwarf surface results in a column density of $\sim 260 \, \mathrm{g \, cm}^{-2}$ and $\sim 785 \, \mathrm{g \, cm}^{-2}$ for the normal and the superoutburst, respectively. Column densities will be higher if the material is accreted only in an equatorial belt.

I consider now that the material, once settled and in hydrostatic equilibrium, follows a density structure as described by a standard model atmosphere. Running the pure–hydrogen LTE atmosphere code described on p. 18 with $T_{\mathrm{eff}} = 100\,000$ K (as observed for the boundary layer, van Teeseling et al. 1993) and $\log g = 8$ down to large optical depths, I find that the column densities estimated for the boundary layer correspond to Rosseland optical depths of $500 - 1600$ where a temperature of $4.4 - 5.9 \times 10^5$ K is reached[12]. These temperatures are still too low to efficiently heat the white dwarf in the Pringle (1988) model. The luminosity of this boundary layer enshrouding the whole white dwarf is $\sim 5 \times 10^{34} \, \mathrm{erg \, s}^{-1}$, higher than the observed EUV and soft X-ray luminosities. If the boundary layer covers only a small fraction of the white dwarf as suggested by X-ray observations ($f \sim 10^{-3}$, van Teeseling et al. 1993), the column density and the bottom temperature will be much higher than estimated above; possible reaching the 10^6 K needed in Pringles model to heat the white dwarf deep enough. In this case, however, the fraction of the white dwarf that can be heated by radiation from the boundary layer is much too small to account for the observed cooling (Sect. 4.3.4.1).

---

[12]Integrating the envelope solution obtained from the equations of stellar structure results in similar, somewhat lower temperatures.

System	P_{orb} [min]	d [pc]	i [°]	R_{wd} $[M_\odot]$	$v\sin i$ [km s^{-1}]	ΔV	t_{out} [d]	τ_{cool} [d]	$E_{\mathrm{outburst}}^{\mathrm{UV/opt}}$ [10^{39} erg]	$E_{\mathrm{stored}}^{\mathrm{UV/opt}}$ [10^{39} erg]
WZ Sge	81	70	76	0.8	1200	6.6	90	687	46	2.10
OY Car	91	100	83	0.9		3.9	17	27	2	0.14
VW Hyi(S)	107	65	60	0.6	400	5.3	16	11	14	0.12
VW Hyi(N)						4.3	3.5	3	1.7	0.02
U Gem	255	81	70	1.1	75	5.5	16	30	11	0.84

Table 4.5: Comparison of the four systems for which cooling of the white dwarf has been observed at ultraviolet wavelengths. Listed are the orbital period, the distance, the inclination, the mass of the white dwarf, the rotational velocity, the visual amplitude of the outburst, the typical duration of an outburst, the cooling timescale, the radiative energy released during an outburst and the thermal energy stored in the white dwarf. The orbital periods, the inclinations, the white dwarf masses and the outburst amplitudes are from Ritter (1990). The distances are from Warner (1987) except that of WZ Sge which is from Sion et al. (1995a). The rotational velocities are from Sion et al. (1994, 95c) and Cheng et al. (1997). The outburst durations were determined from the visual light curves of the AAVSO and the VSS RASNZ. The cooling times are from Sparks et al. (1993); Cheng et al. (1994); Sect. 4.3 and Long et al. (1994), the outburst energies and the thermal energy stored in the white dwarf envelope where derived as described in Sect. 4.3.4.1.

Concluding, it appears that radiative heating by the dissipative boundary layer is an attractive physical mechanism but conflicts with the observed boundary layer characteristics. Compressional heating as modelled by Sion (1995) may be a more realistic mechanism, as it depends only on the amount of mass deposited on the white dwarf envelope.

4.5.2   Comparison with other systems

With the study presented in Sect. 4.3 there are now four dwarf novae in which cooling of the white dwarf following an outburst has been observed at ultraviolet wavelengths[13]. I have summarized in Table 4.5 the characteristics of these four systems. The cooling timescales (and, hence, the thermal energy stored in the white dwarf during an outburst) of WZ Sge, U Gem and OY Car should be regarded with some caution as they are taken from preliminary reports or are based on few observational data.

Comparing the cooling times of the white dwarf in U Gem after a wide outburst ($\tau_{\mathrm{cool}} = 30$ d, Long et al. 1994) and in VW Hyi after a superoutburst ($\tau_{\mathrm{cool}} = 9.8$ d, Sect. 4.3.4.1), heating seems to occur less deeply in VW Hyi. This interpretation is consistent with recent EUV observations of the two systems, revealing a much higher boundary layer luminosity in U Gem than in

---

[13]Some evidence for cooling of the white dwarf has been derived from optical photometry in HT Cas (Wood et al. 1995). However, for the sake of a homogeneous methodology in the measurement of the white dwarf temperatures, I do not include HT Cas in the discussion here.

VW Hyi (Long et al. 1996; Mauche 1996). Furthermore, in U Gem $L_{disc}/L_{BL} \simeq 1$, as expected from standard accretion disc theory (Long et al. 1996), whereas for VW Hyi $L_{disc}/L_{BL} \simeq 20$ (Mauche 1996), indicating that the systems differ substantially. In fact, $L_{disc}/L_{BL} = 1$ is expected only for a non–rotating white dwarf. From recent high–resolution *HST* spectroscopy, Sion et al. (1994, 95b) derive a much higher rotational velocity for the white dwarf in VW Hyi ($\sim 20\%$ Keplerian) than in U Gem (~ 75 km/s), indicating a first possible reason for the low boundary layer luminosity and the less deep heating of the white dwarf in VW Hyi. However, this encouraging picture is somewhat weakened by the recent measurement of the high rotational velocity of the white dwarf in WZ Sge (Cheng et al. 1997): even though this white dwarf is rotating at $\sim 30\%$ of its breakup velocity, it provided up to now the most impressive case of afterglow following a dwarf nova outburst, lasting several years. Admittedly, WZ Sge is a member of the rather peculiar dwarf novae showing very rare but intense outbursts (in the case of WZ Sge the outburst cycle is 33 yrs), and the comparison with U Gem and VW Hyi may not be entirely valid. Obviously, we are still missing some basic understanding of these systems.

To close this chapter, I would like to draw the attention to the following question:

Why can we detect the photospheric emission of the white dwarf at ultraviolet wavelengths in some dwarf novae during quiescence while in other systems there is no obvious spectroscopic evidence of the accreting primary?

I won't be able to answer this question, but I think that it is fundamental for our understanding of dwarf novae as a class and I will illustrate the point with the two dwarf novae VW Hyi (where the white dwarf is clearly the dominant source of ultraviolet flux, see Sect 4.3) and WX Hyi (where no spectroscopic evidence from the white dwarf is found in the *IUE* spectra; see e.g. Fig. 8 of Hassall et al. 1983). Both systems have almost identical (within one minute) orbital periods, and, hence, have similar dimensions (unless the mass ratios differ largely). Both systems have similar outburst cycles (VW Hyi: $f_N = 27$ d, $f_S = 179$ d; WX Hyi: $f_N = 14$ d, $f_S = 140$ d), indicating similar accretion rates. The two dwarf novae differ somewhat in the inclination, $i \simeq 60°$ for VW Hyi and $i \simeq 40°$ for WX Hyi. A lower inclination will result in a larger contribution of the accretion disc. However, considering the small difference in the inclinations, the accretion disc in WX Hyi should contribute a flux only ~ 35 % higher than that in VW Hyi, not sufficient to outshine a white dwarf with similar characteristics as that found in VW Hyi. Both systems show a clear decline of the ultraviolet flux following an outburst (Hassall et al. 1985; Verbunt et al. 1987). In the case of VW Hyi, this decline is clearly due to the decrease of the photospheric white dwarf temperature (Sect. 4.3.4.1). In WX Hyi, this decline may also be due to the cooling of the white dwarf which must, however, be veiled by another source of ultraviolet light. Another speculative hypothesis is that the white dwarf in WX Hyi is too cold to contribute at ultraviolet wavelengths and that the observed flux decline is due to disc evaporation as outlined in the model by Meyer & Meyer–Hofmeister (1994).

Chapter 5

Concluding discussion

5.1 Heating mechanisms

From the analysis and discussion presented in Chapter 3 and 4, it becomes clear that heating of the white dwarf induced by mass accretion is an important effect, both in magnetic and non–magnetic cataclysmic variables. Apart from the geometrically implied differences between the two types of systems, heating of the polar cap in magnetic systems against heating of the equatorial region in disc–accretors, there is apparently also a difference in the physical mechanism which causes the heating. In the disc–accreting dwarf novae, the white dwarf is heated several 1000 K above its equilibrium temperature during the dwarf nova outbursts, and cools subsequently during the quiescent interval. The cooling time can be as short as a few days, e.g. in VW Hyi (Sect. 4.3.4.1) or as long as a few years, e.g. in WZ Sge (Sect. 4.5). The basic parameter which determines the observed cooling times is the heat capacity and, therefore, the mass of the heated envelope. The large spread among the few cooling times observed so far clearly indicates that heating proceeds to different depths of the white dwarf envelope in the individual systems. One factor controlling the depth to which heating proceeds is the duration for which the white dwarf is exposed to mass accretion. In contrast to the post–outburst cooling observed in dwarf novae, the cooling timescale for the hot pole cap in the polar AM Her must be rather short, certainly less than one month (Sect. 3.5.4). Considering that the polar cap in AM Her is heated during high states which can last several years, this cooling timescale may seem surprisingly short. I will now discuss the likely heating mechanisms in both types of cataclysmic variables as well as the shortcomings of the different models for the accretion–induced heating of the white dwarf developed so far.

The physical mechanisms which may heat the white dwarf in dwarf novae have been summarized in Sect. 4.2. Even though the heating mechanism effective in dwarf novae can not yet be unmistakably identified from the available observations of the four systems known to cool after an outburst (Sect. 4.5), it seems clear that irradiation from the hot boundary layer (Pringle 1988) alone is not sufficient to explain the long cooling times observed e.g. in WZ Sge. The short cooling times observed in VW Hyi requires rather high temperatures ($\sim 10^6$ K) of the ex-

ternal radiation field in order to heat a layer of the white dwarf envelope with a corresponding Kelvin–Helmholtz timescale of a few days to two weeks (Sect. 4.3.4.1, 4.5). This high boundary layer temperature and the resulting boundary layer luminosity are in disagreement with the observations. In order to heat a layer of the white dwarf envelope with a Kelvin–Helmholtz timescale of a few years, necessary to describe the observations of WZ Sge, unrealistically high temperatures would be required in the irradiation model of Pringle (1988). It seems, therefore, likely that in dwarf novae the dominant mechanism which heats the white dwarf involves directly the accreted mass, i.e. by compression of the white dwarf envelope (Sion 1995), and/or the accreted angular momentum, i.e. by shear mixing from a rapidly rotating accretion belt (Kippenhahn & Thomas 1978; Kutter & Sparks 1989). Sion's (1995) simulations of compressional heating are able to describe the cooling timescales observed in VW Hyi and U Gem with realistic input values for the mass accreted during a dwarf nova outburst. The only application of shear mixing from a rapidly rotating accretion belt to the heating of white dwarfs in dwarf novae provides a satisfying description of the observations of WZ Sge (Sparks et al. 1993). However, a detailed modelling of this mechanism and its application to a wider range of observations are still missing. A major shortcoming both, in the compression model by Sion (1995) and in the irradiation model by Pringle (1988), is the assumption of spherically symmetric accretion. In dwarf novae, mass and angular momentum are very likely accreted in a relatively narrow equatorial belt. The resulting locally confined heating of the equatorial regions will initiate meridional circulations which re–distribute the energy from the equator towards the poles of the white dwarf. A more realistic approach in describing the effect that accretion of mass and of angular momentum has on the temperature of the white dwarf will have to be based on a *simultaneous* modelling of the boundary layer and the white dwarf envelope. Even though first two–dimensional time–dependent models that include the outer layers of the accreting star have been developed by Kley (1989, 91), a detailed description of the processes transporting matter, energy and angular momentum into the white dwarf is not yet available[1].

   The short cooling timescale of the polar cap observed in AM Her (Sect. 3.5.4) implies that the mass of the heated envelope is rather small. Based on energetical arguments, I concluded in Sect. 3.7 that irradiation from the hot post–shock plasma is the dominant mechanism heating the pole cap of the white dwarfs in polars. As discussed above, heating by irradiation does not proceed to deep layers of the white dwarf envelope; the short cooling timescale observed for the heated pole cap seems, therefore, entirely plausible. However, a self–consistent solution of the radiation transfer in the white dwarf including irradiation by thermal bremsstrahlung and cyclotron radiation is necessary to confirm my conclusions drawn from the energy balance of the accretion luminosities.

---

[1]Another hypothetical mechanism heating the white dwarf is advection of thermal energy from the disc. However, Popham (1997) showed that for the typical parameters found in cataclysmic variables, the advected thermal energy is only $\sim 1\,\%$ of the total accretion luminosity
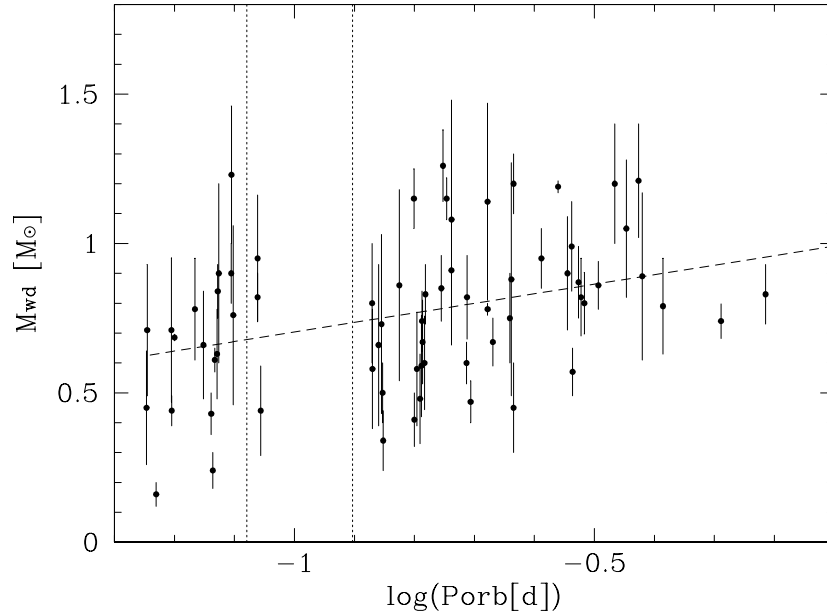
Figure 5.1: Mass spectrum of the cataclysmic variables listed in Ritter & Kolb (1997), where the uncertain values indicated in the catalogue by a colon have been omitted. The 2–3 h period gap is indicated by dotted lines, a least–square fit to the data yields $R_{\mathrm{wd}} = 0.32 \log(P_{\mathrm{orb}}(d)) + 1.023$ and is plotted as a dashed line.

5.2 Long–term evolution

Despite the different short–term response that magnetic and non–magnetic white dwarfs show to accretion, both types of systems share a common characteristic: the accreting white dwarfs are noticeably hotter than expected from their evolutionary ages. If the timescales predicted from the standard evolutionary scenario (Sect. 2.1) are correct, cataclysmic variables above the period gap should be several 10^8 years old. While the cooling theory for single white dwarfs (Sect. 2.2) predicts typical temperatures of 15 000–20 000 K, the observed temperatures for accreting white dwarfs in cataclysmic variables are generally higher, especially in systems with high accretion rates, i.e. novalike variables (see Fig. 2.4). The only long–period system harbouring a white dwarf that has a temperature which agrees with that expected from the cooling theory for single white dwarfs is the polar RX J1313–32. As discussed in Sect. 3.7, it may be that this system started mass transfer only recently, so that its white dwarf was cooling during the detached pre–cataclysmic variable phase in the same way as single white dwarfs do. Cataclysmic variables below the period gap are expected to be a few 10^9 years old, the corresponding temperatures of single non–accreting white dwarfs are $T_{\mathrm{wd}} \lesssim 10\,000$ K. While such

low temperatures are estimated for a few systems[2], the bulk of the short–period cataclysmic variables contains white dwarfs with typical temperatures of $T_{wd} \simeq 15\,000$ K. Concluding, there is overwhelming observational evidence that accretion retards the secular core cooling of the white dwarfs in cataclysmic variables. The somewhat lower temperatures observed in polars compared to dwarf novae and novalike variables may result from the differences in the accretion geometry, i.e. magnetically funnelled vs. disc accretion, in the white dwarf mass or in the accretion rate.

The long–term evolution of the white dwarf temperature is tightly connected with the mass–balance of the accretion process. The white dwarf will re–adjust its radius to an increasing mass by contracting adiabatically, thereby partly transforming gravitational energy into heat. A decrease of the mass will result in an adiabatic expansion and an according cooling of the white dwarf. The secondary stars in cataclysmic variables have typical initial masses of a few tenths of a solar mass to about one solar mass. White dwarfs in cataclysmic variables will, therefore, accrete up to one solar mass during their lifetime. If there were no mechanism for the white dwarf to also lose mass, accretion might cause it to exceed the Chandrasekhar mass and turn it into a type Ia supernova. However, as described in detail in Sect. 2.3, white dwarfs in cataclysmic variables undergo repetitive nova eruptions due to self–ignited thermonuclear burning at the bottom of the accreted hydrogen layer. During the nova explosion, part of the white dwarf envelope is ejected. The mass–balance of the accretion process depends, therefore, on the ratio of accreted to ejected mass during the nova eruptions. Recent nova simulations predict, as shown in Fig 2.3, that the mass of the white dwarf decreases for accretion rates $\dot{M} \lesssim 10^{-9} M_{\odot}\,\mathrm{yr}^{-1}$. As typical cataclysmic variables undergo probably several 10^4 nova explosions during their lifetime, it should be expected that their white dwarf primary will ultimately lose mass.

Inspection of the latest cataclysmic variable catalogue by Ritter & Kolb (1997) yields white dwarf masses for 82 systems. Excluding the 13 values which are flagged as uncertain and the white dwarf mass for CH UMa, quoted as $R_{wd} = 1.9 \pm 0.3\,M_{\odot}$, the mass distribution shown in Fig 5.1 is obtained. Even though the scatter of the individual data points is rather large, the figure suggests a decrease of the white dwarf mass with the orbital period. Indeed, the weighted mean of the white dwarf masses is $R_{wd} = 0.71 \pm 0.06$ ($N = 20$) below the period gap and $R_{wd} = 0.85 \pm 0.03$ ($N = 48$) above the gap. The intrinsic mass distribution of cataclysmic variables may decrease even more steeply towards shorter periods than indicated in Fig. 5.1 due to the following selection effect: The white dwarf mass determines the depth of the potential well and, hence, the amount of energy released by the accreted matter. Cataclysmic variables with massive white dwarfs have, therefore, a higher chance to be detected due to their higher luminosity compared to systems harbouring a low–mass white dwarf. This effect should be stronger for orbital periods below the gap, as these systems have a lower mass transfer rate than long–period systems, and, are, therefore, less luminous and more difficult to discover.

A non–parametric Spearman rank order test of the data plotted in Fig. 5.1 results in a high

---

[2]Candidates for rather low temperatures are the two polars VV Pup (Liebert et al. 1978) and RX J1015+09 (Burwitz et al. 1997b).

statistical significance for a correlation between R_{wd} and P_{orb}. However, a detailed discussion of this correlation will have to be preceeded by a thorough study of the reliability of the mass values. Nevertheless, it is clear that the mass does *not* increase towards shorter periods. Hence, heating by contraction of the white dwarf should not contribute to the observed temperature excess discussed above. It seems, therefore, necessary that either some fraction of the accretion luminosity or the extreme heating by thermonuclear surface burning during a nova eruption transfer heat deep into the white dwarf to counteract the secular core cooling. No model of the evolution of an accreting and intermittently hydrogen burning white dwarf which continues to lose mass is available in the literature.

In the Introduction I raised the question whether the temperature of the white dwarf in cataclysmic variables may be considered as an indicator of the age of the system, in a way similar to the case of single white dwarfs. The present thesis has demonstrated that competing heating but also cooling of the outer layers changes the decrease in effective temperature caused by core cooling. I have studied the short–term heating and cooling processes in the two main types of cataclysmic variables and pointed out the wealth of information that can be gathered from these processes about the behaviour of the envelope of the white dwarf. At the same time, I have demonstrated that the phenomenology of the studied systems is much more complicated than that of single white dwarfs. Part of my findings may provide constraints for a future more comprehensive theory of the heating and cooling of accreting white dwarfs.

Chapter 6

Summary and future targets

The aim of this thesis was to expand our knowledge of the influence that mass accretion has on the temperature of white dwarfs in cataclysmic variables. Following the structure kept throughout the text, I summarize below the major results of this thesis in two separate sections, outlining also valuable future observational projects.

6.1   Polars

I analysed ultraviolet spectroscopy of seven AM Herculis systems in order to determine the photospheric temperatures of their white dwarfs, and, if possible, to detect the presence of accretion–heated pole caps on the white dwarfs.

The most detailed analysis was possible for AM Herculis, the bright prototype of the class, where a large body of phase–resolved *IUE* observations was available. The observed ultraviolet continuum flux varies in phase with the hard X–ray flux, both in the high state and in the low state, and, hence, originates in the vicinity of the main accretion region. Along with this ultraviolet flux modulation, a varying width of the Lyα absorption profile is observed, being narrowest during the flux maximum and broadest during the flux minimum. An intuitive model capable to describe both, the flux modulation and the varying width of the Lyα profile, is a rotating white dwarf with an accretion–heated pole cap. A quantitative description of the data is achieved for a white dwarf of $T_{\mathrm{wd}} \simeq 20\,000\,\mathrm{K}$ with a moderately heated cap covering ~ 0.08 of the white dwarf surface. The mean effective temperature of this pole cap is $T_{\mathrm{spot}} \simeq 24\,000\,\mathrm{K}$ and $T_{\mathrm{spot}} \simeq 37\,000\,\mathrm{K}$ in the low state and the high state, respectively. In contrast to observations of dwarf novae, where a cooling of the white dwarf is observed after the end of an outburst in several systems, I could detect no evidence for cooling of the heated pole cap in AM Her during prolonged low states.

The ultraviolet luminosity of this moderately hot polar cap quantitatively agrees with the sum of the observed bremsstrahlung and cyclotron luminosities, both in the high and the low state: $L_{\mathrm{UV}} \simeq L_{\mathrm{tb}} + L_{\mathrm{cyc}}$. I, therefore, identify the ultraviolet emission from the heated pole cap

as the reprocessed radiation component of the post–shock emission intercepted by the white dwarf. This finding confirms the standard model by Lamb & Masters (1979) and King & Lasota (1979). However, at least in AM Her, this reprocessed component is located in the ultraviolet rather than in the soft X–ray regime as originally suggested. In this picture, the intense soft X–ray flux observed in AM Her must originate from an accretion mode in which the primary bremsstrahlung is unseen, i.e. totally reprocessed. A viable hypothesis is heating of the photosphere by high–density blobs which penetrate deep into the atmosphere, causing the shock to be buried by optically thick material (Kuijpers & Pringle 1982; Beuermann & Woelk 1996).

IUE and *HST* observations of V834 Cen, DP Leo, QQ Vul and RX J1313-32 indicate that a large spot ($f \sim 0.03 - 0.1$) is heated also in these systems to $\sim 10\,000\,\mathrm{K}$ above the photospheric white dwarf temperature. These ultraviolet emitting spots are without exception much larger than the usually very small EUV/soft X-ray emitting spots. It seems, therefore, likely, that irradiation of the white dwarf atmosphere from rather high standing accretion shocks plays an important rôle in many polars. The only system where the presence of a large heated spot can almost certainly be ruled out is the polar AR UMa. The extremely high magnetic field in this system causes a corresponding compression of the free–falling matter, leads to a buried shock (see above), and, hence, prevents heating of the white dwarf surface by irradiation from above.

Combining the white dwarf temperatures derived for seven polars in Chapter 3 with the values published for 11 other systems, I present in this thesis the so far largest set of white dwarf temperatures in AM Her stars. I find, in agreement with Sion (1991), a tendency for lower temperatures at shorter periods, where the systems are likely to be rather old. However, RX J1313–32, being a long–period system is found to have a remarkably low temperature compared to all other previously analysed long–period cataclysmic variables. An appealing hypothesis for this low temperature is that RX J1313–32 presently undergoes a prolonged episode of accretion activity below the secular mean or that the system entered contact only "recently", and that the white dwarf had the chance to cool during the pre–cataclysmic variable stage just as his non–accreting relatives do.

Future targets: Hitherto, all ultraviolet observations[1] of polars suffered from low spectral resolution and from strong contamination by geocoronal Lyα emission. Especially the broad geocoronal Lyα line hampers a reliable temperature determination, as it covers large parts of the white dwarf photospheric absorption profile. Our team in Göttingen has obtained the first high–resolution spectra of a polar, AM Her itself, using the *Goddard High Resolution Spectrograph* onboard *HST*. The observations were carried out during cycle 6 when the system was in a high state. A first inspection of the spectra reveals that the core of Lyα is largely filled in by emission, indicating that the strong irradiation during the high state apparently causes deviations from the temperature stratification of an unirradiated white dwarf. Future modelling of these and similar high–state observations need to include a self–consistent treatment of the radiation transfer with irradiation by cyclotron emission and/or thermal bremsstrahlung.

Obviously, "warm" ultraviolet emitting spots play an important rôle in the energy balance of the accretion process in polars. The actual size and shape of the heated region on the white

---

[1] both, *IUE* and *HST/FOS* achieved a spectral resolution of FWHM$\sim 6 - 9\,$Å.

dwarf strongly depends on the geometry of the accretion region, i.e. the height and the lateral extent of the shock. Future ultraviolet observations, using the high time and wavelength resolution of the *Space Telescope Imaging Spectrograph* (*STIS*) onboard *HST* will be needed to resolve the position, shape and temperature distribution of the irradiation–heated spots. These observations should be accompanied by reliable measurements of the hard X–ray and cyclotron fluxes. Incorporating the heating of the white dwarf by irradiation from the shock region in the accretion scenario for polars will ultimately improve our knowledge of magnetically funneled accretion in general.

Another important question which can be addressed with *HST/STIS* observations is the distribution of the accreted material over the surface of the magnetic white dwarf in polars. The knowledge of the distribution of the accreted material is an important ingredient e.g. for simulations of nova eruptions in magnetic cataclysmic variables. The low–state ultraviolet spectrum of AM Her obtained with *IUE* indicates the presence of heavy elements in the photosphere of the white dwarf. Nevertheless, the observed features are rather weak compared to the metal absorption spectra observed from the white dwarfs in dwarf novae. Apparently, the magnetic field prevents the accreted material from spreading perpendicular to the field lines over the white dwarf surface. However, the *IUE* low–state observations are too limited in both, S/N and spectral resolution, to draw any firm conclusion.

6.2 Dwarf Novae

I analysed the post–outburst evolution of the SU UMa dwarf nova VW Hyi based on the complete set of *IUE* archive data. From the large bulk of data available, I could show for the first time that the decrease of the observed ultraviolet flux is indeed due to a decrease of the photospheric temperature of the white dwarf. Furthermore, VW Hyi is the first SU UMa dwarf nova which allowed to derive cooling times of the accretion–heated white dwarf both after normal and superoutbursts. Following both types of outbursts, the accretion–heated white dwarf cools exponentially to a mean temperature $T_{\mathrm{wd}} \simeq 19\,000\,\mathrm{K}$. The temperature decay time is significantly longer after a superoutburst ($\tau_S = 9.8$ days) than after a normal outburst ($\tau_N = 2.8$ days). The declining luminosities and temperatures are in general agreement with models based on radiative or compressional heating of the outer layers of the white dwarf. However, from the present data it is not possible to unequivocally identify the heating mechanism. There is observational evidence that accretion as well as heating occurs in an equatorial belt and that the polar region of the white dwarf is not effectively swamped by metal–rich newly accreted material. There is also the distinct possibility that the equatorial region of the white dwarf never reaches an equilibrium state due to the frequent repetitive heating.

A dwarf nova very similar to VW Hyi, but with a much longer outburst cycle is EK TrA. This system, even though fainter than VW Hyi, may be better suited to study the thermal response of the white dwarf to dwarf nova outbursts. I have analysed the single available quiescent *IUE* spectrum of EK TrA yielding an estimate of the white dwarf temperature of $T_{\mathrm{wd}} \simeq 18\,000\,\mathrm{K}$. This spectrum is, however, still disc–dominated and has a white dwarf contribution to the SWP

flux of $\sim 25\,\%$ only. In contrast to VW Hyi, no ultraviolet spectrum of EK TrA in quiescence exists so far. Optical spectroscopy of the system deep in quiescence confirms the flux level of the white dwarf derived from the *IUE* data. Additional optical emission arises from a cool ($T \simeq 6500\,\mathrm{K}$) accretion disc (or a corona situated on top of a colder disc), possibly extending over much of the Roche radius of the primary. Both, optical and ultraviolet data yield a distance of $d \simeq 180\,\mathrm{pc}$, about three times that of VW Hyi.

Future targets: Detailed information of the white dwarf properties in dwarf novae, such as temperature, post–outburst cooling timescale, rotational velocity, and chemical abundances have been derived so far only for a handful of dwarf novae (see Sect. 4.5). The best–studied white dwarfs are harboured in systems with extremely different properties: VW Hyi is a short–period SU UMa dwarf nova, U Gem is the prototype of its own class of long–period dwarf novae, and WZ Sge is a TOAD, an ultrashort–period SU UMa dwarf nova with an extremely long outburst period. It is, therefore, clear that the white dwarf characteristics derived so far are only of snapshot character. However, all these characteristics are important ingredients to probe the thermal response of the white dwarf to intermittent accretion (Pringle 1988; Sion 1995), to verify the presence of a differentially rotating accretion belt (Kippenhahn & Thomas 1978; Kutter & Sparks 1987) and to test the theory of disc evaporation (Meyer & Meyer–Hofmeister 1994). As the few dwarf novae studied at a sufficient level of detail form an extremely heterogeneous set, a more general understanding of these phenomena presently evades us.

In order to progress to a deeper understanding of the mutual relation between the white dwarf properties and the accretion process, a comparative study of several objects with *similar* overall properties is necessary. The poorly studied SU UMa dwarf nova EK TrA proved to be similar in many respects to the well–known system VW Hyi, except for the outburst cycle and, thereby, for the accretion rate. The long outburst period of EK TrA makes the system a unique candidate to study the evolution of both accretion disc and white dwarf into deep quiescence.

Appendix A

Glossary

AAVSO	American Association of Variable Star Observers
ANS	Astronomical Netherlands Satellite
EUVE	Extreme Ultraviolet Explorer
EXOSAT	European X–ray Observatory Satellite
FOS	Faint Object Spectrograph
FWHM	Full Width Half Maximum
GHRS	Goddard High Resolution Spectrograph
HUT	Hopkins Ultraviolet Telescope
IUE	International Ultraviolet Explorer
LWP	Long Wave Prime camera
LWR	Long Wave Redundant camera
HST	Hubble Space Telescope
IUESIPS	IUE Spectral Image Processing System
NEWSIPS	Newly developed IUE Spectral Image Processing System
ORFEUS	Orbiting Retrievable Far and Extreme Ultraviolet Spectrometer
PSPC	Position Sensitive Proportional Counter
RASS	ROSAT All Sky Survey
RIASS	ROSAT IUE All Sky Survey
ROSAT	Röntgensatellit (X-ray satellite)
S/N	Signal–to–noise
STIS	Space Telescope Imaging Spectrograph
SWP	Short Wave Prime camera
VSS RASNZ	Variable Star Section of the Royal Astronomical Society of New Zealand

Appendix B

Evolution Strategies

In Chapter 4, I used an evolution strategy algorithm to decompose observed *IUE* spectra of dwarf novae into contributions from the white dwarf, from the accretion disc and from selected emission lines. This algorithm, even though a very powerful tool for multi–parameter optimisation, has so far never been applied to astrophysical problems[1]. The great strengths of the evolution strategies are their flexibility which allows them to be adopted to (almost) any kind of optimisation problem, their stability against local optima and the easy way to implement any additional constraints.

The initial concept of the evolution strategies was developed in 1964 by H.–P. Schwefel and I. Rechenberg at the Technische Universität Berlin in order to optimise the aerodynamic properties of a wing in a wind tunnel experiment. The idea was to transcribe the evolutionary mechanisms of nature, i.e. mutation, recombination and selection, into an algorithm applicable to technical problems. Rechenberg and collaborators continuously improved the algorithm and a comprehensive review is given by Rechenberg (1994, in German). As there exists little introductory literature in English, I outline below the very basic concepts of evolution strategy algorithms.

Very generally spoken, the process of optimisation is the search for a set of parameters which satisfy a certain number of constraints for a given problem. In nature, this means to evolve a large number of characteristics of a creature in order to maximize its fitness function, i.e. its chances to survive. Formally, this corresponds to the search of a parameter vector $\underline{X}$ which optimises a quality function $q(\underline{X})$. As an example, consider the following function

$$f(\underline{X}) = 2^{2N} \sum_{i=1}^{N} (1 - X_i) \sin(m\pi X_i) \tag{B.1}$$

where N is the dimension of the parameter vector $\underline{X}$ and m^N is the number of local maxima for

---

[1]A description of the more widespread genetic algorithms can be found in Charbonneau (1995). Even though similar in the basic approach, i.e. copying some of nature's optimisation procedures, the genetic algorithms differ substantially from the evolution strategies presented here.
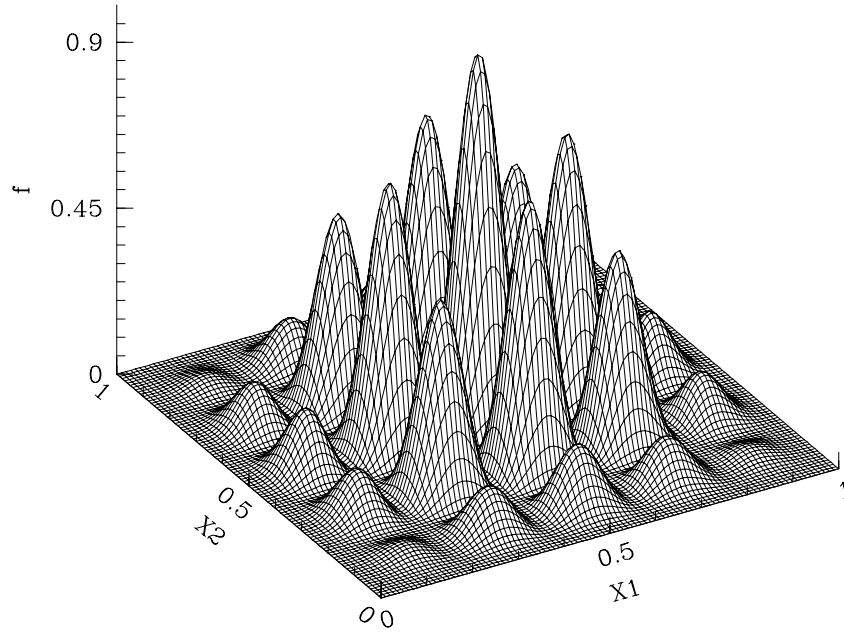
Figure B.1: Surface plot of $f(\underline{X})$ from equ. B.1 with $N = 2$ and $m = 5$.

$X_i = [0, 1]$. Fig. B.1 shows this function for $N = 2$ and $m = 5$. The optimisation problem in this case is to find the vector $\underline{X}$ which yields the *absolute* maximum of $f(\underline{X})$, which is located at $X_i = 0.5$ if m is odd. From Fig. B.1, it is clear that any simple gradient search has very high chances to end up in a local maximum of $f(\underline{X})$. The function $f(\underline{X})$ will demonstrate below the capability of the evolution strategies.

The simplest evolution strategy involving one parent and λ offsprings works as follows. (a) Choose an initial point P in the parameter space, called the *parent*. (b) Distribute λ points O_i regularly over a sphere of radius 1, centered on P. These are the *offsprings*. (c) Offset each offspring O_i by an amount δ_{O_i} along the line passing through O_i and P. (d) Compute for all O_i offspring the value of their quality, $q(O_i)$. (e) Choose the best offspring O_{best}, declare him parent P for the next generation and go to (a).

Steps (b) and (c) are called *mutation*, step (e) is called *selection*. Formally, the mutation can be expressed as follows:

$$
\begin{aligned}
\delta_{O_i}^g &= \delta_P^g \cdot \xi_i \\
\underline{X}_{O_i}^g &= \underline{X}_P^g + \delta_{O_i}^g \cdot \underline{z}_i
\end{aligned}
\qquad \text{with } i = 1, \ldots, \lambda
$$

where $\underline{X}_P^g$ is the parent parameter vector, δ_P^g is the parent mutation step width, $\underline{z}_i$ is a normalized vector with random orientation in the parameter space and ξ_i is set randomly either to α or to

$1/\alpha$. α is a parameter which controls the rate of mutation between two generations. Empirical tests yield $\alpha = 1.3$ as optimal value for problems with $\lesssim 100$ parameters. The selection is expressed as follows:

$$
\begin{aligned}
\delta_P^{g+1} &= \delta_{O\,\text{best}}^g \\
\underline{X}_P^{g+1} &= \underline{X}_{O\,\text{best}}^g
\end{aligned}
$$

As an illustrative example, I used an evolution strategy[2] with $\lambda = 30$ offsprings to find the global maximum of equ. B.1 with $N = 2$ and $m = 9$, i.e. 81 local maxima. Additional constraints in this problem are that $0 \leq X_{1,2} \leq 1$. These constraints were implemented by decreasing the quality of an offspring $X_{O_i}^g$ by a factor of ten if X_1 or X_2 fall outside the allowed range. Fig. B.2 shows the result of this test. The evolution strategy was started with an initial parent vector $X_{1,2} = 0$. The global maximum is found after $\simeq 300$ generations, using $\sim 0.6\,\text{sec}$ of CPU time on a 120 MHz Pentium.

The spectral decomposition described in Sect. 4.3.3 and Sect. 4.4.3 was solved with the same evolution strategy, defining as quality function the value of χ^2, i.e. $(F_{\text{obs}} - F_{\text{model}})^2/\sigma^2$, where F_{obs}, F_{mod} and σ are the observed flux, the model flux and the error of the observed flux, respectively. The optimisation included 12 free parameter: the scaling factors of the white dwarf flux and the disc flux, the white dwarf temperature, and the FWHM, central wavelengths and amplitudes of three Gaussians describing the emission of N v, Si iv and C iv. Additional constraints were as follows: the white dwarf temperature had to be $11\,000\,\text{K} \leq T_{\text{wd}} \leq 30\,000\,\text{K}$, no flux contribution had to be less than zero (i.e. no absorption lines allowed), $2\,\text{Å} \leq \text{FWHM} \leq 12\,\text{Å}$ and the central wavelengths were allowed to vary $|\lambda_c - \lambda_{\text{lab}}| \leq 3\,\text{Å}$.

Concluding, evolution strategies are a flexible tool for multiparameter optimisation problems. Further astronomical applications may include the search for $(P_{\text{orb}}, \dot{P}_{\text{orb}})$ in time–resolved observations of pulsars, mapping of the intensity distribution along accretion streams in polars[3], or the deconvolution of the magnetic field distribution of a white dwarf from spin–phase–resolved spectropolarimetry[4].

---

[2]based on a library of evolutionary strategy routines developed by U. Utecht and K. Trint, Technische Universität Berlin.

[3]An similar approach using genetic algorithms has been reported by Hakala (1995).

[4] An extension of this method is underway in two diploma theses at the Universitäts–Sternwarte Göttingen .
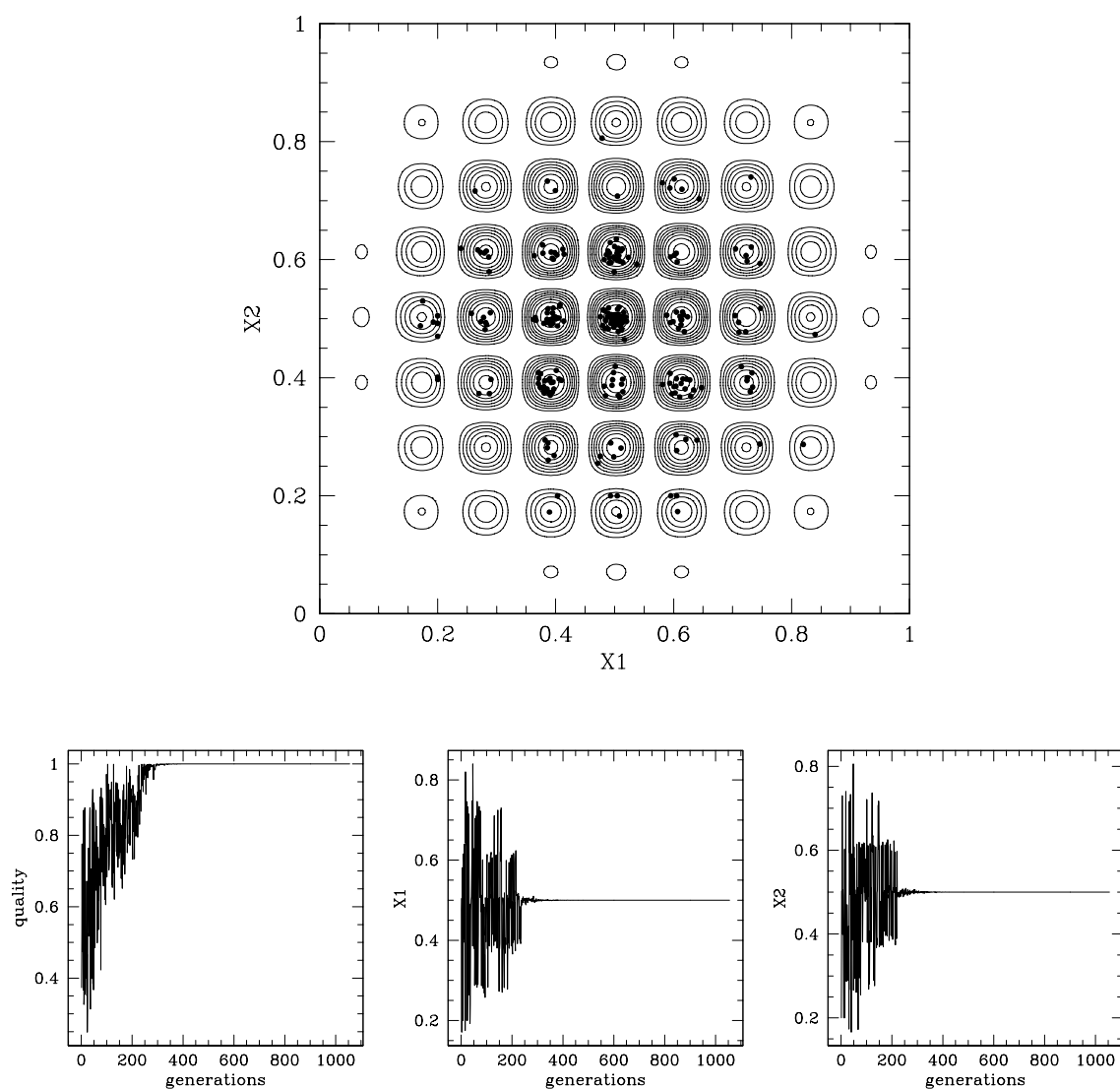
Figure B.2: Application of an evolution strategy with λ offsprings to $f(\underline{X})$ (equ. B.1) with $N = 2$ and $m = 9$. Top: contour plot of $f(\underline{X})$. The dots mark the position of the best offspring from each generation. Bottom, from left to right: the values for $f(\underline{X})$, X_1 and X_2 as a function of the generation.

References

Aizu, K., 1973, Progr. Theor. Phys., 49, 1184

Armitage, P.,J., Livio, M., 1996, ApJ 470, 1024

Bahcall, N. A., Harris, D.E., Strom, R.G., 1976, ApJ 209, L17

Bath, G.T., 1973, Nature Phys. Sci 246, 84

Bath, G.T., Pringle, J.E., Whelan, J.A.J., 1980, MNRAS 190, 185

Bailey, J., 1981, MNRAS 197, 31

Bailey, J., Cropper, M., 1991, MNRAS 253, 27

Bailey, J., Watts, D.J., Sherrington, M.R., Axon, D.J., Giles, A.B., Hanes, D.A., Heathcote, S.R., Hough, J.H., Hughes, S., Jameson, R.F., McLean, I., 1985, MNRAS 215, 179

Bailey, J., Hough, J.H., Wickramasinghe, D.T., 1988, MNRAS 233, 395

Bailey, J., Ferrario, L., Wickramasinghe, D.T., 1991, MNRAS 251, 37p

Beardmore, A.P., Done, C., Osborne, J.P., Ishida, M., 1995a, MNRAS 272, 749

Beardmore, A.P., Ramsay, G., Osborne, J.P., Mason, K.O., Nousek, J.A., Baluta, C., 1995b, MNRAS 273, 742

Belloni, T., Verbunt, F., Beuermann, K., Bunk, W., Izzo, C., Kley, W., Pietsch, W., Ritter, H., Thomas, H.-C., Voges, W., 1991, A&A 246, L46

Berg, R.A., Duthie, J.G., 1977, ApJ 211, 859

Bergeron, P., Saffer, R.A., Liebert, J., 1992, ApJ 394, 228

Beuermann, K., 1997, in *Perspectives in High Energy Astronomy & Astrophysics*, Proceedings of the International Colloquium to Commemorate the Golden Jubilee of the Tata Institute of Fundamental Research.

Beuermann, K., Burwitz, V., 1995, in *Cape Workshop on Magnetic Cataclysmic Variables*, eds. Buckley, D.A.H. & Warner, B., p. 99 (ASP Conf. Ser. 85)

Beuermann, K., Thomas, H.-C., 1993, Adv. Space Res. 13, (12)115

Beuermann, K., Woelk, U., 1996, in *Cataclysmic Variables and related objects*, IAU Coll 158, eds. A. Evans, & J.H., Wood, p. 199 (Dordrecht: Kluwer)

Beuermann, K., Thomas, H.-C., Schwope, A., 1988, A&A 195, L15

Beuermann, K., Thomas, H.-C., Pietsch, W., 1991a, A&A 246, L36

Beuermann, K., Predehl, P., Thomas, H.-C., de Martino, D., Barwig, H., Mantel, K.-H., 1991b, IAU Circ. No. 5244

Biermann, P., Schmidt, G.D., Liebert, J., Stockman, H.S., Tapia, S., Kühr, H., Strittmaier, P.A., West, S., Lamb, D.Q., 1985, ApJ 293, 303

Boeshaar, P.C., 1976, PhD thesis, Ohio State University

Boggess, A., Carr, F.A., Evans, D.C., Fischel, D., Freeman, H.R. et al., 1978, Nature 275, 372

Bond, H.E., Wagner, R.L., 1977, IAU Circ. 3049

Bonnet-Bidaud, J.-M., Mouchet, M., 1987, A&A 188, 89

Brett, J.M., Smith, R.C., 1993, MNRAS 264, 641

Buckley, D.A.H., Warner, B. (eds.), 1995, *Cape Workshop on Magnetic Cataclysmic Variables* (ASP Conf. Ser. 85)

Buckley, D.A.H., O'Donoghue, D., Hassall, B.J.M., Kellet, B.J., Mason, K.O., Skiguchi, K., Watson, M.G., Wheatley, P.J., Chen, A., 1993, MNRAS 262, 93

Burwitz, V., Reinsch, K., Schwope, A.D., Beuermann, K., Thomas, H.-C., Greiner, J., 1996, A&A 305, 507

Burwitz, V., Reinsch, K., Beuermann, K., Thomas, H.-C., 1997a, A&A *in press*

Burwitz, V., Reinsch, K., Schwope, A.D., Hakala, P.J., Beuermann, K., Rousseau, Th., Thomas, H.-C., Gänsicke, B.T., Piirola, V., Vilhu, O., 1997b, *A&A submitted*

Charbonneau, P., 1995, ApJS 101, 309

Cheng, F.H., Marsh, T.R., Horne, K., Hubeny, I., 1994, AIP conf. proc. 308, 197

Cheng, F.H., Sion, E.M., Szdoky, P., Huang, M., 1997, ApJ 484, L149

Cropper, M., 1988, MNRAS 231, 597

Cropper, M., 1990, Space Sci. Rev. 54, 195

Dahn, C.C., Riepe, B.Y., Guetter, H.H., Walker, R.L., Vrba, F.J., Hewitt, A. V., Harrington, R.S., Christy, J.W., Kallarakal, V.V., Miranian, M., 1982, AJ 87, 419

de Martino, D., Buckley, D.A.H., Mouchet, M., Mukai, K., 1995, A&A 298, L5

de Martino, D., Mouchet, M., Rosen, S.R., Gänsicke, B.T., Clayton, K.L., Mason, K.O., 1997, A&A *in press*

Ferrario, L., Wickramasinghe, D.T., Bailey, J., Hough, J.H., Tuohy, I.R., 1992, MNRAS 256, 252

Finley, D.S., Basri, G., Bowyer, S., 1990, ApJ 359, 483

Friedrich, S., Staubert, R., La Dous, C., 1996, A&A 315, 411

Frank, J., King, A. R., Lasota, J.-P., 1988, A&A 193, 113

Gänsicke, B.T., 1993, *Berechnung von Atmosphären weißer Zwerge mit H-line blanketing und Anwendung auf kataklysmische Veränderliche*, Diplomarbeit, Technische Universität Berlin. (MSc Thesis)

Gänsicke, B.T., Beuermann, K., 1996, A&A 309, L47

Gänsicke, B.T., Beuermann, K., de Martino, D., 1995, A&A 303, 127

Gänsicke, B.T., Beuermann, K., Thomas, H.-C., 1997, MNRAS 289, 388

Glenn, J., Howell, S.B., Schmidt, G.D., Liebert, J., Grauer, A.D., Wagner, R.M., 1994, ApJ 424, 967

Götz, W., 1993, AN 314, 69

Greenstein, J.L., 1957, ApJ 126, 23

Hakala, P.J., 1995, A&A 296, 164

Hamada, T., Salpeter, E.E., 1961, ApJ 134, 683

Hameury, J.M., King, A.R., 1988, MNRAS 235, 433

Hassall, B.J.M., 1985, MNRAS 216, 335

Hassall, B.J.M., La Dous, 1996, in *Cataclysmic Variables and related objects*, IAU Coll 158, eds. A. Evans, & J.H., Wood, p. 85 (Dordrecht: Kluwer)

Hassall, B.J.M., Pringle, J.E., Schwarzenberg-Czerny, A., Wade, R.A., Whelan, J.A.J., Hill, P.W., 1983, MNRAS 203, 865

Hassall, B.J.M., Pringle, J.E., Verbunt, F., 1985, MNRAS 216, 353

Haswell, C.A., Patterson, J., Thorstensen, J.R., Hellier, C., Skillman, D.R., 1997, ApJ 476, 847

Hearn, D.R., Richardson, J.A., Clark, G.W., 1976, ApJ 210, L23

Heise, J., Verbunt, F., 1988, A&A 189,112

Heise, J., Brinkman, A.C., Gronenschild, E., Watson, M., King, A.R., Stella, L., Kieboom, K., 1985, A&A 148, L14

Heise, J., van Teeseling, A., Kahabka, P., 1994, A&A 288, L45

Hessman, F.V., 1997, MNRAS *submitted*

Holberg, J.B., Wesemael, F., Wegner, G., Bruhweiler, F.C., 1985, ApJ 293, 294

Holberg, J.B., Wesemael, F., Basile, J., 1986, ApJ 306, 629

Huang, M., Sion, E.M., Hubeny, I., Cheng, F.H., Szkody, P., 1996, in *Cataclysmic Variables and related objects*, IAU Coll 158, eds. A. Evans, & J.H., Wood, p. 247 (Dordrecht: Kluwer)

Jordan, S., 1992, A&A 265, 570

Keys, C.D., 1995, *FOS Instrument Handbook*, Space Telescope Science Institute, Version 6.0

King, A.R., 1988, Quart. Jour. Roy. Astr. Soc., 29, 1

King, A.R., 1989, MNRAS 241, 365

King, A.R., Lasota, J.P., 1979, MNRAS 188, 653

King, A.R., Frank, J., Kolb, U., Ritter, H., 1995, ApJ 444, L37

Kippenhahn, R., Thomas, H.-C., 1978, A&A 63, 265

Kiplinger, A. L., Sion, E. M., Szkody, P., 1991, ApJ 366, 569

Kley, W., 1989, A&A 222, 141

Kley, W., 1991, A&A 247, 95

Koester, D., Weidemann, V., Zeidler-K.T., E.-M., Vauclair, G., 1985, A&A 142, L5

Kolb, U., 1995, in *Cape Workshop on Magnetic Cataclysmic Variables*, eds. Buckley, D.A.H. & Warner, B., p. 440 (ASP Conf. Ser. 85)

Kolb, U., 1996, in *Cataclysmic Variables and related objects*, IAU Coll. 158, eds. Evans, A. & Wood, J.H., p. 433 (Dordrecht: Kluwer)

Kolb, U., Stehle, R., 1996, MNRAS 282, 1454

Kraft, R.P., Matthews, J., Greenstein, J.L., 1962, ApJ 136, 312

Kraft, R.P., Krzeminski, W., Mumford, G.S., 1969, ApJ 158, 589

Krzeminski, W., Kraft, R.P., 1964, ApJ 140, 921

Krzeminski, W., Serkowski, K., 1977, ApJ 216, L45

Kuijpers, J., Pringle, J.E., 1982, A&A 114, L4

Kutter, G.S., Sparks, W.M., 1987, ApJ 321, 386

Kutter, G.S., Sparks, W.M., 1989, ApJ 340, 985

Lamb, D.Q., Masters, A.R., 1979, ApJ 234, L117
Liebert, J., Stockman, H.S., Angel, J.R.P., Woolf, N.J., Hege, K., 1978, ApJ 225, 201
Litchfield, S.J., King, A.R., 1990, MNRAS 247, 200
Livio, M., Pringle, J.E., 1994, ApJ 427, 956
Long, K.S., Blair, W.P., Bowers, C.W., Davidson, A.F., Kriss, G.A., Sion, E.M., Hubeny, I.,
     1993, ApJ 405, 327
Long, K.S., Sion, E.M., Huang, M., Szkody, P.,1994, ApJ 424, L49
Long, K.S., Blair, W.P., Raymond, J.C., 1995, ApJ 454, L39
Long, K.S., Mauche, C.W., Raymond, J.C., Szkody, P., Mattei, J., 1996, ApJ 469, 841

Maraschi, L., Treves, A., Tanzi, E.G., Mouchet, M., Lauberts, A., Motch, C., Bonnet-Bidaud,
     J.M., Phillips, M.M., 1984, ApJ 285, 214
Mateo, M., Szkody, P., 1984, AJ 89, 863
Mattei, J. A., 1994, observations from the AAVSO International Database, private communica-
     tion.
Mauche, C.W., 1996, in *Cataclysmic Variables and related objects*, IAU Coll 158, eds. A.
     Evans, & J.H., Wood, p. 243 (Dordrecht: Kluwer)
Mauche, C.W., Raymond, J.C., Cordova, F.A., 1988, ApJ 355, 829
Mauche, C.W., Wade, R.A., Polidan, R.S., van der Woerd, H., Paerels, F.
McDermott, P.N., Taam, R.E., 1989, ApJ 342, 1019
Meyer, F., Meyer-Hofmeister, E., 1994, A&A 288, 175
Mittaz, J.P.D., Rosen, S.R., Mason, K.O, Howell, S.B., 1992, MNRAS 258, 277
Mukai, K., Charles, P.A., 1986, MNRAS 222, 1p
Mukai, K., Charles, P.A., 1987, MNRAS 226, 209

Nelan, E.P., Wegner, G., 1985, ApJ 289, L31
Nousek, J.A., Takalo, L.O., Schmidt, G.D., Tapia, S., Hill, G.J., Bond, H.E., Grauer, A.D.,
     Stern, R.A., Agrawal, P.C., ApJ 277, 682

O'Donoghue, D., Mason, K.O., Chen, A., Hassall, B.J.M., Watson, M.G., 1993, MNRAS 265,
     545
Osaki, Y., 1996, PASP 108, 39
Osborne, J.P., Bonnet-Bidaud, J.-M., Bowyer, S., Charles, P.A., Chiappetti, L., Clarke, J.T.,
     Henry, J.P., Hill, G.J., Kahn, S., Maraschi, L., Mukai, M., Treves, A., Vrtilek, S., 1986,
     MNRAS 221, 823
Osborne, J.P., Beuermann, K., Charles, P., Maraschi, L., Mukai, K., Treves, A., 1987, ApJ 315,
     L123
Osborne, J.P., Beardmore, A.P., Wheatley, P.J., Hakala, P., Watson, M.G., Mason, K.O., Hassall,
     B.J.M., King, A.R., 1994, MNRAS 270, 650
Oswalt, T.D., Smith, J.A., Wood, M.A., Hintzen, P., 1996, Nature 382, 692

Panek R.J., Holm A.V., 1984, ApJ 277, 700

Paerels, F., Heise, J., van Teeseling, A., 1994, ApJ 426, 313

Patterson, J., 1984, ApJS 54, 443

Patterson, J., Raymond, J.C., 1985a, ApJ 292, 535

Patterson, J., Raymond, J.C., 1985b, ApJ 292, 535

Paresce, F., 1984, AJ 89, 1022

Polidan, R.S., Holberg, J.B., 1987, MNRAS 225, 131

Popham, R., 1997, ApJ 478, 734

Prialnik, D., Kovetz, A., 1995, ApJ 445, 789

Priedhorsky, W., Matthews, K., Neugebauer, G., Werner, M., Krzeminski, W., 1978, ApJ 226, 397

Pringle, J.E., 1988, MNRAS 230, 587

Pringle, J.E., Bateson, F.M., Hassall, B.J.M., Heise, J., van der Woerd, H., Holber, J.N., Polidan, R.S., van Amerongen, S., van Paradijs, J., Verbunt, F., 1987, MNRAS 225, 73

Puchnarewicz, E.M., Mason, K.O., Murdin, P.G., Wickramasinghe, D.T., 1990, MNRAS 244, 20p

Ramsay, G., Mason, K.O., Cropper, M., Watson, M.G., Clayton, K.L., 1994, MNRAS 270, 692

Ramseyer, T.F., 1994, ApJ 425, 243

Rappaport, S., Verbunt, F., Joss, P.C., 1983, ApJ 275, 713

Raymond, J.C., Black, J.H., Davis, R.J., Dupree, K., Gursky, H., Hartmann, L., 1979, ApJ 230, L95

Raymond, J.C., Mauche, C.W., Bowyer, S., Hurwitz, M., 1995, ApJ 440, 331

Rechenberg, I., 1994, *Evolutionsstrategie '94* (froommann–holzboog: Stuttgart)

Remillard, R.A., Schachter, J.F., Silber, A.D., Slane, P., 1994, ApJ 426, 288

Reinsch, K., Burwitz, V., Beuermann, K., Schwope, A.D., Thomas, H.-C., 1994, A&A 291, L1

Ritter, H., 1990, A&AS 85, 1179

Ritter, H., Kolb, U., 1997, A&AS, *submitted*

Robinson, E.L., Nather, R.E., Patterson, J., ApJ 219, 168

Rothschild, R.E., Gruber, D.E., Knight, F.K., Matteson, J.L., Nolan, P.L., Swank, J.H., Holt, S.S., Serlemitos, P.J., Mason, K.O., Tuohy, I.R., 1981, ApJ 250, 723

Rousseau, Th., Fischer, A., Beuermann, K., Woelk, U., 1996, A&A 310, 526

Schmidt, G.D., Smith, P.S., 1995, ApJ 448, 305

Schmidt, G.D., Stockman, H.S., Margon, B., 1981, ApJ 243, L157

Schmidt, G.D., Stockman, H.S., Grandi, S.A., 1983, ApJ 271, 753

Schmidt, G.D., Liebert, J., Stockman, H.S., 1995, ApJ 441, 414

Schmidt, G.D., Szkody, P., Smith, P.S., Silber, A., Tovmassian, G., Hoard, D.W., Gänsicke, B.T., de Martino, D., 1996, ApJ 473, 483

Schwarzenberg-Czerny, A., Ward, M., Hanes, D.A., Jones, D.H.P., Pringle, J.E., Verbunt, F., Wade, R.A., 1985, MNRAS 212, 645

Schwope, A.D., 1990, in *Reviews in Modern Astronomy 3*, p. 44

Schwope, A.D., 1991, *Akkretion in AM–Herculis–Sternen*, Dissertation, Technische Universität Berlin. (PhD Thesis)

Schwope, A.D., Thomas, H.-C., Beuermann, K., 1993, A&A 271, L25

Schwope, A.D., Beuermann, K., Jordan, S., Thomas, H.-C., 1993, A&A 278, 487

Schwope, A.D., Beuermann, K., Jordan, S., 1995, A&A 301, 447

Sekiguchi, K., Nakada, Y., Bassett, B., 1994, MNRAS 266, L51

Shafter, W., Szkody, P., Liebert, J., Penning, W.R., Bond, H.E., Grauer, A.D., 1985, ApJ 290, 707

Shakura, N.I., Sunyaev, R.A., 1973, A&A 24, 337

Silber, A.D., Bradt, H.V., Ishida, M., Ohashi, T., Remillard, R.A., 1992, ApJ 389, 704

Singh, K.P., Szkody, P., Barret, P., White, N.E., Fierce, E., Silber, Hoard, D.W., Hakala, P.J., Piirola, V., Sohl, K., 1995, ApJ 453, L95

Sion, E.M., 1991, AJ 102, 295

Sion, E.M., 1995, ApJ 438, 876

Sion, E.M., Leckenby, H.M., Szkody, P., 1990, ApJ 364, L41

Sion, E.M., Long, K., Szkody, P., Huang, M. 1994, ApJ 430, L53

Sion, E.M., Cheng, F.H., Long, K., Szkody, P., Gilliland, R.L., Huang, M., Hubeny, I., 1995a, ApJ 439, 957

Sion, E.M., Szkody, P., Cheng, F.H., Huang, M., 1995b, ApJ 444, L97

Sion, E.M., Huang, M., Szkody, P., Cheng, F.H., 1995c, ApJ 445, L31

Sion, E.M., Cheng, F.H., Huang, M., Hubeny, I., Szkody, P., 1996, ApJ 471, L41

Sion, E.M., Cheng, F.H., Sparks, W.M., Szkody, P., Huang, M., Hubeny, I., 1997, ApJ 480, L17

Smak, J., 1984, AcA 34, 317

Sparks, W.M., Sion, E.M., Starrfield, S.G., Austin, S., 1993, Ann. Isr. Phys. Soc. 10, 96

Staubert, R., König, M., Friedrich, S., Lamer, G., Sood, R.K., James, S.D., Sharma, D.P., 1994, A&A 288, 513

Stella, L., Beuermann, K., Patterson, J., 1986, ApJ 306, 225

Stockman, H.S., Schmidt, G.D., 1996, ApJ 468, 883

Stockman, H.S., Schmidt, G., Lamb, D.Q., 1988, ApJ 332, 282

Stockman, H.S., Schmidt, G., Liebert, J., Holberg, J.B., 1994, ApJ 430, 323

Szkody, P., Silber, A., 1996, AJ 112, 289

Szkody, P., Raymond, J.C., Capps, R.W., 1982, ApJ 257, 686

Szkody, P., Liebert, J., Panek, R.J., 1985, ApJ 293, 321

Szkody, P., Downes, R., Mateo, M., 1988, PASP 100, 362

Szkody, P., Downes, R., Mateo, M., 1990, PASP 102, 1310

Szkody, P., Silber, A., Hoard, D.W., Fierce, E., 1995, ApJ 455, L43

Tapia, S., 1976a, IAU Circ. No. 2987

Tapia, S., 1976b, IAU Circ. No. 2994

Tapia, S., 1977, IAU Circ. No. 3054

Thomas, H.-C., Beuermann, K., Schwope, A.D., Burwitz, V., 1996, A&A 313, 833

Tovmassian, G., Greiner, J., Zickgraf, F.-J., Kroll, P., Krautter, J., Thiering, I., Zharykov, A.V., Serrano, A., 1997, A&A *in press*

van Amerongen, S., Damen, E., Groot, M., Kraakman, H., van Paradijs, J., 1987, MNRAS 225, 93

van der Woerd, H., Heise, J., 1987, MNRAS, 225, 141

van Paradijs, J., Augusteijn, T., Stehle, R., 1996, A&A 312, 93

van Teeseling, A., Verbunt, F., Heise, J., 1993, A&A, 270, 159

van Teeseling, A., Heise, J., Paerels, F., 1994, A&A 281, 119

van Teeseling, A., Kaastra, J.S., Heise, J., 1996, A&A 312, 186

Verbunt, F., 1984, MNRAS 209, 227

Verbunt, F., 1987, A&AS 71, 339

Verbunt, F., Zwaan, C, 1981, A&A 100, L7

Verbunt, F., Hassall, B.J.M., Pringle, J.E., Warner, B., Marang, F., 1987, MNRAS 225, 113

Vidal, C.R., Cooper, J., Smith, E.W., 1973, ApJS 25, 37

Voges, W. et al., 1997, A&A *in press*

Walter, F.M., Wolk, S.J., Adams, N.R., 1995, ApJ 440, 834

Warner, B., 1987, MNRAS 227, 23

Warner, B., 1995, *Cataclysmic Variable Stars* (Cambridge University Press)

Warner, B., 1997, in *proceedings of the 13th North American Workshop on Cataclysmic Variables*, eds S. Howell et al., (ASP Conf. Ser. *in press*)

Wheatley, P.J., Verbunt, F., Belloni, T., Watson, M.G., Naylor, T., Ishida, M., Duck, S.R., Pfeffermann, E., 1996, A&A 307, 137

Wesemael, F., Auer, L.H., Van Horn, H.M., Savedov, P., 1980, ApJS 43, 159

Wickramasinghe, D.T., Visvanathan, N, Tuohy, I.R., 1984, ApJ 286, 328

Williams, R.E., 1980, ApJ 235, 939

Woelk, U., Beuermann, K., 1992, A&A 256, 498

Woelk, U., Beuermann, K., 1993, A&A 280, 169

Woelk, U., Beuermann, K., 1996, A&A 306, 232

Wolf, M., 1924, AN 220, 255

Wood, J.H., Naylor, T., Hassall, B.J.M., Ramseyer, T.F., 1995, MNRAS 273, 772

Wood, M.A., 1995, in *White Dwarfs*, ed. D. Koester, K. Werner, 41 (Berlin: Springer)

Wunner, G., 1987, Mitt. Astron. Ges. 70, 1987

Young, P., Schneider, D.P., 1981a, ApJ 245, 1043

Young, P., Schneider, D.P., 1981b, ApJ 247, 960

Acknowledgements

List of publications

Refereed Journals

Burwitz, V., Reinsch, K., Schwope, A.D., Hakala, P.J., Beuermann, K., Rousseau, Th., Thomas, H.–C., Gänsicke, B.T., Piirola, V., Vilhu, O., 1997. A new ROSAT discovered polar near the lower period limit: RX J1015.5+0904 in Leo, *A&A in press*

de Martino, D., Mouchet, M., Rosen, S.R., Gänsicke, B.T., Clayton, K.L., Mason, K.O., 1997. Insights into the accretion flow in QS Tel (RE1938–461), *A&A in press*

Gänsicke, B.T., Beuermann, K., 1996. The cooling of the white dwarf in VW Hydri, *A&A* 309, L47

Gänsicke, B.T., Beuermann, K., de Martino, D., 1995. The white dwarf in AM Herculis, *A&A* 303, 127

Gänsicke, B.T., Beuermann, K., Thomas, H.–C., 1997. EK TrA, a close relative of VW Hyi, *MNRAS* 289, 388

Gänsicke, B.T., van Teeseling, A., Beuermann, K., de Martino, 1997. Hubble Space Telescope ultraviolet spectroscopy of the Supersoft X–ray binaries CAL 83 and RX J0513.9–6951, *A&A in press*

Sion, E.M., Cheng, F.H., Szkody, P., Sparks, W., Gänsicke, B.T., Huang, M., Mattei, J., 1997. Anomalous cooling of the massive white dwarf in U Geminorum following a narrow dwarf nova outburst, *ApJ in press*

Schmidt, G.D., Szkody, P., Smith, P.S., Silber, A., Tovmassian, G., Hoard, D.W., Gänsicke, B.T., de Martino, D., 1996. AR Ursae Majoris: The first high–field magnetic cataclysmic variable, *ApJ* 473, 483

Conference proceedings

Gänsicke, B.T., 1997. Accretion heated magnetic white dwarfs, in *Proceedings of the 13th North American Workshop on Cataclysmic Variables*, eds. S. Howell & E. Kuulkers, *in press* (ASP conf. series)

Gänsicke, B.T., Beuermann, K., 1996. VW Hyi: a rapidly cooling white dwarf, in *Cataclysmic Variables and Related Objects*, IAU Coll. 158, eds. A. Evans, J.H. Wood, p. 251 (Dordrecht: Kluwer)

Gänsicke, B.T., Beuermann, K., 1996. The cooling of the white dwarf in VW Hyi, in *Röntgenstrahlung from the Universe*, eds. H.U. Zimmermann et al., MPE Report 263, p. 137

Gänsicke, B.T., Beuermann, K., 1996. Detection of the white dwarf in EK TrA, in *AG Abstracts 12*, p. 197

Gänsicke, B.T., Beuermann, K., 1997. EK TrA, a spectroscopic twin of VW Hyi, in *IAU Coll. 163, Accretion Phenomena and Related Outflows*, eds. D. Wickramasinghe et al., *in press*

Gänsicke, B.T., Beuermann, K., de Martino, D., 1994. The white dwarf in AM Herculis, in *AG Abstracts* 10, 71

Gänsicke, B.T., Beuermann, K., de Martino, D., 1995. The white dwarf in AM Her, in *White Dwarfs*, eds. D. Koester, K. Werner, p. 263 (Berlin: Springer)

Gänsicke, B.T., Beuermann, K., de Martino, D., 1995. AM Her: The reprocessed radiation component identified, in *Cape Workshop on Magnetic Cataclysmic Variables*, eds. D.A.H. Buckley, B. Warner, p. 331 (ASP Conf. Ser. 85)

Gänsicke, B.T., Beuermann, K., de Martino, D., 1996. Phase–resolved UV spectroscopy of RX J0019.8+2156, in *Supersoft X–ray Sources*, ed. J. Greiner, Lecture Notes in Physics 472, p. 105 (Berlin: Springer)

Gänsicke, B.T., Beuermann, K., de Martino, D., Jordan, S., 1996. Accretion–heated magnetic white dwarfs, in *AG Abstracts 12*, p. 32

Gänsicke, B.T., Beuermann, K., de Martino, D., Jordan, S., 1997. White Dwarfs in AM Herculis Systems, in *White Dwarfs*, ed. J.Isern et al., p. 353 (Dordrecht: Kluwer)

Gänsicke, B.T., Beuermann, K., Mattei, J., 1997. Polars, a growing family, in *Proceedings of the 86th spring meeting of the AAVSO.*, ed. J. Mattei, *in press* (ASP conf. series)

Viotti, R., de Martino, D., Gänsicke, B.T., Gonzales-Riesta, R., 1997. The impact of 18.5 years of space observations with the International Ultraviolet Explorer on variable star research, in *Proceedings of the 86th spring meeting of the AAVSO.*, ed. J. Mattei, *in press* (ASP conf. series)

Curriculum Vitae

Name	Boris Teddy Gänsicke
Born	September 7, 1968 in Berlin
Nationality	German
Marital status	Single

Education

Sept. 74 - July 78	Zinnowwald Grundschule, Berlin
Sept. 78 - June 86	Französisches Gymnasium, Berlin
June 86	Acquisition of the German and French matriculation standards, Abitur and Baccalauréat (D)
Oct. 86 - Nov. 93	Studies of physics at the Technische Universität Berlin
Nov. 93	Diploma in physics with the thesis *Calculation of H-line blanketed white dwarf atmospheres and application to cataclysmic variables*
since April 94	PhD studies in astrophysics at the Universitäts-Sternwarte Göttingen, supervisor: Klaus Beuermann

Professional activities

Jan. - Apr. 89	Industrial practical studies at BMW, Berlin
Oct. 89 - Sept.92	Teaching assistant in physical laboratory lectures
April 93 - March 94	Teaching assistant for lectures on experimental physics and on FORTRAN
Since April 94	Research assistant at the Universitäts-Sternwarte Göttingen